Politecnico di Torino

Politecnico di Torino

Corso di Laurea magistrale in Ingegneria energetica e nucleare
A.a. 2021/2022
Sessione di Laurea marzo 2022

Synthetic natural gas generation by co-electrolysis in SOEC and methanation: experimental and techno-economic analysis

Relatori:
Prof. Massimo Santarelli
Co-relatore:
Prof. Domenico Ferrero

Candidata
Giorgia Bove

Abstract

The usage of renewable energy sources (RES) is an alternative to fossil energy sources and their growth aims to disjoin the society from carbon sources. However, many renewable sources of energy, such as wind and solar, provide energy in an intermittent manner and very often, the peak of production and the peak of consumption do not match.

Electrical energy storage (EES) is seen as a solution to these issues. EES has the potential to smooth out variability of power generation from renewable energy sources and store renewable energy to lower the cost of integrating RES within the electricity grid, increase the market penetration of RES, and lead to GHG reductions. Reversible solid oxide cells (rSOCs) working in both fuel cell (power producing) and electrolysis (fuel producing) modes are a technology capable of providing highly efficient and cost-effective EES.

Power-to-gas (P2G) is an energy conversion path where electrical energy is converted into chemical energy which is suitable for relatively long-term and large-scale storage. In power to-gas processes, energy carrier gases such as methane and hydrogen are produced by utilizing surplus electricity coming from RES, and then stored or transported. In particular, methane is a promising energy carrier because it can be used in the existing infrastructure for natural gas.

This work deals with the coupling between high temperature co-electrolysis of CO_2 and H_2O using solid oxide cells (SOEC) and a methanation process to produce a synthetic natural gas (SNG) directly injectable in the natural gas distribution grid via a Power-to-gas pathway. Downstream methanation of the syngas produced in the SOEC plant is carried out to yield a SNG stream with grid quality.

The work consists of a first theoretical section where the main concepts of fuel cells and electrolyzers are treated, focusing on both the thermodynamics of the systems and the state of the art of the technologies. Then, attention is paid on methanation process coupled with SOEC. Section 4 deals with the experimental analysis: studies on the behavior of reversible SOCs have been carried out at Environment Park in Turin, results of the polarization curves of the tests at different compositions and temperatures are reported, as well as a description of all the components (hardware and software) that make up the test bench and the procedure of assembling. The model of the system is presented in section 5: carbon dioxide present in the flue gases coming from a cement oxyfuel plant and demineralized water are considered to feed the cell. The SOEC, as well as the methanation system and the cleaning section of the gas, are modeled on AspenPlusv10.

Eventually, an economic analysis is carried on with the aim of assess the feasibility of the plant and compare the costs with those of natural gas currently marketed in the residential and industrial sector.

Contents

List of figures

List of tables

Symbols

$\dot{n}$	mol/s	Molar flow
I	A	Current
Z	-	Charge number
F	C/mol	Faraday constant
ϕ	W	Heat flux
W	W	Power
h	J/kg	Specific enthalpy
s	J/kgK	Specific entropy
T	°C or K	Temperature
p	bar	Pressure
l	J/kg	Specific work
Δg	kJ/mol	Giggs free energy variation
E	V	Nernst voltage
ν	-	Stoichiometric coefficient
R	J/molK	Universal molar constant of gas
A	cm^2	Area
j	A/ cm^2	Specific current
η	-	Efficiency
OCV	V	Open circuit voltage
ASR	Ωcm^2	Area specific resistance
V	V	Voltage
Kr	A	Rate constant
K	A	Exchange current
n_{RDS}	-	n° e- at rate determining step
β	-	Symmetric factor
ρ	kg/m^3	Density
D_{eff}		Di
ε	-	Porosity
τ	-	Tortuosity
R	Ω	Resistance
ρ	Ωm	Resistivity
V_{op}	V	Operational voltage
V_G	V	Gibbs voltage
V_{TN}	V	Thermoneutral voltage
G	kg/s	Mass flow rate
c	kJ/kgK	Specific heat

LHV	kJ/kg	Lower heating value
HHV	kJ/kg	High heating value
MM	g/mol	Molecular mass
Na	Particle/mol	Number of Avogadro
q_{e-}	C	Charge of an electron

Abbreviations

RES	Renewable energy sources
EES	Electrical energy storage
SOEC	Solid Oxide Electrolytic Cell
SNG	Synthetic natural gas
rSOC	Reversible solid oxide cell
LCOE	Levelized cost of energy
IPCC	Intergovernmental Panel on Climate Change
GHG	Greenhouse gas
IEA	International Energy Agency
UNFCC	United Nations Framework Convention on Climate Change
COP	Conference of parties
CDM	Clean Development Mechanism
JI	Joint implementation
ET	Emissions trading
GDP	Gross domestic product
INDC	Intended Nationally Determined Contributions
USD	United State dollar
NDCs	Nationally determined contributions
P2X	Power-to-X
P2G	Power-to-Gas
P2L	Power-to-Liquid
AEL	Alkaline Electrolyzer
PEMFC	Proton exchange membrane electrolytic cell
SMR	Steam methane reforming
FR	Fischer-Tropsch
MEA	Membrane electrode assembly
SOFC	Solid oxide fuel cell
RU	Reactant utilization
YSZ	Yttria stabilized zirconia
TPB	Three-phase boundary
LSCM	Lanthanum Strontium Manganese Chromate
LSM	Strontium-doped Lanthanum Manganite
ScSZ	Scandia stabilized zirconia
LSF	Lanthanum strontium ferrite

LSCo	Lanthanum strontium cobalt
LSCF	Lanthanum strontium cobalt ferrite
LSCuF	Lanthanum strontium copper ferrite
TREMP™	Topsøe Recycle Energy-efficient Methanation Process
AGR	Acid gas removal
LNG	Liquefied natural gas
MFC	Mass flow controller
CEM	Controlled evaporator mixed
AC	Alternative current
DC	Direct current
NG	Natural gas
DS	Design specification
CB	Calculator block
GG	Gas Gravity
WI	Wobbe Index
PP	Pinch point
PV	Photovoltaic
NPC	Net present cost
CAPEX	Capital expenditure
OPEX	Operational expenditure
REPL	Replacement
CF	Capacity factor
O&M	Operation and maintenance

Introduction

The tangible effects of climate change and pollutants emissions have brought to attention the urgent need to employ carbon free or carbon neutral technologies.

The energy sector accounts for a huge part of greenhouse gases emissions and it is one of the most influential concerning environmental pollution.

Among the renewable energy sources (RES), wind power and solar energy are nowadays considered the most exploitable to achieve carbon neutrality. However, these technologies are strongly dependent on atmospheric conditions and meteorological fluctuations. Moreover, it usually happens that power production from RES does not necessarily coincide with demand of end user.

Managing the intermittency of RES and their integration with the existing electric grid is not straightforward: the expected increased penetration level may lead to higher integration costs.

Large amounts of surplus electricity can be stored for long periods to balance seasonally RES electric production via chemical conversion and storage into synthetic fuels.

Low-priced surplus electricity is used to feed electrolyzers which can produce at the cathode a stream of pure hydrogen or a mixture of H_2 and CO, following the "Power-to-Gas" pathway, starting from water or a mixture of H_2O and CO_2 as feed reactants.

Converting renewable electricity into a synthetic natural gas is an innovative concept: electricity is stored as chemical energy in existing storage capacities, which is an advantage over hydrogen.
The combustion of natural gas produces the lowest ratio of emitted CO_2 per unit of thermal energy produced. Natural gas is flexible because is largely used in transportation, electricity production and civil heating sectors.

The use of solid oxide electrolysis cells (SOECs) for energy conversion has generated a great deal of interest in recent years. SOECs are able to convert electrical energy into chemical energy via electrolysis of steam or co-electrolysis of both steam and CO_2.

The aim of this work is to simulate a plant for SNG production. The final product can be directly injected into the national distribution gas grid. The plant consists of mainly three parts: the electrolysis section followed by a catalytic process called methanation and a cleaning section in order to meet the grid parameters for SNG.

The electrolyzers used are the SOEC working in co-electrolysis. They are fed by demineralized water and by carbon dioxide present in the flue gases coming from a cement oxyfuel plant. Pressurized stack operation (33.1 bar) is analyzed in this work mostly because methanation is favored at high pressure and generally employed in commercial reactors. Moreover, high pressure in SOECs favors methanation in the cathode.

The work consists of:

A first introduction on global warming situation, the international treaties to contrast it and the current energy mix.

Chapter 2 deals with the physics of electrochemical systems and their state of the art.

In chapter 3 the SNG production through the coupling of pressurized SOEC and methanation is introduced.

Chapter 4 is dedicated to the experimental results of the test carried out at the Environment Park in Turin: studies on the behavior of reversible SOCs have been carried and the results of the polarization curves of the tests at different compositions and temperatures are reported, as well as a description of all the components that make up the test bench and the procedure of assembling.

Then, the modeling of a plant coupling high temperature co-electrolysis and methanation is presented. The modelling of the plant is carried out on AspenPlusv10 and in particular, two different layouts of methanation plant are implemented to compare the produced SNG quality according to molar composition and heating value.

The main goal of this analysis is the calculation of overall plant efficiency as the ratio of SNG chemical energy and electricity input required. Results are reported in chapter 6 as well as the pinch analysis carried out on both the layouts in order to minimize the external heating requirement: heat produced from the exothermal methanation is entirely used for water evaporation before the co-electrolysis.

In the last chapter, an economic analysis is carried out to assess the feasibility of the plant and to calculate the LCOE in order to compare it with the cost of natural gas currently marketed in the residential and industrial sector.

1.Global warming and environmental problem

1.1 Climate change and global warming

According to the Intergovernmental Panel on Climate Change (IPCC) climate change is "a change in the state of the climate that can be identified (e.g., by using statistical tests) by changes in the mean and/or the variability of its properties and that persists for an extended period, typically decades or longer" [1].

The major cause of climate change is the persistence in time of greenhouse gases in the Earth's atmosphere, mainly caused by human activities.

Greenhouse gases (GHG) have the capability to absorb infrared radiation emitted from Earth's surface; after absorbing this energy, gas molecules start to vibrate and re-emit it in all directions. Part of the energy returns to Earth as heat, contributing to the so-called greenhouse effect [2]. The primary greenhouse gases in Earth's atmosphere are water vapor (H_2O), carbon dioxide (CO_2), methane (CH_4), nitrous oxide (N_2O), and ozone (O_3).

These gases are able to remain in atmosphere for extended times, causing an increase of the temperature in the lower strata of atmosphere.

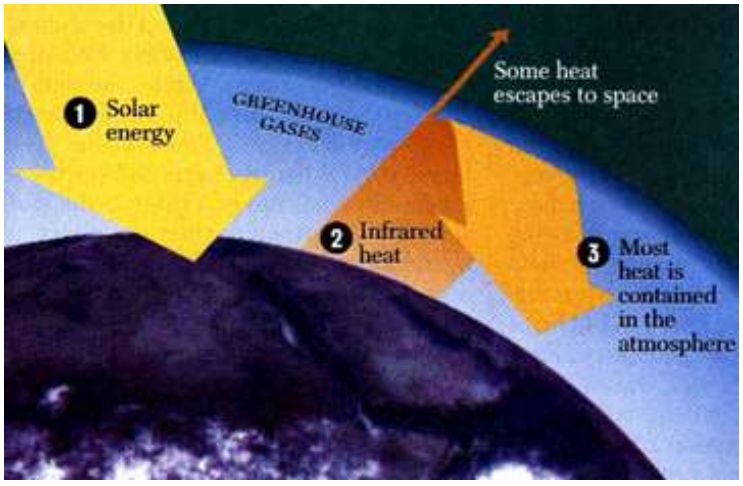

Figure 1 – Green house effect [3]

Among all the GHGs, carbon dioxide is able to exert a larger overall warming. Moreover, it has an atmospheric lifetime that increases through the years due to the growing amount of fossil carbon extracted and burned. Therefore, it can be stated that a fraction of 20-35% of the fossil carbon transferred thus far will persist in the atmosphere as elevated CO_2 levels for many thousands of years [3]. CO_2 emissions are growing through the years as we can see from the following figure [4].

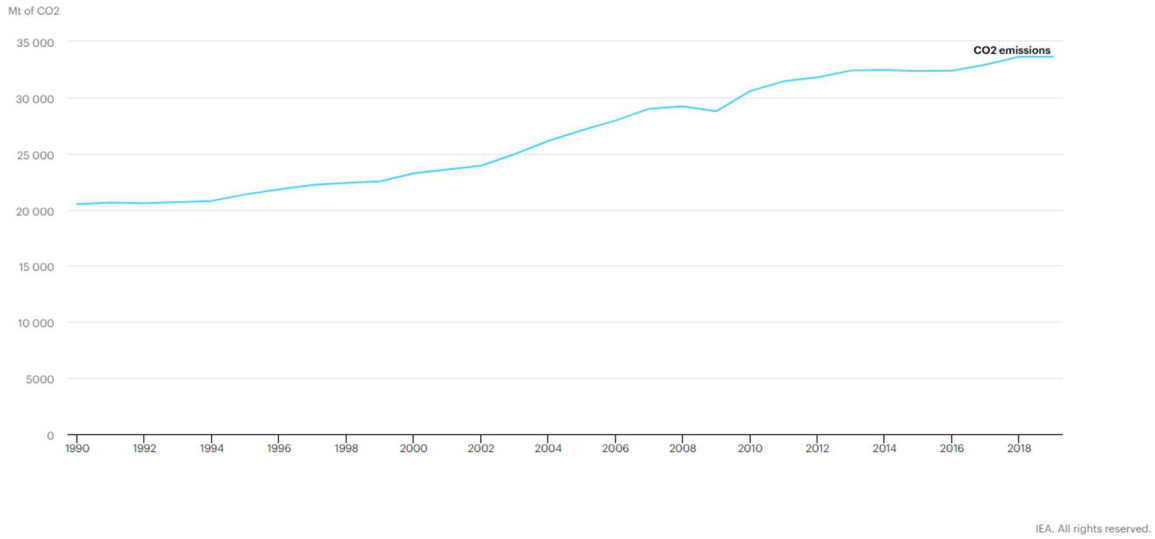

Figure 2 – Total CO2 emissions, World 1990-2019

Most CO_2 from human activities is released from burning coal, petroleum, and natural gas, as is depicted in fig.3 [4]. Other anthropogenic activities are important emissions sources such as cement production, deforestation, and biomass burning. Currently, about half of the carbon dioxide released from the burning of fossil fuels remains in the atmosphere and is not absorbed by vegetation and the oceans.

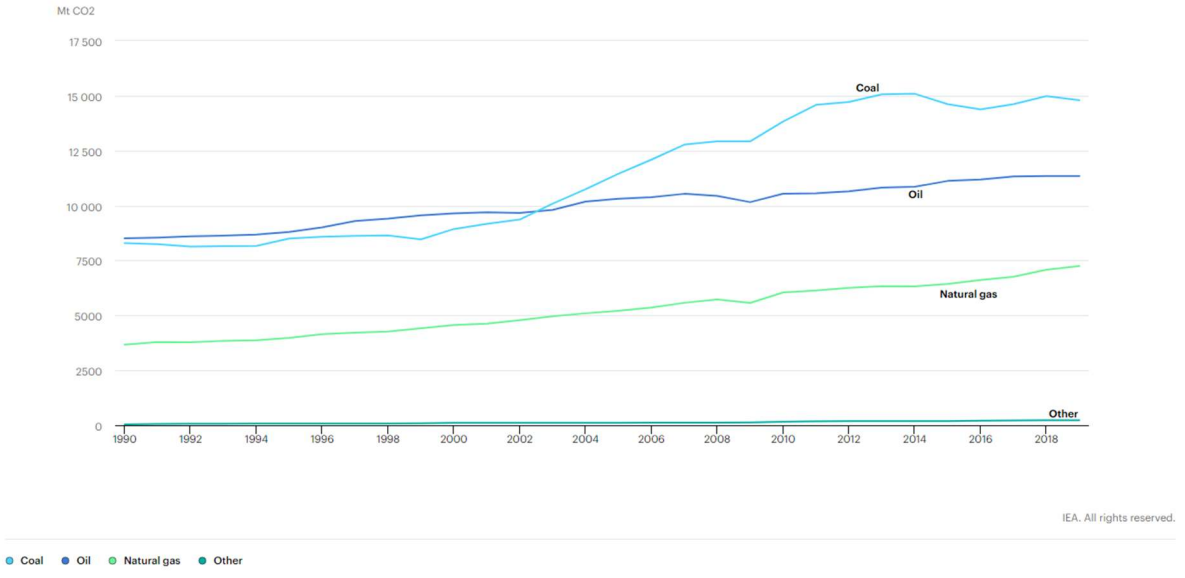

Figure 3 – CO2 emissions by energy source, World 1990-2019

Global climate change is increasing over time and requires the adoption of several coping methods. As we can see from fig.4 electricity sector is one of the most imputable for CO_2 emissions [4].
As an alternative for conventional electricity systems, renewable energies are considered to be fundamental for reducing greenhouse gas emissions, and therefore, they play an important role in climate change mitigation strategies [5].

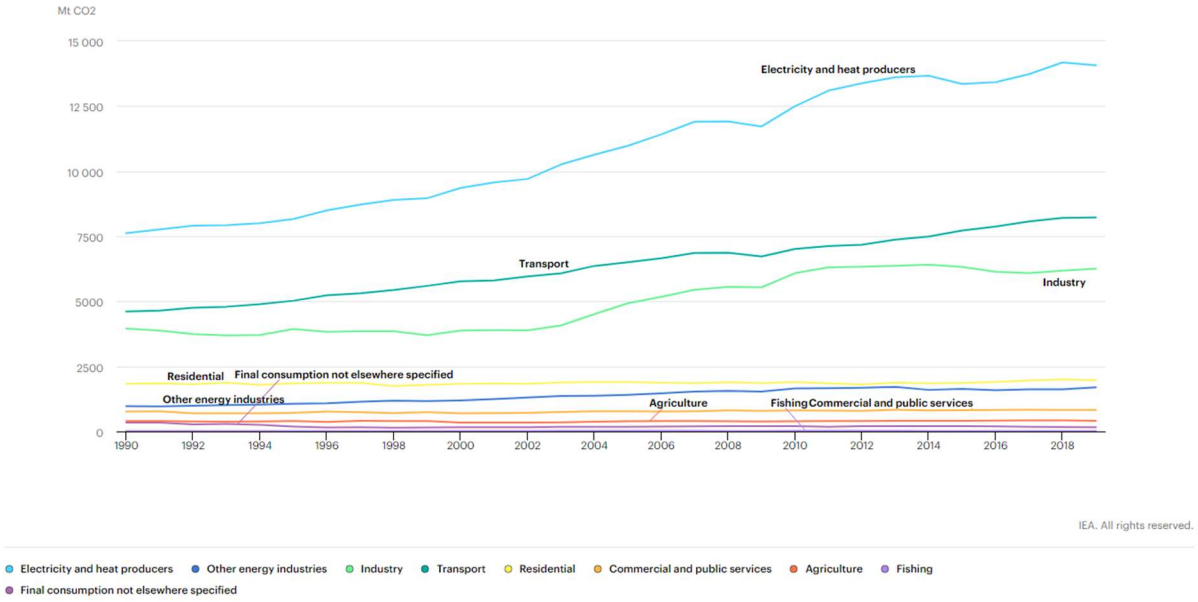

Figure 4 – CO2 emissions by sector, World 1990-2019

1.2 International treaties

The United Nations Framework Convention on Climate Change UNFCCC is an international convention that has as objective the reduction of greenhouse gas emissions and the containment of the average global temperature increase, defined during the Conference on Environment and Development of the United Nations (Rio de Janeiro, 1992) and entered into effect in 1994, when the threshold of 50 signatory countries was reached. The contracting parties participate in an annual meeting, called Conference of Parties (COP) [6].

The COP is the supreme decision-making body of the Convention. All States that are Parties to the Convention are represented at the COP, at which they review the implementation of the Convention and any other legal instruments that the COP adopts and take decisions necessary to promote the effective implementation of the Convention, including institutional and administrative arrangements [7].

1.2.1 COP3-Kyoto climate change conference

The COP3 took place from 1 to 10 December 1997 in Kyoto, Japan. In this occasion, first treaty in the world to reduce greenhouse gas emissions was approved. The Kyoto Protocol implemented the objective of the UNFCCC to reduce greenhouse gas concentrations in the atmosphere to "a level that would prevent dangerous anthropogenic interference with the climate system" (Article 2).

A first phase has been established, covering the period 2008-2012, in which the quantity of global emissions had to be reduced below the level reached in 1990.

The Protocol was based on the principle of common but differentiated responsibilities: it was stated that individual countries have different skills and opportunities to contrast climate change, firstly due to their economic development. Parties were asked to reduce current emissions on the basis that they were historically responsible for the current levels of greenhouse gases in the atmosphere. The Kyoto Protocol also provided for the possibility for member countries to use a system of flexible mechanisms for the acquisition of emission credits [6]:

- Clean Development Mechanism (CDM): allows industrialized countries to carry out projects in developing countries which can bring to a reduction of greenhouse gas emissions as well as economic and social development of the host countries; the countries leading these projects can obtain emission credits (CER).
- Joint Implementation (JI): allows industrialized countries and countries with economies in transition to carry out projects which can bring to a reduction of greenhouse gas in another country in the same group and to use the resulting credits jointly with the host country.
- Emissions Trading (ET): a country that has achieved a reduction in its greenhouse gas emissions greater than its own target can transfer their credits to a country which wasn't able to achieve its targets.

In order to be effective, the protocol needed the ratification by at least 55 countries responsible for a total of at least 55% of emissions, this was possible only in 2005 after ratification by Russia. The USA has never ratified the Protocol [6].

1.2.2 COP21-Paris climate change conference

The COP21 took place from 30 November to 11 December 2015, in Paris. The agreement reached on December 12, committed to keeping temperature rise below 2° and - if possible - below 1.5° above pre-industrial levels.

As with the Kyoto Protocol, the entry into force of the agreement required ratification by at least 55 countries responsible for at least 55 of global emissions. The agreement was signed by 177 countries, including Italy, on April 22,2016 in New York.
Each Party that has ratified the agreement had to define an emission reduction target called Intended Nationally Determined Contributions (INDCs) on voluntary basis and without penalties in case the target was no reached [6].
Pledges of the countries are depicted in the following table [6]:

UE	-40% of GHG emissions in 2030 with respect to 1990
Russia	-25/30% of GHG emissions in 2030 with respect to 1990
China	60/65% of reduction on carbon intensity per GDP unit in 2030 with respect to 2005 Peak CO2 emissions before 2030 20% of renewable energies in the energy mix
India	-33/35% of carbon intensity per GDP unit in 2030 with respect to 1990
Japan	-26% of GHG emissions in 2030 with respect to 2013
USA	-2628% of GHG emissions in 2025 with respect to 2025

Table 1 – Summary of pledges of the parties

The Paris Agreement brought attention to the important role of providing incentives for emission reduction activities, including tools such as domestic policies and carbon pricing [8]. In November 2019, Donald Trump began the process of exiting from the Paris Accords. His successor Biden, elected in 2020, is negotiating to officially re-enter the agreements.

1.2.3 COP26-Glasgow climate change conference

The Glasgow Climate Pact is an agreement reached on November 13, 2021 at the 2021 United Nations Climate Change Conference (COP26) and signed by the 197 countries that participated.

With this agreement, more than 140 countries have committed to zero emissions, which together account for 90% of current global greenhouse gas emissions [9].

Previous COP agreements have not mentioned coal, oil, gas, or even fossil fuels in general, as a major cause of climate change; this makes Glasgow Climate Pact the first agreement ever to explicitly plan to reduce coal.

The goals of the parties are the following:

1. Mitigation: zero net emissions by 2050 and limit the increase in temperatures to no more than 1.5 °C by accelerating the phase-out of coal, reducing deforestation and increasing the use of renewable energy.
2. Adaptation: supporting the most vulnerable countries to mitigate the impacts of climate change, to safeguard communities and natural habitats.
3. Climate finance: reaching the target of USD 100 billion per year of funding for developing countries.
4. Finalization of the "Paris Rulebook: make the Paris Agreement operational, with particular reference to:
    - transparency: the set of modalities for reporting GHG emissions and monitoring the commitments made by countries through Nationally Determined Contributions (NDCs);
    - mechanisms (Article 6 of the Paris Agreement);
    - Common timeframes (common time horizons for NDC definition) [10].

1.3 Current energy scenario

Despite the important decisions taken to counter the increase in GHG emissions and the technological advancement that has characterized the last decades, the world energy mix is still far from what it should be to limit climate change and global warming but in the recent years we can see some positive changes.

At a global level, the largest amount of energy comes from oil, followed by coal, gas and hydroelectric power. The global energy mix is still deeply dominated by fossil fuels, which account for more than 80% of energy consumption [11].

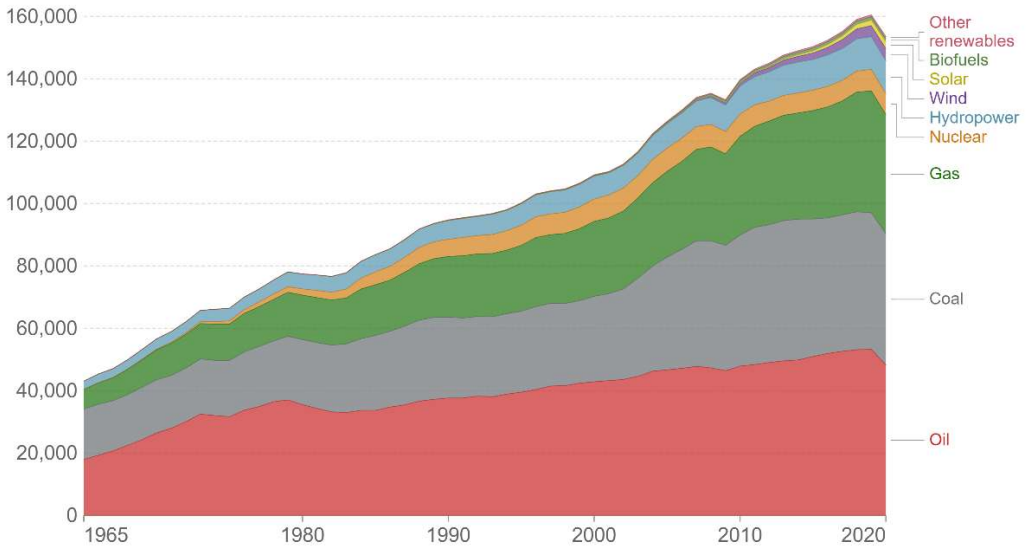

Figure 5 – Energy consumption by source, world [11]

In 2019, almost 16% of global primary energy came from low-carbon sources. Low carbon sources are the sum of nuclear and renewables, in particular:11,4 % came from renewables and 4,3% came from nuclear [11].

The global energy mix is still dominated by coal, oil, and gas, moreover, total production of fossil fuels has increased from 116,214 to 136,761 TWh in the last 10 years [11].

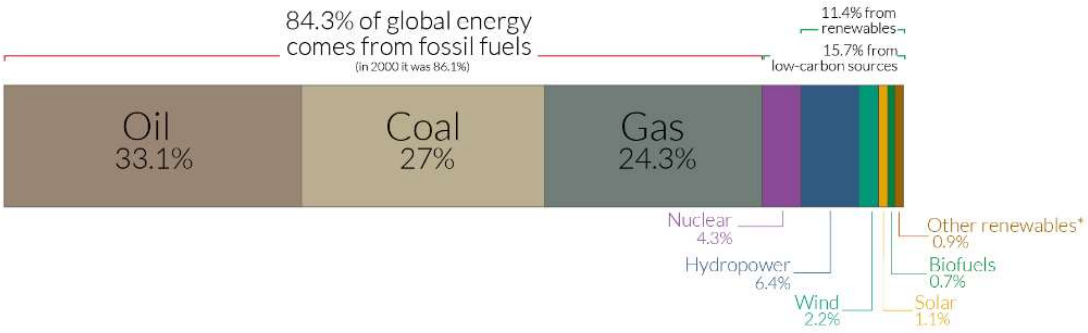

Figure 6 – Global primary energy consumption by source [11]

While in 1994 the low carbon source production were already getting 13.5%, in 2019, 25 years later, this value increased only by two percentage points, as it can be seen in the following chart:

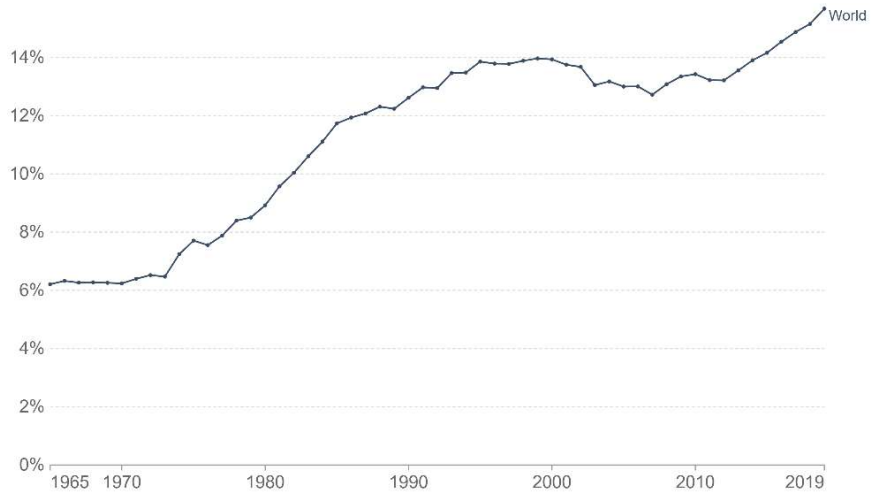

Figure 7 – Share of primary energy from low-carbon sources [11]

The electricity production is still world dependent from fossil fuel:

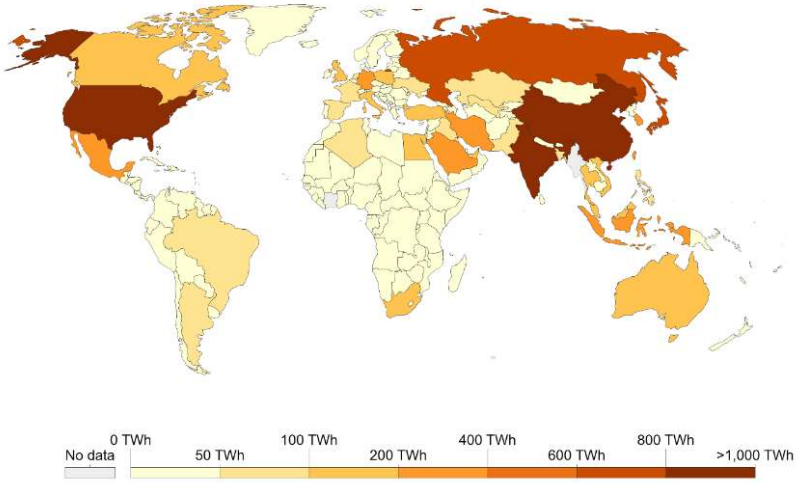

Figure 8 – Electricity generation from fossil fuels [12]

And it can be depicted from the following picture that there is a close connection between carbon dependence and CO_2 emission:

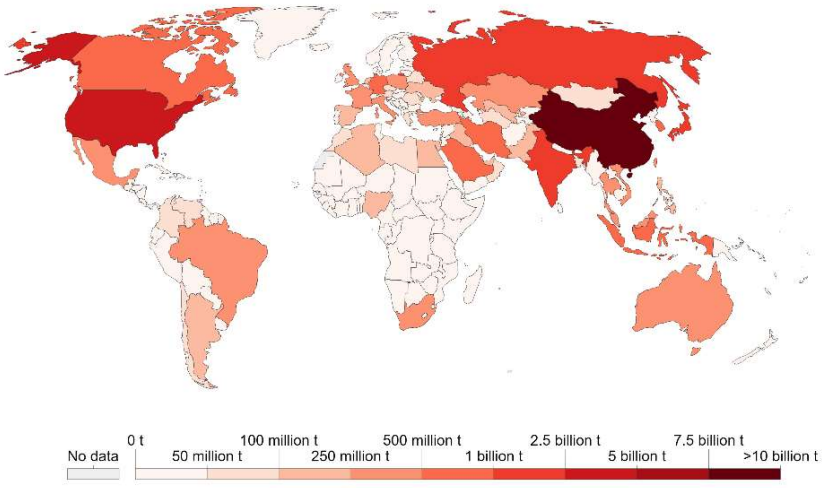

Figure 9 – Annual CO_2 emissions [12]

2.Technologies and processes

Before discussing the plant under analysis, it is important to recall the fundamental principles and the state of the art of technologies useful to the study. Firstly, electrochemical systems will be analyzed, paying attention on the state-of-the-art electrolyzers. Subsequently, hydrogen is introduced, analyzing its chemical properties but also its production and storage as well as its possible uses. Finally, the attention will be focused on P2X pathways.

2.1 Physics of electrochemical cells

An electrochemical cell is a device capable of either generating electrical energy from chemical reactions or using electrical energy to cause chemical reactions. The electrochemical cells which generate an electric current are called voltaic or galvanic cells and those that generate chemical reactions, via electrolysis for example, are called electrolytic cells.

Electrochemical cells are able to drive a redox reaction separating the two steps of the reaction into two different sections of the cell:

- Oxidation occurs in the anode side of the cell;
- Reduction occurs in the cathode side of the cell.

These two semi-reactions generate a charge separation which leads to a voltage gradient. The difference between the anodic voltage gradient and the cathodic voltage gradient is defined as the voltage gradient of the cell.

The flow of ions between anode and cathode is made possible by the presence of the electrolyte layer between them. It's necessary that the electrolyte layer has the following characteristics:

- It has to be a good ionic conductor, in this way molecules can quickly recombine during oxidation and reduction;
- It has to be an extremely low electrons conductor since the electrons have to pass through the external circuit of the system;
- It must have an extremely low molecular diffusion in order to not contaminate the layers.

Considering the electrolysis of water, fig.10 shows the operation mode of electrolyzers and fuel cells:

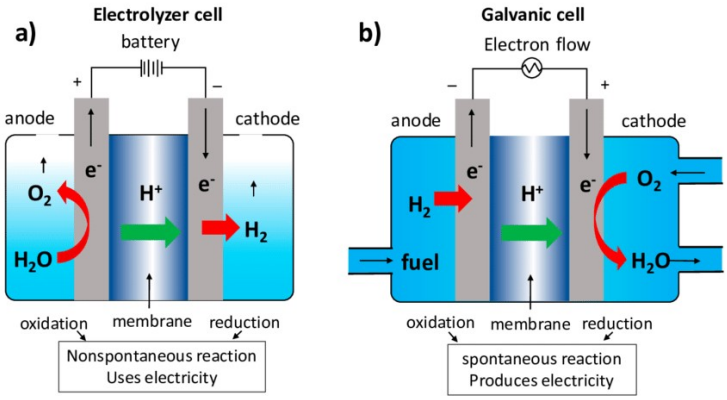

Figure 10 – Components of electrochemical cells. a) Electrolyzer cell (electrolytic) and b) hydrogen cell (galvanic cell) [13]

2.1.1 The Faraday Law

The Faraday's Law of electrolysis expresses the magnitude of electrolysis effects. It quantifies the electric current produced by the flow of electrons:

$$\dot{n} = \frac{I}{Z_i \cdot F} \tag{1}$$

Where:

- $\dot{n}$ is the molar flow, mol/s;
- I is the current, A;
- Z_i is the charge number, representing the number exchanged during the rection (gained by reduction and delivered by oxidation);
- F is the Faraday constant, equal to 96485 C/mol, and it is obtained multiplying the Avogadro constant $N_A = 6.02214076 \times 10^{23}$ mol^{-1} and the charge of an electron $q_{e^-} = -1.60217663 \times 10^{-19}$ C

2.1.2 Nernst equation

Going on with the thermodynamic and chemical analysis of the cell, another fundamental equation, called the Nernst equation, is introduced.

The formula is obtained under the following hypothesis:

- The system is in equilibrium conditions, allowing the transition of state from the initial to the final conditions;
- Steady state conditions are considered, no dynamic behavior is assumed.

Starting from these hypotheses, it is possible to consider the cell as is depicted in the following image:

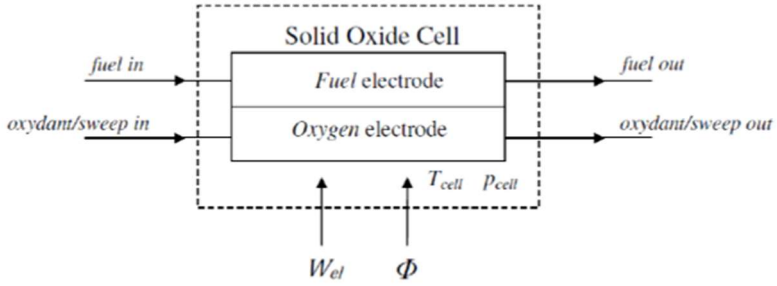

Figure 11 – Energy balance

Let's consider a galvanic cell in which, as it is stated at the beginning of chapter 2, spontaneous reaction take place. The First and the Second Law of Thermodynamics considering the control volume of fig.11 have the following forms:

$$\phi_{th} - W_{el} = \dot{n}_{prod}\hat{h}_{prod} - \dot{n}_{react}\hat{h}_{react} \tag{2}$$

$$\frac{\phi_{th}}{T_{cell}} = \dot{n}_{prod}\hat{s}_{prod} - \dot{n}_{react}\hat{s}_{react} \tag{3}$$

Normalizing them by the moles of the fuel:

$$q - l = \Delta\hat{h}_{reaction} \tag{4}$$

$$\frac{q}{T} = \Delta\hat{s}_{reaction} \tag{5}$$

$$l = \Delta\hat{s}_{reaction}T - \Delta\hat{h}_{reaction} = -[\Delta\hat{h}_{reaction} - \Delta\hat{s}_{reaction}T] = -\Delta\hat{g}_{reaction} \tag{6}$$

The Gibbs Energy, $\Delta\hat{g}_{reaction}$, for definition, is a thermodynamic function which takes into account only variation of other thermodynamic functions of the system and allows to determine the spontaneity of a process which takes place at constant temperature and pressure. In particular, in the electrolyzer mode, the variation $\Delta\hat{g}_{reaction}$ is positive due to the non-spontaneity of the reactions involved, while it is negative in the fuel cell mode.
Recalling that:

$$l = \frac{W_{el}}{\dot{n}_{fuel}} = \frac{I * E}{\frac{I}{Z * F}} = E * Z * F \tag{7}$$

It is possible to write:

$$-\Delta\hat{g}_{reaction} = E * Z * F \text{ , so: } E = -\frac{\Delta\hat{g}_{reaction}}{Z*F} \tag{8}$$

This equation is called the Nernst equation and allows the calculation of the open circuit voltage (OCV) that represents the voltage that would be measured during open circuit conditions, so

without any current flow. It can be stated the is the voltage that a cell can generate without the presence of transport phenomena, in thermodynamics equilibrium.

The specific molar enthalpy and entropy are a function of the cell temperature and partial pressure, so it can be stated that:

$$\Delta \hat{g}_{reaction} = \sum_{p} \nu_p \hat{g}_p(T, p_i) - \sum_{r} \nu_r \hat{g}_r(T, p_i) \tag{9}$$

Applying the ideal gas model, it can be written:

$$\hat{g}(T, p_i) = g(T, p_0) + RT \ln \frac{p_i}{p_o} \tag{10}$$

Where:

- p_o is the reference pressure of 1 bar, p_i is the partial pressure and R is the universal molar constant of gas.

It is finally derived that:

$$OVC_{fuel\ cell} = -\frac{\Delta g_{reaction}(T, p_0)}{Z * F} + RT \ln \frac{\prod_i^{react} \frac{p_i}{p_0}^{\nu_i}}{\prod_i^{prod} \frac{p_i}{p_0}^{\nu_i}} \tag{11}$$

$$OVC_{electrolyzer} = \frac{\Delta g_{reaction}(T, p_0)}{Z * F} + RT \ln \frac{\prod_i^{prod} \frac{p_i}{p_0}^{\nu_i}}{\prod_i^{react} \frac{p_i}{p_0}^{\nu_i}} \tag{12}$$

Where ν_i is the stoichiometric coefficient of the i-th species.

The differences between the two equations are the minus sign before the $\Delta g_{reaction}$ and the logarithm argument.

2.1.3 Polarization curve

A very useful tool to describe the behavior of the voltage as the current increases is the polarization curve of the cell (I-V curve) also called characteristic of the cell. It can be represented on a Cartesian coordinate system in which on the abscissa there is the current I (A), or more often the density of current j (A/cm^2).

As it is stated in 2.1.2, the OCV represents the voltage of the cell only in the case of nil current. As the passage of electrons begins, the value of the current starts to increase, and the voltage

changes its value. When the circuit is closed, the system goes out of equilibrium and so the physics is dominated by transport phenomena such as:

- Charge transfer which is related to the kinetic of the reactions;
- Charge migration which refers to the resistance of passing through the electrolyte layer and through the external circuit by molecules, ions and electrons;
- Mass transport which is related to the molecule diffusion.

Each of these phenomena is related to an overvoltage, respectively: activation overvoltage, ohmic overvoltage, diffusion overvoltage.

They are graphically depicted in the three different slopes of the curve which can be divided in three zones.

So, the complete formula of the voltage can be written as follows:

$$V_{CELL} = OCV \pm \eta_{ACT} \pm \eta_{OHM} \pm \eta_{DIFF} \quad (13)$$

In case of a fuel cell, all minus signs are considered, on the contrary, in case of electrolyzer, all plus signs are used.

Activation overvoltage

Each reaction that occurs in the systems has its own kinetic. Chemical reactions, in fact, are not immediate, as they are made by a succession of intermediate stages each of which is characterized by a particular degree of advancement of the reaction. These stages follow each other leading to the final result of the reaction, so the global rate of reaction is an average value of the kinetic of all the stages.

For electrochemical systems, a kinetic law can be written by the Arrhenius equation as follows:

$$K_r = K\ exp\left[\frac{\beta\ n_{RDS}\ F}{R\ T}\eta\right] \quad (14)$$

Where:

- K_R is measured in C/s, so in Ampere;
- K is the rate constant, which represents Kr when η tends to zero, so in open circuit conditions, when the system is in equilibrium. Indeed, this current is called Exchange current, and it is a characteristic of the given electrochemical reaction and electrode, and it is function of the temperature;
- n_{RDS} is the number of the electrons transferred in the Rate Determining Stage of the reaction;
- β is a symmetry factor which quantifies the energy levels, usually approximated to 0,5;
- R is the universal molar constant of gas;
- T is the absolute temperature;
- η is the activation voltage.

The charge transfer process is regulated by a combination of the forward reaction and the backward reaction. Butler and Volmer, starting from the eq.14 formulate an expression to correlate the current density and the overpotential:

$$I = I_0\, exp\left[\frac{\beta\, n_{RDS}\, F}{R\, T}\eta\right] -\ exp\left[-\ \frac{(1-\beta)\, n_{RDS}\, F}{R\, T}\eta\right] \tag{15}$$

Substituting β with its value:

$$I = I_0\, exp\left[\frac{0{,}5\, n_{RDS}\, F}{R\, T}\eta\right] -\ exp\left[-\ \frac{(1-0{,}5)\, n_{RDS}\, F}{R\, T}\eta\right] \tag{16}$$

Taking into account the formula of the hyperbolic sin: $\sinh(x) = \frac{e^x - e^{-x}}{2}$

Eq.17 is achieved:

$$\eta_{ACT} = \frac{R\, T}{\beta\, n_{RDS}\, F}\sinh^{-1}\left(\frac{I}{2I_0}\right) \tag{17}$$

Considering the current density:

$$\eta_{ACT} = \frac{R\, T}{\beta\, n_{RDS}\, F}\sinh^{-1}\left(\frac{i}{2i_0}\right) \tag{18}$$

Ohmic overvoltage

This contribution is related to the migration of charged species, regulated by the Ohm Law:

$$\Delta V = R \cdot I \tag{19}$$

Where:

- R is the resistance of the material, Ω;
- I is the current, A.

The ohmic overvoltage is expressed as follows:

$$\eta_{OHM} = R \cdot I = \rho\frac{L}{S}\, i\, S = \ \rho\, L\, i \tag{20}$$

Where:

- ρ is the resistivity od the conductor, Ωm;
- L is the length of the conductor, m;
- S is the section of the conductor, m^2.

The overvoltage refers to both electrons and ions, but since the resistivity of the electrons is order of magnitude lower than the conductivity of the ions, it can be neglected.

Diffusion overvoltage

Due to the diffusive phenomena on the porous electrode, two different conditions of the reactants flow are found:

- The bulk condition, which represents the concentration in the supply channel, before interacting with the electrode;
- The reactant concentration condition, when the stream reaches the point of activation on the electrode surface [8].

The diffusion or concentration overvoltage is caused by mass transport phenomena. As the cell reaction proceeds, in fact, a concentration gradient of both reactants and products in the bulk electrolyte and on the electrode surface is formed. Due to mass transport, in fact, reactant molecules cannot reach, or the product molecules cannot depart from, the reaction sites under the specified current. Consequently, is formed an excess of product and a burnout of reactants on the electrode surface [14].

The diffusive coefficient of the i-th species can express the real concentration of the gas:

$$D_i^{eff} = D_{bulk}\left(\frac{\varepsilon}{\tau}\right)^n \tag{21}$$

Where:

- D_{bulk} is the diffusive coefficient in the bulk condition, which describes the concentration of the gas species before any interaction with the electrode;
- ε is the porosity;
- τ is the tortuosity.

In the ideal conditions, the diffusive coefficient and the bulk coefficient coincide, as the diffusive phenomenon doesn't produce any loss. In the real case, losses came from the porosity of the material and on the path of the stream inside the electrode.

The diffusion phenomenon reduces the concentration of the reactant in the reaction point related to the voltage.

Applying the Fick' s model to 1D system, it is possible to calculate the current density:

$$i = 2FD_i\frac{C_i^{bulk} - C_i^{CAT}}{L_{electr}} \tag{22}$$

In the hypothesis of C_{cat}=0, the so-called Limiting current density is obtained:

$$i_l = 2FD_i\frac{C_i^{bulk}}{L_{electr}} \tag{23}$$

Where:

- C_i^{bulk} is the concentration of the i-th species in the bulk condition;
- C_i^{CAT} is the concentration of the i-th species inside the electrode;
- L_{electr} is the thickness of the electrode.

Taking the case of a fuel cell, the OCV can be written in the following form starting from the Nernst equation but considering concentration instead of partial pressures:

$$OCV_{fuel\ cell} = -\frac{\Delta g_{reaction}(T, p_0)}{Z * F} + \frac{RT}{Z * F} \ln \frac{\prod_i^{react} C_i^{\nu_i}}{\prod_i^{prod} C_i^{\nu_i}} \quad (24)$$

$$\Delta V_{cat-bulk} = OCV(cat) - OCV(bulk) = \eta_{diff} = \frac{RT}{ZF} ln \frac{C_i^{CAT}}{C_i^{BULK}} \quad (25)$$

It is possible to finally obtain:

$$\eta_{diff} = \left| \frac{R\,T}{Z\,F} ln\left(1 - \frac{i}{i_l}\right) \right| \quad (26)$$

A typical trend of the characteristic curve of an electrolyzer and a fuel cell is depicted in the following image:

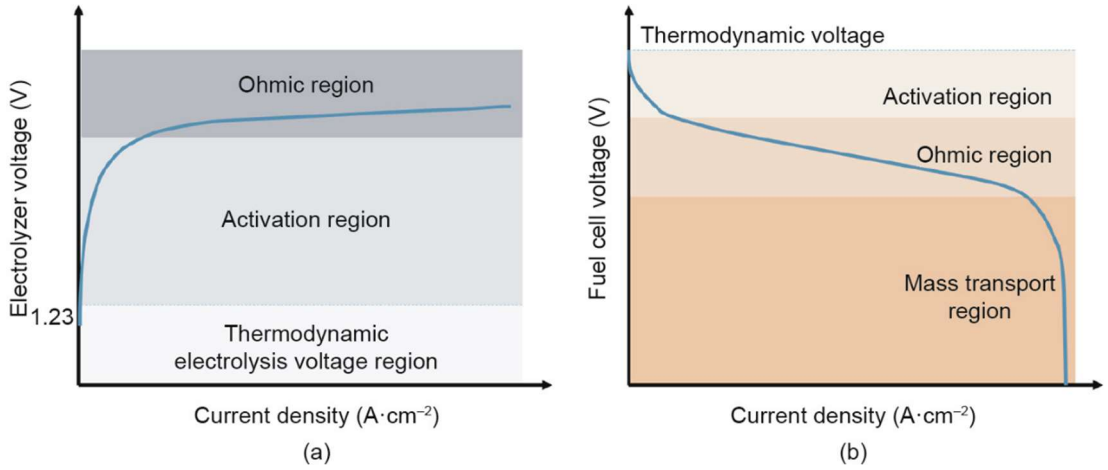

Figure 12 – Example of polarization curves: (a) electrolyzer, (b) fuel cell [15]

Simplyfing hypothesis

Very often, when considering the polarization curve, a simplifying assumption is done: as the greatest overvoltage contribution appears to be the ohmic one, the curve is linearized, so a linear relationship between voltage and current density is considered
Obviously, this is a simplifying hypothesis, but for some type of cells like solid oxide ones is not senseless. As a matter of fact, the polarization curve is quite linear also for low values of current density, because activation overpotential is not as high as that of low temperature electrolysis; this is because high temperature makes the kinetic of reactions higher.

Area specific resistance

With the hypothesis of linear relationship between voltage and current density, it is possible to define the angular coefficient of the curve. This is called "Area Specific Resistance":

$$ASR = \frac{V_{op} - V_G}{j} \quad (27)$$

Where:

- V_{op} is the operative voltage, V;
- V_G is the "Gibbs Voltage", which has the same meaning of Reversible Voltage,V;
- j is the current density, A/cm^2.

The unit of measurement of the ARS is $\Omega \cdot cm^2$.
So it's also possible to express the operating voltage in a simplified way, but still as a function of current density:

$$V_{op}(j) = V_G + ASR \cdot j \tag{28}$$

And similarly:

$$\eta_{ohm} = ASR \cdot j \tag{29}$$

ASR can be seen as the sum of different terms:

$$ASR = R_{el} + R_{conn} + R_{echem} + R_{diff} + R_{conv} \tag{30}$$

Where:

- R_{el} is the electrolyte resistance calculated from the specific conductivity and the thickness;
- R_{conn} is the resistance due to non-optimized contact and current collection;
- R_{eche} is the electrode polarization originating from all the chemical and electrochemical processes on the electrode surfaces, on the electrolyte/electrode interfaces and in the bulk electrode material;
- R_{diff} accounts for the contribution of the gas phase diffusion;
- R_{conv} is the contribution due to gas conversion [16].

According to literature ASR can essentially be calculated in two ways:

1. From the polarization curve obtained at constant mole flow;
2. Through Electrochemical Impedance Spectroscopy (EIS). EIS is a method that allows identifying and recognizing all the different fuel cell loss terms. From the analysis of polarization curves, it is possible to evaluate the cell resistance [16].

Assuming for a system a fix operating voltage and a fixed Faradic current, modifying the ASR brings to a change in the current density, and so on the active area of the cell. In fact, the active area can be calculated as follows:

$$Area = \frac{I}{j} \tag{31}$$

Moreover, ASR depends on operational parameters like pressure and temperature.

Data provided by researchers of Risø Laboratory and DTU (Technical University of Denmark) can be used to estimate ASR, following this procedure [16]:

- Ebbesen et al. derived the increasing of ASR passing from single cell to a stack [17];
- Mogensen et al. estimated the change of ASR varying temperature both for steam electrolysis and co-electrolysis of steam and carbon dioxide [18];
- Jensen et al. studied the behavior of ASR at different pressures for steam electrolysis [19].

By fitting and interpolating of these literature data, both for steam and co-electrolysis a relationship with the following form was derived:

$$ASR(p,T) = A \cdot exp(-B \cdot T) \cdot exp(-C \cdot p) \tag{32}$$

Where:

	Steam electrolysis	Co-electrolysis
A	35,71	34,22
B	0,0057	0,0054
C	0,0217	0,0217

Table 2 – ASR coefficients

In modelling the plant, the previous relationship is used to calculate the ASR at 850 °C and 33,1 bar.

2.1.4 Thermodynamics

The thermodynamics of an electrochemical cell is the result of the sum of two heating effects: one is purely thermodynamic, represented by the heat of reaction ϕ_{REACT}, the other is the result of transport processes, and it is the heat related to the irreversibilities, ϕ_{IRR}.

As it is stated in section 2.1, electrochemical systems can work in two modes: fuel cells and electrolyzers. The different thermodynamics of the reactions that take place in the different modes leads to a difference in the thermodynamic of the whole system. The thermal behavior of the fuel cell is completely exothermic, while the thermal behavior of the electrolyzer, can be either exothermic or endothermic.

Case 1: $\Delta g<0$

Considering a fuel cell, being $\Delta g<0$ it can be state that $\Delta s<0$.

The heat of reaction is:

$$\hat{q}_{REACT} = T\ \Delta\hat{s}_{reaction} \tag{33}$$

$$\phi_{REACT} = |\hat{q}_{REACT}|\ \dot{n}\ F = |\hat{q}_{REACT}|\ \frac{I}{Z\ F} \tag{34}$$

$$\phi_{REACT} = |\hat{q}_{REACT}|\ \dot{n}\ F = -\frac{T\ \Delta\hat{s}_{reaction}}{Z\ F}\ I \tag{35}$$

This is an exothermic contribution.

The heat due to the irreversibilities is:

$$\phi_{IRR} = I \sum_{j=I}^{3} \eta_j \tag{36}$$

This contribution in exothermic too.

The sum of the two is:

$$\phi_{cell} = \phi_{REACT} + \phi_{IRR} = -\frac{T\,\Delta\hat{s}_{reaction}}{Z\,F}\,I + I\sum_{j=I}^{3}\eta_j = I\left[-\frac{\Delta\hat{h}}{Z\,F} + \frac{\Delta\hat{s}}{Z\,F} + \sum_{j=I}^{3}\eta_j\right]$$
$$= I\left[-\frac{\Delta\hat{h}}{Z\,F} - \left(-\frac{\Delta\hat{g}}{Z\,F} - \sum_{j=I}^{3}\eta_j\right)\right] = I\left(-\frac{\Delta\hat{h}}{Z\,F} - V_c\right) \quad (37)$$

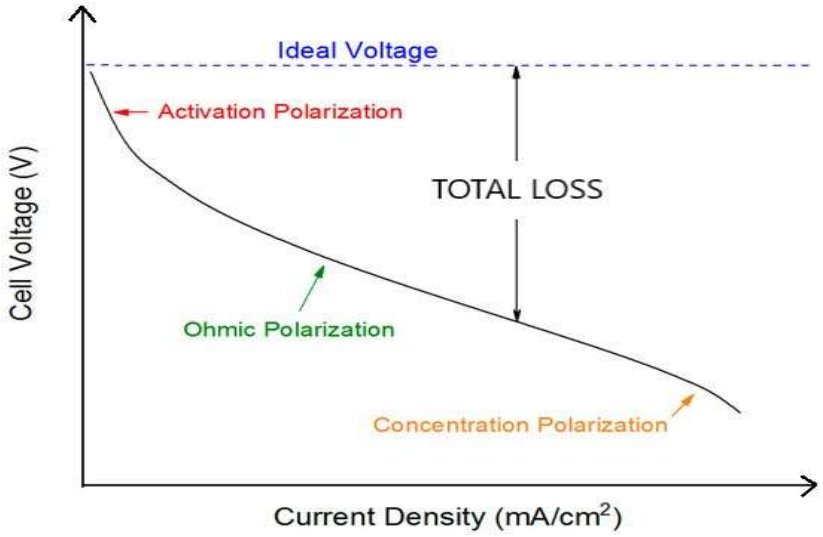

Figure 13 – Losses [20]

Case 2: Δg>0

In this case, the heat of reaction is an endothermic contribution while the heat due to the irreveribilities remains exothermic:

$$\phi_{cell} = \phi_{REACT} - \phi_{IRR} = \frac{T\,\Delta\hat{s}_{reaction}}{Z\,F}\,I - I\sum_{j=I}^{3}\eta_j$$
$$= I\left[\frac{\Delta\hat{h}}{Z\,F} - \left(-\frac{\Delta\hat{g}}{Z\,F} - \sum_{j=I}^{3}\eta_j\right)\right] = I\left(\frac{\Delta\hat{h}}{Z\,F} - V_c\right) \quad (38)$$

So there will be a value of the operating voltage such that ϕ_{cell} will be zero. This value is called Thermoneautral voltage V_{TN}:

$$V_{TN} = \frac{\Delta\hat{h}}{Z\,F} \quad (39)$$

This threshold value separates the endothermic behavior of the electrolyzer from its exothermic behavior.

The point of operation in which the voltage is the thermoneutral voltage is called thermo neutrality and the cells work in adiabatic conditions. In the following image, the point of thermo-neutrality is depicted by the circle:

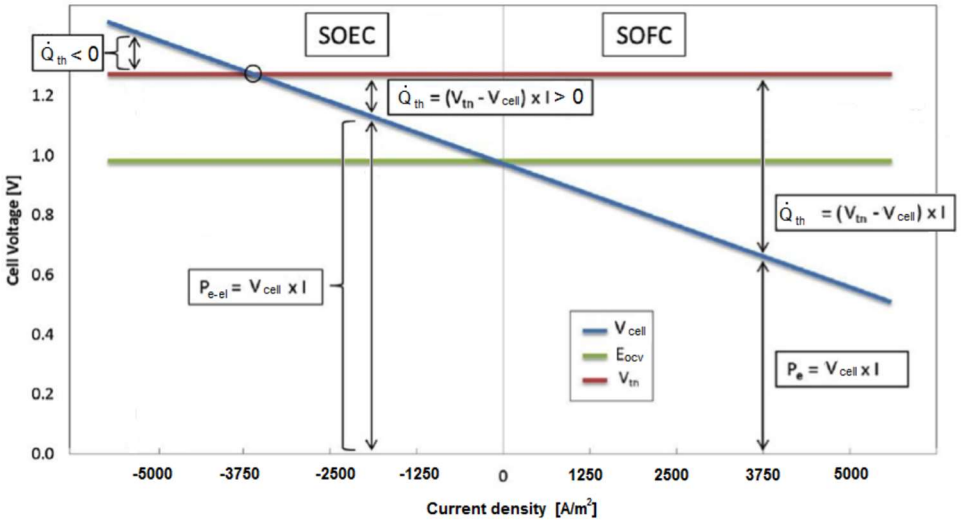

Figure 14 – rSOC polarization curve: electrical and thermal power in fuel cell and electrolysis mode [21]

When an electrolyzer is assumed to work in thermoneutrality, a 100% of electrolysis efficiency is reached.

Considering that:

$$\phi_{REACT} = |\hat{q}_{REACT}|\, \dot{n}\, F = -\frac{T\, \Delta\hat{s}_{reaction}}{Z\, F}\, I = \frac{T\, \Delta\hat{s}_{reaction}\, j}{Z\, F} = \frac{j}{Z\, F}\, (\Delta_h - \Delta_g)$$
$$= j\, (V_{TN} - V_G)$$

Setting V_{OP}=V_{TN}, ϕ_{REACT} *and* ϕ_{OHM} have the same form with opposite sign. This confirms that the V_{TN} makes the global heat flux null.

The cell efficiency can be defined, using the Faraday Law and the definition of Thermoneautral voltage, as follows:

$$\eta = \frac{n_R \cdot \Delta_h}{W_{el}} = \frac{\frac{I}{Z \cdot F} \cdot Z \cdot F \cdot V_{TN}}{V_{OP} \cdot I} = \frac{V_{TN}}{V_{OP}} \qquad (40)$$

2.2 Electrolyzers: state of the art

An electrolytic cell is an electrochemical system capable of operating chemical reactions with Δ_g>0. This type of reactions is not spontaneous and so requires a level of energy to occur, accordingly they are also defined as endothermic. Electrolysis technologies are usually grouped in two categories according to the temperature of operation. The low temperature technologies are the alkaline electrolyzers and the PEM electrolyzsers, while the high temperature ones are represented by the SOEC.

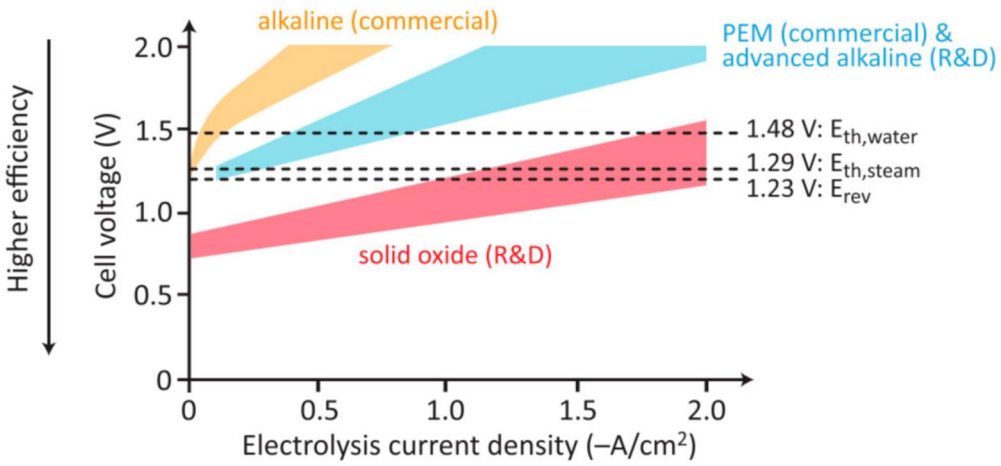

Figure 15 – Comparison between alkaline, polymer electrolyzer membrane (PEM), and solid oxide electrolyzers [22]

2.2.1 Alkaline electrolyzers

Alkaline water electrolyzers have been widely used in chemical industry and nowadays are the most commercialized among electrolyzers. The electrolyte layer consists of a solution with 30% in weight of potassium hydroxide (KOH) or sodium hydroxide (NaOH), here the hydroxide ions (OH-) passes from the cathode to the anode.

The electrodes are usually made by nickel-based metals and they are typically separated by a thin porous foil (with a thickness between 0.050 to 0.5 mm), commonly referred to as diaphragm or separator. The ionic conductivity is supplied by the aqueous alkaline solution, which penetrates in the pores of the diaphragm.

The semi reactions that occur on the electrodes are:

- Cathode (reduction): $2H_2O(l) + 2e^- \rightarrow H_2(g) + 2OH^-(l)$
- Anode (oxidation): $2OH^-(l) \rightarrow \frac{1}{2}O_2 + H_2O(l)$

The main advantages of alkaline electrolyzers are:

- The use of a cheap catalyst;
- The use of an exchangeable electrolyte with a lo dissolution of anodic catalyst in it;
- The production of a quite pure gas due to the low gas diffusivity in alkaline electrolyte.

Co-electrolysis is possible using a bicarbonate electrolyte. CO_2 is sent through an aqueous media or in form of a gas.

2.2.2 Proton exchange membrane electrolyzers

Polymer electrolyte membrane (PEM) electrolyzers perform water electrolysis trough proton exchange membrane electrolyte made by Nafion. The electrolyte layer conduct protons from the anode to the cathode while insulating the electrodes electrically. The proton exchange membrane shows a very low gas crossover rate, this brings to an extremely high purity of the product gas [23].

A high gas purity is important for storage safety and for the direct usage in a fuel cell. Furthermore, this type of electrolyte allows to operate with a very thin membrane (~100-200 μm), resulting in low ohmic losses [24].

PEM electrolyzers were first introduced in the 1960s by General Electric to overcome the issues of partial load, low current density, and low-pressure operation currently plaguing the alkaline electrolyzers [25]. This type of electrolyzers have indeed a fast dynamic and a low start-up time, large operational ranges, and high efficiencies.

The semi reactions that occur on the electrodes are:

- Cathode (reduction): $4H^+(aq) + 4e^- \rightarrow 2H_2(g)$
- Anode (oxidation): $2H_2O(l) \rightarrow O_2(g) + 4H^+(aq) + 4e^-$

The temperature range of operation of a PEM electrolyzer is 60-80 °C. The low temperature has the great advantage to cut the start-up time but, on the other hand, low-temperature electrochemical cells need a more precious catalyst.

PEM electrolyzers are able to operate at high current densities, reducing operation costs especially for systems coupled with very dynamic energy sources.

2.2.3 SOEC

A solid oxide electrolyzer achieves the electrolysis of water (and/or carbon dioxide) by using a ceramic electrolyte. The products of the electrolyzer are hydrogen gas (and/or carbon monoxide) and oxygen, as depicted in the following reactions:

- Cathode (reduction): $2H_2O(l) + 4e^- \rightarrow 2H_2(g) + 2O_2^-(g)$
- Anode (oxidation): $2O_2^-(g) \rightarrow O_2(g) + 4e^-$

This type of electrolyzers operate in a range of temperature between 500 and 850 °C. These temperatures are like those of a solid oxide fuel cell.

The high temperature of operation needs a meticulous choice of materials.

2.3 Hydrogen

Hydrogen is an energy carrier that can transform our fossil-fuel dependent economy into a hydrogen economy, which can provide an emissions-free transportation fuel. The fields of application of hydrogen are growing up and are becoming key players in decarbonization. Even if hydrogen is the most present element on Earth -constituting roughly 75% of all normal matter- it cannot be found in nature, so it cannot be defined as a primary energy source. However, it can be obtained from several sources and processes, that will be analyzed in detail in section 2.4.2.

The combustion reaction of hydrogen produces water and heat, being of course an exothermic reaction:

$$2H_2 + O_2 \rightarrow 2H_2O \qquad \Delta\hat{h}_0 = -286 kJ/mol \tag{41}$$

Where:

- $\Delta\hat{h}_0$ is the variation of enthalpy calculated at normal conditions (20 °C and 1 bar).

$\Delta\hat{h}_0$ represents the amount of heat released, as its sign is negative. The only physical product of this reaction is water, so the combustion of hydrogen is totally free from GHG emissions.

The use of hydrogen as a fuel for the mobility can extremely reduce smog and pollutants emissions. Moreover, combined with CO, it forms the so-called syngas, which can be immitted in the national gas grid.

Another important aspect of hydrogen exploitation is the storage of energy that can perform. Energy storage by means of hydrogen is fundamental not only for deficit periods but also to improve the transportation of energy from the place of production to the place of consumption.

Thus, considering its huge potential, the hydrogen economy will emerge in the near future.

2.3.1 Properties

Hydrogen is the lightest element on Earth. At standard conditions it is in form of gas of diatomic molecules having the formula H_2.

Hydrogen results to be colorless, odorless, tasteless, non-toxic, and highly combustible. Its most abundant form on Earth is molecular such as water and organic compounds. For the most common isotope of hydrogen each atom has one proton, one electron, and no neutrons. Its molecule has two different configurations: ORTO and PARA. The difference between the two is the spin of the single electron outside the nucleon. The molecule configuration strictly depends on temperature: at 298 K, the 75% of the molecules are in the ORTO configuration. The decrease of temperature leads to the exothermic conversion from ORTO to PARA. The following table report some of the most interesting properties of this molecule:

Property	Value
Gas density @ 273,15 K, Kg/Nm^3	0,08988
Liquid density @ 20,3 K, Kg/m^3	70,79
Boiling point @ 1 bar, K	20,3
Freezing/Melting point, K	13,95
Lower Heating Value (LHV), MJ/kg	120
Higher Heating Value (HHV), MJ/kg	141,7
Specific heat at constant pressure, kJ/kgK	14,33
Specific heat at constant volume, kJ/kgK	10,296
Specific volume, m^3/kg	11,99
Low Flammable Limit, %	4
High Flammable Limit, %	74
Liquefaction latent heat, kWh/kg	3,92
Coefficient of diffusivity, cm$_2$/s	0,61

Table 3 – Hydrogen properties

As it turns out from table 3, hydrogen has a very low density. Its LHV(g) is one of the highest if compared to all the other fuels. LHV(g) represents the energy content in function of the mass taken into account, but considering it from a volumetric point of view, this value considerably decreases, arriving to around 9,72 MJ/m^3. A low volumetric energy content leads to an economic disadvantage, as it is necessary more space to store the hydrogen.

Fortunately, it is possible to overcome this issue by acting on the density. Considering the Law of natural gases, it can be written that:

$$\rho = p \cdot R \cdot T \tag{42}$$

By increasing the pressure, or decreasing the temperature, the density will increase too, so the less volume the hydrogen will occupy with the same space, because it will have a greater weight.

By increasing the pressure of the gas to 200 bar the density arrives to the value of 16642 kg/m^3. Bringing the gas to 700 bar, the improvement in terms of density becomes still more evident, reaching the value of 57,47 kg/m^3. Even if these values can bring to an evident reduction of space, the processes involved are not economically feasible yet.

By operating on temperature, it is possible to obtain a density of 71 kg/m^3 through a liquefaction process of the hydrogen. However, liquefaction involves cryogenic processes, which result to be very expensive in terms of energy.

A third new technology seems to be fundamental in the future of the hydrogen storage, and it is based on the chemical absorption of the gas in a solid matrix, where the most performants are the metal hydrides. This method is less expensive than the previous ones, and it allows to achieve a higher density level, with an average of ρ between 100 ÷ 200 kg/m^3, confirming itself as an important method of hydrogen storage for the future.

Hydrogen is characterized by an extremely high specific heat, to highlight its energy potential it can be noticed that, at standard condition, hydrogen specific heat is 14,33 kJ/kgK, while air value is 1,055 kJ/kgK, and water one is 4,186 kJ/kgK. As a matter of fact, its exploitation in a thermal cycle, considering the same amount and the same variation of temperature, produces an higher amount of thermal energy compared to the referent elements. However, there are still some issues related to materials that do not allow the exploitation of hydrogen in thermal plants: the temperatures reached in both the combustion chamber and turbine are too high for several construction materials.

The high value of the coefficient of diffusivity is important for safety reasons being it the tendency to escape from the storage system which contains the gas, so it is extremely important to take into consideration all the possible leaks and the environments that would be in direct contact with the escape of this gas.

2.3.2 Means of production

As mentioned in 2.4, hydrogen cannot be found as a raw material in nature, and it can only be obtained as a product of several processes. For this reason, hydrogen has been classified according to the GHG emission profile of the process used to extract it into [26]:

- Brown hydrogen: is made from coal and is produced trough gasification. This process has been largely used in many industries and converts carbon-rich materials into hydrogen and carbon dioxide. Gasification releases CO_2 into the atmosphere.
- Grey hydrogen: is extracted from natural gas using a process called steam reforming. In this process steam is used to separate hydrogen from natural gas, emitting GHGs which are released into the atmosphere.
- Blue hydrogen: is produced using steam reforming too, but carbon capture and storage technologies capture and store those related-process emissions.
- Green hydrogen: is extracted using a method that does not produce GHG emissions. The most used methods involve electrolyzers, which split water into hydrogen and oxygen consuming electricity. Electricity has a key role in this classification since it has to come from renewable sources, such as wind, solar, which have no associated GHG emissions.

Now, in details, gasification and steam reforming processes are analyzed.

Gasification

The gasification process converts any raw carbonaceous material such as coal into syngas. Syngas can be treated in order to produce hydrogen or another alternative chemical compound, more convenient and suitable for the target process [8]. During gasification, the coal is blown through with steam and oxygen, while also being heated (and in some cases pressurized).

During this reaction, oxygen and water molecules oxidize the coal and produce a gaseous mixture of carbon dioxide (CO_2), carbon monoxide (CO), water vapor (H_2O), and molecular hydrogen (H_2). The desired end product is usually syngas, but the produced coal gas may also be further refined to produce additional quantities of H_2:

$$3C + O_2 + H_2O \rightarrow H_2 + 3CO \tag{43}$$

Several technologies for coal gasification exist, but they all employ the same chemical processes.

For low-grade coals which contain significant amounts of water, are used technologies which do not employ the use of steam with coal and oxygen being the only reactants. As well, some coal gasification technologies do not require high pressures, some other utilize pulverized coal as fuel while others work with relatively large fractions of coal [27].

Steam reforming

The most mature technology to produce hydrogen involves the steam methane reforming (SMR). The reaction is represented by this equilibrium:

$$CH_4 + H_2O \leftrightarrow 3\,H_2 + CO \qquad \Delta\hat{h}_0 = +206 kJ/mol \tag{44}$$

A metal catalyst is usually used to favor the reactions between methane and steam, producing syngas which is a mixture of H_2 and CO [8]. Through this reaction, one molecule of methane and one of water are useful to obtain three molecules of hydrogen, and only one of carbon monoxide is obtained. This reaction is strongly endothermic, so it need energy to be activated,

generally, in a polygenerative plant, this kind of reactions are used as thermal sink to reduce the heat dissipated. Furthermore, it has been seen that the high temperatures shift the equilibrium towards the products, and specifically at 800 °C SMR is considered complete.

Furthermore, to increase the amount of hydrogen, the Water Gas shift reaction can be performed:

$$CO+H_2O \rightarrow H_2+CO_2 \qquad \hat{\Delta h_0} = -41 kJ/mol \qquad (45)$$

The reaction is thermodynamic characterized by a low exothermic behavior; hence a low amount of heat is produced during the process.

2.3 P2X pathways

Power-to-X (also P2X and P2Y) is a term used for a number of electricity conversion, energy storage, and reconversion pathways. Power-to-X schemes are particularly useful in energy systems with high shares of renewable generation and/or with strong decarbonization targets. The surplus of electric power coming from renewable energy is used, generally wind and solar.

The term "X" stands for the kind of energy into which the electricity is converted: these are usually gases, liquid or heat. Indeed, the "X" can stand for: power-to-ammonia, power-to-hydrogen, power-to-gas, power-to-liquid, power-to-power, and more.

These schemes allow the use of power production from energy sector in other sectors such as transport or chemicals.

The production of electricity from wind and solar technologies are strongly affected by meteorological conditions and seasonal imbalances, so it is required a large-scale energy storage to compensate for the intermittent production. The excess of electricity can be converted trough one of the Power-to-X pathways [28]. Hydrogen can be used to enable large-scale integration of renewables into the power generation network: both as means of distributing energy across sectors and as a storage buffer. As seen in section 2.3.2, hydrogen can be produced in several ways: this is why hydrogen is seen as the ideal energy carrier. One of the main targets of the Power-to-X concept is to use the excess renewable electricity production to split water into hydrogen and oxygen thorough an electrolyzer.

In the electrolyzers, direct current can be used to produce hydrogen which can be converted to methane via methanation. Another possibility is converting hydrogen and carbon dioxide to methanol. Both these fuels can be stored and used to produce electricity again, hours to months later.

Power-to-X concepts also offer an opportunity to reduce GHG emissions in heavy transportation vehicles, ships and air traffic. For instance, synthetic kerosene obtained using electricity from renewables is currently the only fuel enabling climate-neutral flight. Linking traditionally separated sectors of the energy system like electricity, gas, heat and transport, can raise energy efficiency and lower network investment costs.

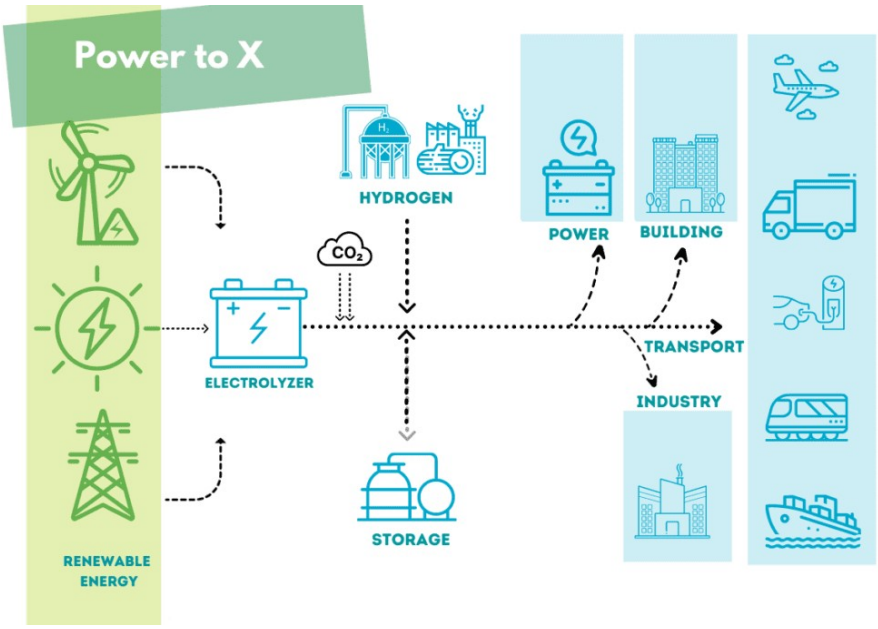

Figure 16 – Scheme of P2X pathways [29]

2.4.1 Power-to-Gas (P2G)

Power-to-gas is often considered the most promising technology for seasonal renewable energy storage. The P2G scheme can provide significant amounts of hydrogen or synthetic methane utilizing excess electrical power from renewables to produce a gas fuel. Hydrogen is produced by electrolysis, and it can be directly used or further converted to syngas, methane or liquefied petroleum gas (LPG). The obtained gases can either be used as fuels or re-converted back into electricity when it is needed.

There are currently three different electrolysis technologies that are considered commercially mature and they are based on: alkaline electrolyzers (AEL), polymer electrolyte membrane electrolyzers (PEM) and solid oxide electrolyzers (SOEC). Solid oxide electrolysis is the newest technology. An advantage of this technology is its reversible operation, which in P2G systems could be used to "return" electricity to the grid when needed.

Thermochemical methanation is a catalytic process that takes place between 250 and 550 °C and high pressures. The reaction is strongly exothermic, so the temperature control is a complex aspect; nonetheless the exothermicity of the reaction allows to have as by-product an amount of heat, which can be used in industrial processes or in solutions like local district heating network or greenhouses.

A second option for CO_2 hydrogenation is biological methanation, in which methanogenic microorganisms act as biocatalysts, at temperatures between 20 and 70 °C and at pressures higher than atmospheric pressure.

One of the greatest aspects of P2G is the decarbonization of the energy production, the possibility of long-term storage, the possibility to transport and distribute energy over long distances. Indeed, the technologies involved in P2G schemes allow the storage of electricity in 100% renewable energy carriers, with the possibility to use existent infrastructures such as the gas grid.

Naturally, there are still some drawbacks that prevent a strong access and use of these technologies. Some of them are strictly related to the state of the art, such as the development of electrolyzers efficiently operating in highly dynamic regimes, the optimization of heat recovery in the catalytic methanator, the reduction of volumes in biological methanators. Some others are purely economic. The cost of gas obtained from hydrogen is much higher than the one of the gas obtained by fossil fuels. In this area, the role of governance, research and industrial stakeholders and their synergistic involvement will be crucial [30].

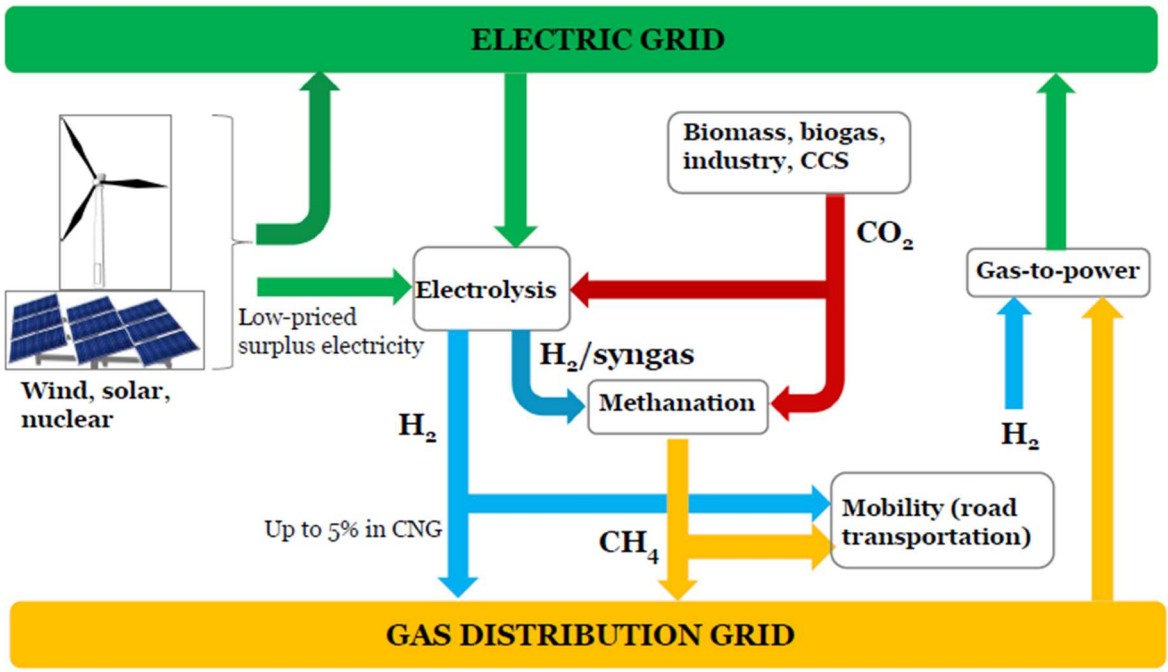

Figure 17 – P2G scheme [31]

2.4.2 Power-to-Liquid (P2L)

Among P2L schemes, there are two main production pathways, the Fischer-Tropsch (FT) pathway and the methanol (MeOH) pathway. The energy efficiency of the two pathways are about the same. Both pathways are highly sensitive regarding how well waste heat from syntheses can be recuperated and used in, e.g., electrolysis or CO_2 provision [32]. The P2L allows the conversion of electricity coming from renewable energy into liquid fuels and chemicals like methanol, oxymethylene ether (OME), ammonia, and Fischer-Tropsch (FT) products.

Wind and solar power are used to produce hydrogen via electrolysis. Liquid hydrocarbons are produced hydrogen and carbon dioxide, then are further refined to obtain specific liquid fuels. These liquids have a surprisingly high energy density making them optimal for aircraft, ships and other applications with a high-power demand and the need to serve long distances. This type of fuels is easier to store and transport than pure hydrogen and can be used as feedstock in industry.

Furthermore, there is the possibility to produce “drop-in” fuels that are compatible with the existing infrastructure, through the usage of advanced thermochemical catalytic processes [33].

The environmental benefits of P2L are evident: greenhouse gas emissions can be made near carbon-neutral when using electricity coming from RES and CO_2 from biomass sources or directly from the air. Moreover, P2L water demand is almost negligible and land requirements are much lower compared to biofuels. Being synthetic fuels, the P2L products offer improved combustion with less pollutants.

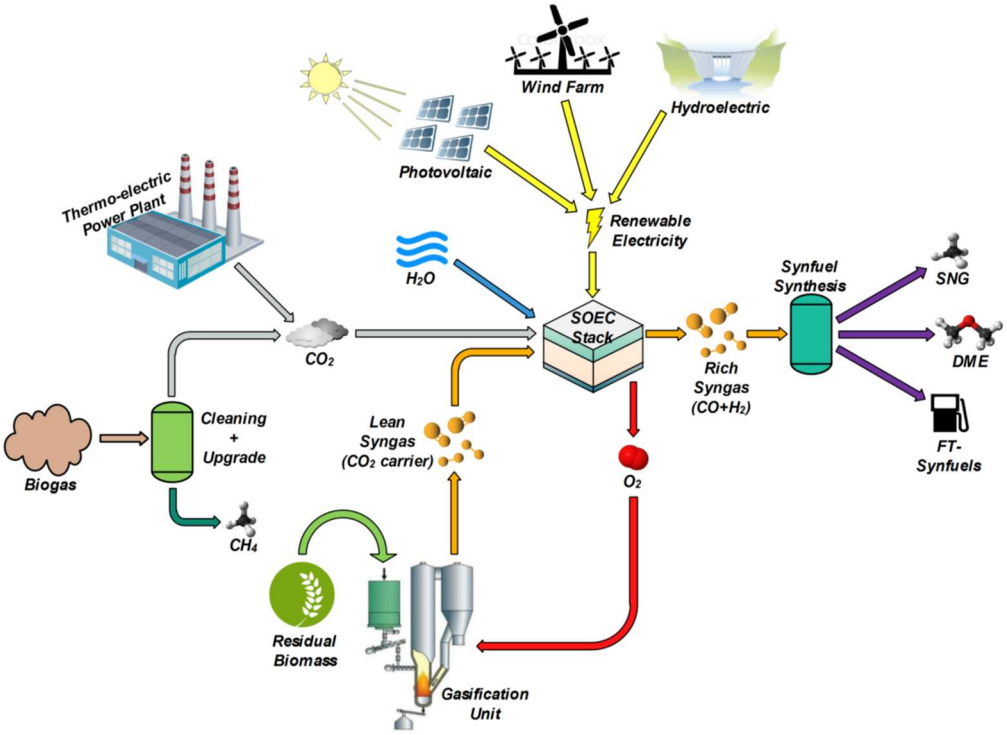

Figure 18 – P2L scheme [34]

3.Syntetic natural gas production: co-electrolysis and methanation

A potential advantage of SNG production through power-to-gas compared to hydrogen production that distribution infrastructure for natural gas already exists.

In this chapter, the thermodynamic aspects of reversible Solid Oxide Cells (rSOCs) and the currently used materials are analyzed more precisely, with particular attention to the stack configuration and its degradation. After that, the methanation process is exposed with particular attention to the various possible processes, their thermodynamics and the necessary components.

3.1 rSOC operating principles

The technology of reversible Solid Oxide Cell allows to exploit innovative processes that also give environmental benefits, since there is the possibility to direct use of polluting gases that would otherwise be released into the atmosphere, foremost the carbon dioxide.
The most relevant feature of such technology is the flexibility of the operation. The system can work in both electrolysis mode, named SOEC, or in fuel cell mode, named SOFC. Although fuel cells are currently the primary application- to generate electrical power consuming fuel- rSOCs operating in SOEC mode produce fuel from reactant species such as H_2O and CO_2 with an input of electrical power [35]. Accordingly to this duality, rSOCs are seen as a technology capable of providing highly efficient and cost-effective EES: power is produced in SOFC mode, while fuel is produced (or stored to be further re-converted in power) through the SOEC mode.

This type of cell, as already explained in section 2.2.3, operates at high temperatures, and it is made up of a membrane electrode assembly (MEA) comprising a laminated fuel electrode, a solid electrolyte, and an oxygen electrode. The rSOC stack is comprised of many single cells in series.

In SOFC mode, oxygen from air is used for the oxidation reactions; while in SOEC mode, air acts as a sweep gas to reduce the partial pressure of the generated oxygen from the reduction of steam/CO_2, so as to increase the efficiency of fuel production [36].

In the system depicted in fig. 19, the fuel and the products can be clearly seen:

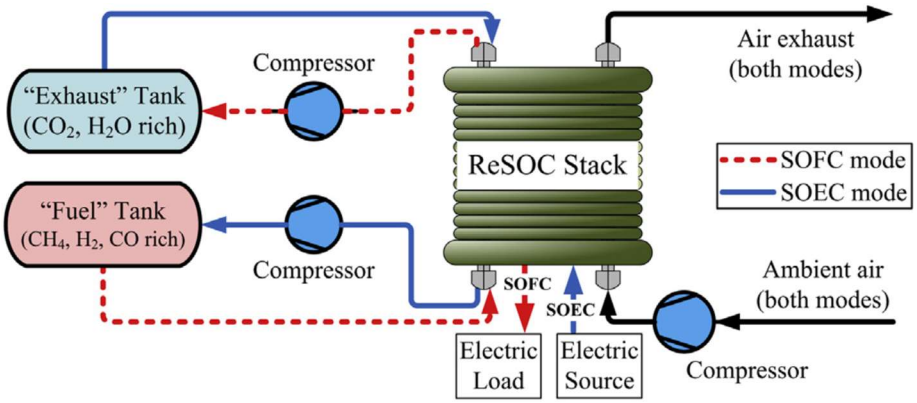

Figure 19 – Simplified scheme of a stand-alone energy storage system utilizing rSOC [36]

The equilibrium reactions that occur in SOFC are the opposite ones occurring in SOEC, so an important and challenging aspect is the thermal management of the system.
Indeed, while the hydrogen oxidation that take place in SOFC is exothermic, the steam and/or carbon dioxide reduction are endothermic: under typical operation the SOFC mode requires excess heat rejection while SOEC mode requires heat supply to maintain the desired operating temperature.

In this present work of thesis, a SOEC system and a methanation section are considered: methanation reaction, being exothermic, can overcome the endothermic co-electrolysis reactions. In this way, the process can operate more efficiently without the need to generate extensive quantities of resistive waste heat. This aspect will be analyzed more in deep in section 6.2 where thermal integration of the systems is treated.
Equilibrium calculations suggest that operating the rSOC stack at an intermediate temperature of about 600 °C or elevated pressure performs sufficient methane formation allowing an efficient thermal self-sustainability of the cell in SOEC mode operation [37].

Pressurized operation of solid-oxide cells is important because it promotes methane formation in SOEC mode. It is proved that pressurization has also the capacity to increase cell electrical efficiency as well as to improve system efficiency when coupled with other system processes [38].

The ability to simultaneously electrolyze steam and CO_2 to produce syngas (i.e., co-electrolysis) allows efficient generation of feedstocks for synthetic natural gas.

3.2 Physics of SOEC

In co-electrolysis, in addition to steam reduction at cathode $2H_2O(l) + 4e^- \rightarrow 2H_2(g) + 2O_2^-(g)$ and oxidation at the anode $2O_2^-(g) \rightarrow O_2(g) + 4e^-$ (see section 2.2.3), the reduction of carbon dioxide takes place at cathode side:

$$2CO_2 + 4e^- \rightarrow 2CO + 2O_2^- \quad (46)$$

Besides these electrochemical reactions, in co-electrolysis also chemical reactions take place. Firstly, water gas shift (WGS) reaction plays an important role. The WGS equilibrium can be written as:

$$H_2O(g) + CO(g) \leftrightarrow H_2(g) + CO_2(g) \qquad \Delta\hat{h}_0 = -41\ kJ/mol \quad (47)$$

It is proved that at high operation temperatures, like the SOEC operation one, WGS is kinetically fast and will quickly reach equilibrium throughout Ni-YSZ electrode. As reported in literature, the amount of water and carbon dioxide electrochemically reduced in SOEC is not clearly understood because of simultaneous catalytic reactions occurring within the cathode electrode. [39]

If occurs that the concentration of CO is high enough, it may be further electrolyzed to solid carbon:

$$CO(g) \rightarrow C(s) + \frac{1}{2}O_2 \quad (48)$$

However, under normal SOEC operating conditions, where both hydrogen and carbon dioxide are present in the cathode gas, this reaction will not be critical.
For pressurized SOEC or in SOEC working with high conversion, methanation reactions may take place:

$$CO(g) + 3H_2(g) \rightarrow CH_4(g) + H_2O(g) \qquad \Delta\hat{h}_0 = -206\ kJ/mol \quad (49)$$

$$CO_2(g) + 4H_2(g) \rightarrow CH_4(g) + 2H_2O(g) \qquad \Delta\hat{h}_0 = -165\ kJ/mol \quad (50)$$

These reactions are highly exothermic, and they are not thermodynamically promoted at high temperatures, while, as already stated, high pressure favors them.
In the same conditions, also Boudouard reactions may take place:

$$CO(g) + H_2(g) \rightarrow C(s) + H_2O(g) \qquad \Delta\hat{h}_0 = -206\ kJ/mol \quad (51)$$

$$2CO(g) \rightarrow C(s) + CO_2(g) \qquad \Delta\hat{h}_0 = -172\ kJ/mol \quad (52)$$

These reactions may be responsible for carbon deposition in Ni-YSZ electrode. Ni is also a good catalyst for carbon deposition.
Carbon deposition represents a potential issue as solid carbon deposits on Ni, reducing the catalytic area, and so decreasing the ability of the cell to realize electrochemical reduction. Furthermore, solid carbon can also occlude pores, blocking the flow of reagents through the porous medium, since mass transport resistance in the gas diffusion electrode increases. Its formation depends on many factors including temperature, pressure, and mixture composition. It is important to fix a utilization parameter (i.e., fuel utilization or reactant utilization) which quantifies the fraction of reactant delivered to the stack that is electrochemically converted. Carbon formation probability increases with pressure (because of equilibrium issues) and reactant utilization RU.

In the next figure, it is possible to see, for RU from 50% to 80% compositions such that the carbon deposition risk is avoided.

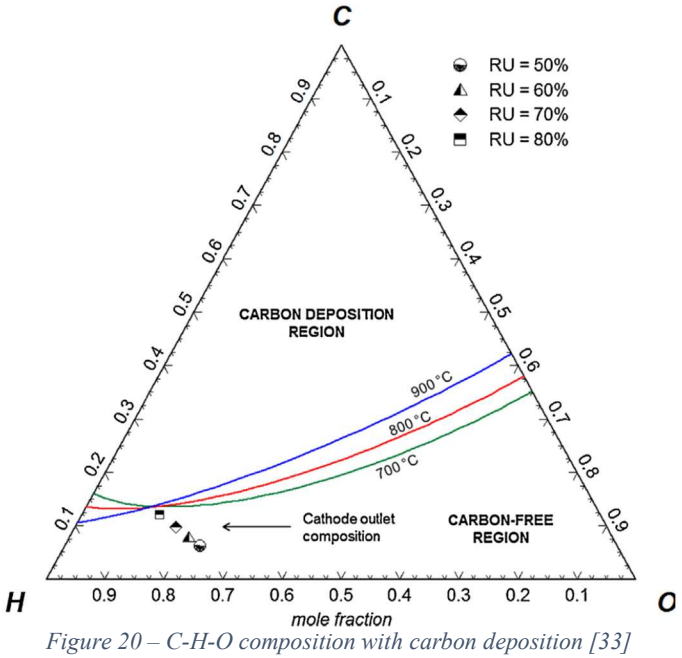

Figure 20 – C-H-O composition with carbon deposition [33]

The possible compositions are bounded by the fully oxidized region and carbon deposition region and the boundary is determined by equilibrium calculations.
The choice of the inlet composition of the gas is done to mitigate carbon deposition and to allow high fuel energy density. Generally, the working hydrogen-to-carbon ratio in the composition is quite low.

3.3 Design of SOEC

In the following section a focus on the state of the art of the materials used in SOEC is presented. Moving on, the stack configuration as well as its degradation is analyzed.

Electrolyte

Generally, the electrolyte material is formed by doping zirconia (ZrO_2) with 8% mol of yttria (yttrium oxide, Y_2O_3). This percentage of yttria produces a "fully stabilized" electrolyte. Zirconia dioxide is used because of its high mechanical strength, high melting temperature (approximately 2700 °C) and very good corrosion resistance. Y_2O_3 is used to mitigate the phase transition from the tetragonal to the monoclinic phase on rapid cooling, which can lead to cracks [40]. Zirconia doped with yttria is called Yttria stabilized zirconia (YSZ).

The dopant purposes are mainly two:

- It "stabilizes" the cubic crystal structure over a wide range of temperatures: indeed, undoped zirconia exhibits a monoclinic crystal structure at room temperature and a tetragonal phase above 1170°C.
- The substitution of trivalent Y instead of tetravalent Zr forms holes (unfilled positions) in the oxygen sub-lattice: oxygen ions can move through the solid by occupying successive holes in the lattice. YSZ is therefore, a good oxygen ion conductor [16].

Other type of materials that are used are Scandia stabilized zirconia (ScSZ), ceria based electrolytes or lanthanum gallate materials. Scandia-Stabilized zirconia has a higher ionic conductivity than YSZ, but is more expensive. Electrolytes made of ceria are the most promising for intermediate temperature SOFC. Cerium oxide is usually doped with (GDC) or (SDC).

In general, the material used for SOEC are very similar to the ones used for SOFC, but the different operating conditions lead to issues such as high steam concentrations at the fuel electrode and high oxygen partial pressures at the electrolyte/oxygen electrode interface. A recent study found that periodic cycling a cell between electrolyzer and fuel cell modes reduced the oxygen partial pressure build up and increased the lifetime of the electrolyzer cell [41].

Steam-Hydrogen Electrode

Nowadays, the most used material for the cathode is porous nickel-zirconia (Ni-YSZ) cermet. During the cell operation, reducing atmosphere need to be maintained, since the cathode contains nickel metal which acts as an electronic conductor and also as a catalyst for steam reduction. Reducing conditions are typically guaranteed by including around 10% or higher mole fraction hydrogen in the inlet flow. Zirconia provides ionic conductivity. Porosity of the electrode makes possible the migration of steam to the active electrochemical reaction sites and allows hydrogen to migrate away from those sites. The active reaction sites correspond to what is typically termed the triple-phase boundary (TPB) where the electronic, ionic, and gas phases coexist.

New materials are being researched such as lanthanum strontium manganese chromate (LSCM), which has proven to be more stable under electrolysis conditions.

Oxygen Electrode

The oxygen electrode, which is the anode in SOEC mode, must operate in a highly oxidizing environment. The most used material is the strontium-doped lanthanum manganite (or LSM). As it generates oxygen vacancies under anodic polarization, it offers high performance in electrolysis mode of operation, enhancing oxygen diffusion. Recent studies underlined the important role of Gd-doped CeO_2 (GDC): impregnating LSM electrode with them was found to increase cell lifetime.

Alternative materials like composite electrodes of YSZ with lanthanum strontium ferrite (LSF), lanthanum strontium cobalt (LSCo), lanthanum strontium cobalt ferrite (LSCF), lanthanum strontium copper ferrite (LSCuF) are under studies, and they are probably more suitable for performances under 800 °C.

Stack configuration

Commonly, cell present dense gas-tight electrolyte layer, with porous electrodes on both sides. In an electrolyte-supported cell, the electrolyte layer is thicker than both anode and cathode and must have sufficient mechanical strength to withstand any stresses. However, the increased thickness of the electrolyte leads to higher ionic resistance. The best performing SOFC cells at present are the anode-supported ones (cathode-supported in case of SOEC). In this layout the mechanical strength is provided by a thick layer of anode (cathode) material.
In the SOEC mode, air-electrode-supported cells should exhibit a lower concentration polarization than steam-hydrogen-electrode supported cells, due to the direction of steam and oxygen diffusion in the two modes.

In fig.21 is shown a stack cell: the flow fields conduct electrical current through the stack and provide flow passages for gas streams.
The bipolar plate separates the process gas streams. It is usually metallic since it must be electrically conducting and acts as current distributors. Each interconnect includes an impermeable separator plate with edge rails and two corrugated "flow fields", one on the anode side and one on the cathode side.

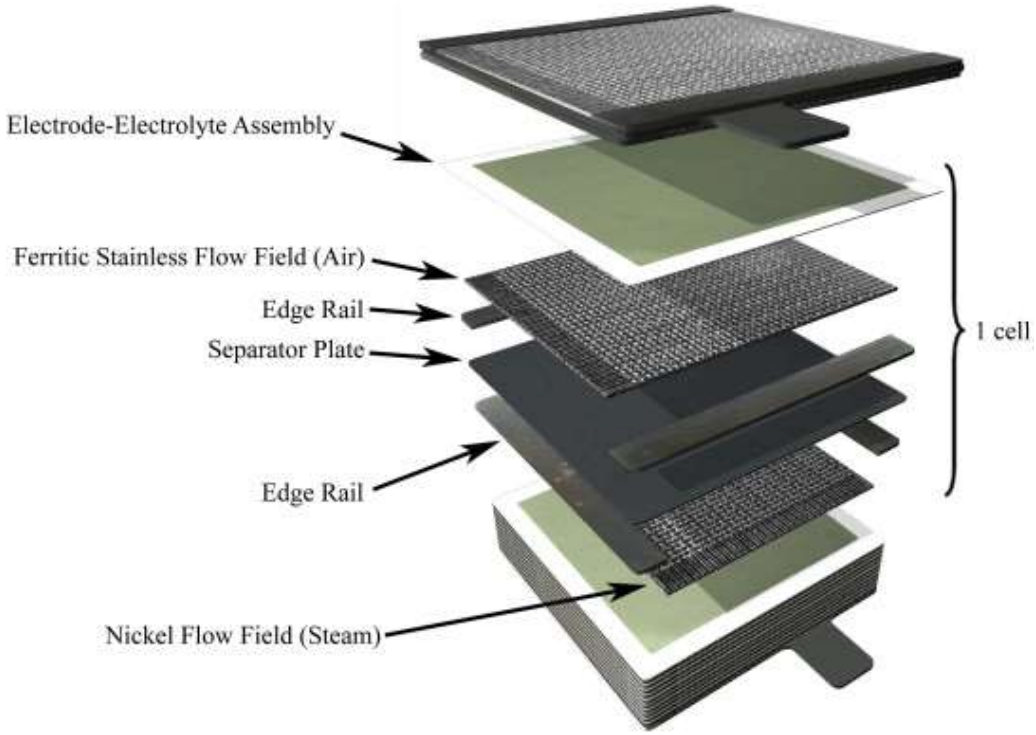

Figure 21 – Stack stratification [42]

Degradation

It is still not clear which is the main cause of degradation in rSOCs. It is confirmed that degradation mechanisms in a stack are not identical to those in a single cell as well as degradation in an SOEC is not identical to that in an SOFC. Long-term tests run on single cells show that SOEC operation generally exhibits greater degradation rates than SOFC operation. Therefore, SOFC degradation can be used for background information and guidance.
Moreover, some researchers have observed that higher operating temperatures increase degradation rates in SOECs, but higher current density does not increase degradation.

A common degradation mechanism between the SOFC and SOEC modes of operation is chromium poisoning originating either from interconnects or from balance-of-plant piping: volatile chrome oxide may deposit at the electrode–electrolyte interface or TPB. This deposition can bring to deactivation of electrochemical reaction sites and/or separation of the bond layer from the oxygen electrode.

Interconnects can also be a source of serious degradation as they segregate and build-up at interfaces:

- Sr segregates to the interconnect–bond layer interface;

- Mn segregates to the interconnect surface;
- Si and Ti segregate to the interconnect–passivation layer interface.

3.4 Principles of methanation

Now the technology of methanation, which allows to convert a generic syngas - a mixture of hydrogen and carbon monoxide - into Synthetic Natural Gas (SNG) is presented.

The principle of catalytic synthetic production of methane from carbon monoxide and hydrogen was discovered by Sabatier and Senderens.
The reactions of CO methanation and CO_2 methanation have already been introduced in the previous section as the can develop into pressurized SOECs:

$$CO + 3H_2 \rightarrow CH_4(s) + H_2O \quad (48)$$

$$CO2 + 4H_2 \rightarrow CH_4(s) + 2H_2O \quad (49)$$

Both reactions are linked by eq.44, the water gas shift conversion, which is always observed simultaneously whenever active catalysts are used. It has been observed that the whole transformation of carbon dioxide into methane starts with a reverse shift conversion reaction with hydrogen to obtain steam and carbon monoxide which is subsequently transformed into methane.

$$CO + H_2O \rightarrow CO_2(s) + H_2 \quad (44)$$

Methanation reactor technologies can be classified into three categories: fixed bed, fluidized bed and other types of reactors.

In the next section TREMP™ ("Topsøe Recycle Energy-efficient Methanation Process") process will be analyzed. This process will be then modeled coupled to SOEC.

3.5 TREMP™ process description

In fig.22, a block diagram of the SNG plant is depicted. The feedstock is initially gasified in the presence of O_2 and H_2O. Three different types of gasifiers can be employed for SNG generation: fixed beds, fluid beds and entrained-flow gasifiers. After being cooled, the gas is cleaned from tars, salts and dust. The WGS reaction that occurs un the sour shifts adjusts the H_2/CO ratio. The syngas exiting the sour shift is rich in sulphur (H_2S) and CO_2. Being the sulphur an inhibitor for the methanation catalyst it must be removed. The CO_2, as well, has to be removed in order to reach the right hydrogen to carbon ratio. Their removal is performed in the acid gas removal (AGR) unit.

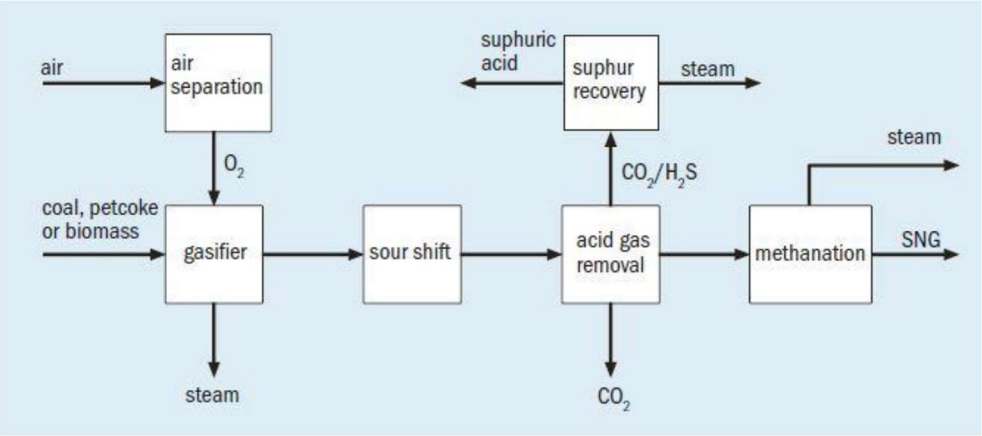

Figure 22 – Block diagram with major units of a "Solid fuel to SNG" plant [43]

As already stated, the methanation reactions are strongly exothermic: as an example, if the resulting gas mixture enters an adiabatic methanation reactor at a temperature of 300 °C, after the reaction, it will exit at a temperature of around 900 °C. The adiabatic temperature increase requires a high-temperature stable catalyst that must have also a high activity at low temperatures.

In order to obtain at the end of the methanation step a product with more than 95% of methane, the methanation process has to be performed in more step, so more adiabatic reactors working at decreasing temperature levels and split by intermediate cooling. The exact number of reactors is chosen considering a trade-off between requirements of product gas quality and heat recovery.

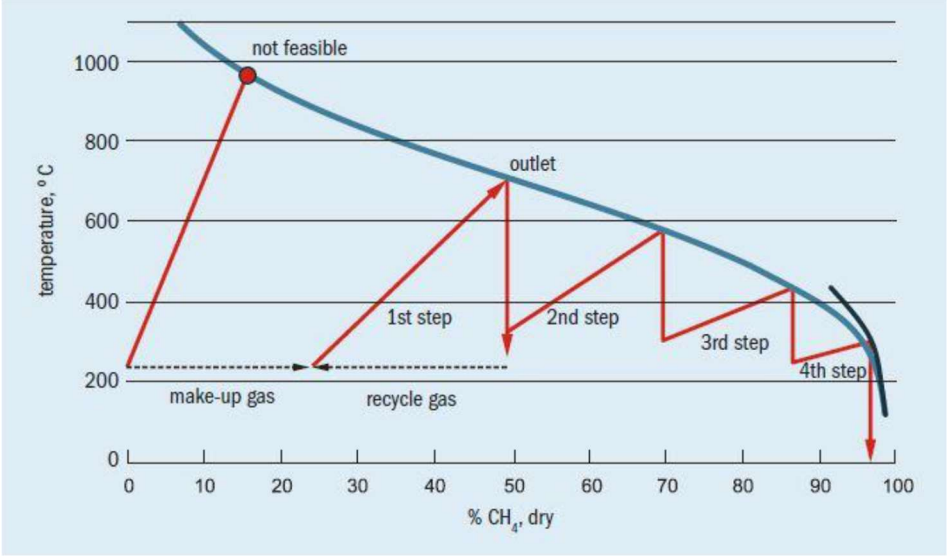

Figure 23 – Equilibrium curve for methanation process at a specific pressure [44]

In fig.24 a representation of the TREMP™ methanation process is shown. Based on the limitations and opportunities mentioned, TREMP™ works in the following way.

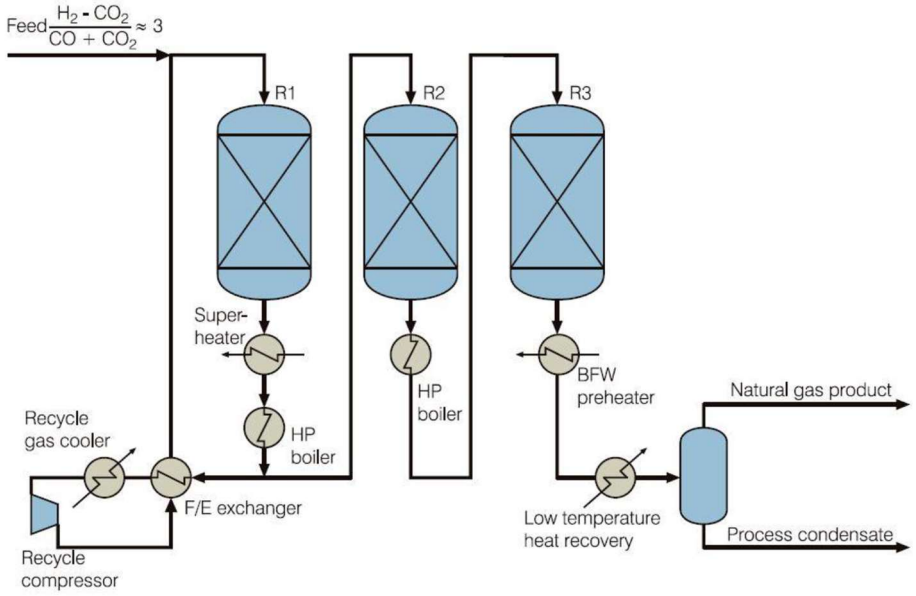

Figure 24 – Example of TREMPTM methanation plant [40]

Initially, the feed runs through a sulphur guard bed in which the sulphur traces that have not been removed by the AGR unit are taken off. The feed is mixed with recycled gas for temperature control and then is passed to the first methanation reactor. The mixture exiting has high outlet temperature, the reaction heat can be recovered for generation of superheated high-pressure steam in the downstream heat exchangers or for plant thermal integration, as is described in section 6.2. The partially methanated syngas, after being cooled down, is sent to other methanation reactors, which are separated each other by coolers. The methanation reactors to obtain a complete conversion of CO and/or CO_2 into methane are generally three or four; the number will depend on parameters like pressure, as well as the SNG product specification.

If the reactors are four or more, usually, before the last methanation step, the water generated in upstream methanation steps is removed in order to push the equilibrium further towards methane production [44].

The mixture exiting the last reactor is cooled and dried, If the feed is directly sent to the gas network, it is "corrected" to meet the pipeline specifications or LNG production requirements.

The methanation reaction is favored by high pressure and works well with syngas from all types of coal or biomass gasifiers.

<u>The feed gas module</u>

Having an inlet composition with the correct ratio between the reactants, i.e. CO, H_2 and CO_2, is fundamental to achieve a product with as high methane content as possible.

The prevailing methanation reaction is usually the methanation from CO, in which the stoichiometric ratio between H_2 and CO is 3.

To consider the content of CO_2 in the feed gas for the methanation, the "feed gas module" has been introduced:

$$FEED = \frac{[H_2]-[CO_2]}{[CO]+[CO_2]} = 3$$

Since this ratio is defined from a stoichiometric value for the methanation reactions, it will be unchanged throughout the methanation section. However, because the methanation section

"amplifies" the phase shift in modulus, a small change in the ratio of reactants in the feed gas results in a large change in the composition of the product SNG [44].

Module control

The value of the module is controlled by varying the by-pass of the sour shift unit: when it is increased, less CO and water are converted into H2 and CO_2 through the water gas shift reaction. Being the CO_2 removed downstream in the AGR at an almost constant level, the module will decrease when the sour shift by-pass is increased.

Heat integration

The high temperature waste heat at the exit of the reactors can be used to produce superheated steam at high pressure which can be exploited into steam turbines.

Heat exchangers dealing with superheated steam are exposed to high pressure on one side and to a particular chemical composition on the other, where metal dusting could verify. This corrosion phenomenon takes place in atmospheres with high CO partial pressure and metal temperatures typically in the range of 450-650°C. Both in the waste heat boilers and in the steam superheaters, parts of the metal surfaces are subjected to this temperature range, so it is fundamental to design them in order to better respond to this phenomenon. Actually, for what concerns the waste heat boilers, the problem is narrowed as the areas exposed to temperatures in the critical range will be limited due to the fact that the boiling water is characterized by a high heat transfer coefficient. For the steam superheater, on the other hand, the potential of metal dusting increases as a significant part of the metal surface exposed to process gas will be in the critical range of temperatures.

Product quality

The concentration of the inerts in the feed will be quadrupled in the SNG product because of the molar reduction by the methanation reaction, while most of the carbon dioxide will be converted to methane.

Generally, the SNG produced by TREMP™ coupled with gasification of solid fuels is composed by methane (94-98%), hydrogen (0,05-2%), carbon dioxide (0,2-2%), carbon monoxide (<100 ppm), Nitrogen and Argon (2-3%). This SNG is characterized by a Higher Heating Value (HHV) around 37380-38370 KJ/Nm^3 [43].

4.Experimental analysis

In this chapter are reported the experimental procedure and results of several tests made on commercial Solid Oxide Cells (electrolyte-supported, 5cm x 5 cm cell) both in SOFC and SOEC mode at the Environment Park in Turin. Before going in details with the experiment, the components of the test bench as well as the experimental setup will be briefly described. For both SOFC and SOEC mode of operation, different types of feed are used. The SOEC performs both electrolysis and co-electrolysis.

4.1 Test bench description

The solid oxide cells characterization needs a proper testing environment, which is mainly composed by:

- Gas distribution lines;
- Mass flow controllers;
- Water distribution line;
- Water evaporator;
- Oven;
- Electronic auxiliaries for the oven and for the cell;
- Data acquisition and control system;
- Instrument for the electrical characterization of the cells.

4.1.1Gas distribution lines

They allow the flow of gases used in the experiment, such as CH_4, CO_2, H_2, CO_2, N_2 and air. For safety reason the gas cylinders are placed outside the laboratory. A pressure reducer is present between the laboratory's distribution line and the test-bench lines.

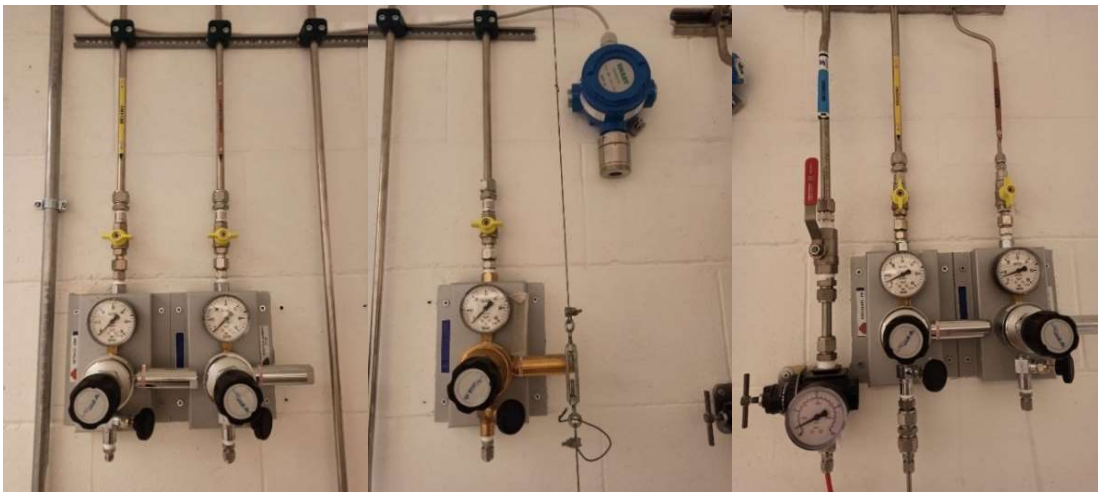

Figure 25 – Focus on gas distribution lines, test bench side

4.1.2 Mass flow controllers (MFCs)

They measure and control the mass flow rates in order to send the desired quantities of gases. In the test bench, there are nine MFCs used to control the flows of H_2, CH_4, CO, CO_2, N_2 and one which controls the air entering the cathode in SOFC mode. Upstream and downstream of each MFC there are two manually controlled valve.

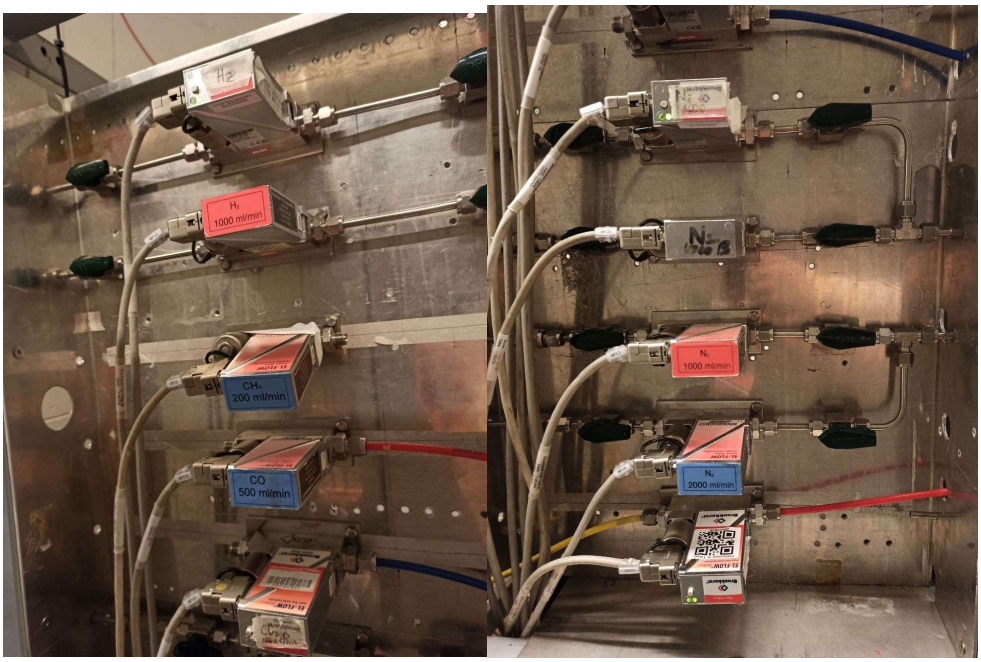

Figure 26 – Focus on mass flow controllers

4.1.3 Water evaporator

The controlled evaporator mixer enables the humidification of the gas that enters the cell. The CEM is made up of three main components: a mixing valve, a mixing chamber and a heater. It is integrated with a liquid flow meter and with the gas line, by means of a three-way valve.

The obtained humidified gas leaves the CEM from the bottom path of the evaporator. The temperature of the evaporator chamber is controlled by means of a heater with an integrated temperature sensor. The set-point temperature of the evaporator is modified by the user through the control software of the test bench.

It's recommended to install the CEM on a rigid structure, which is not influenced from mechanical vibrations and heat sources.

Figure 27 – Controlled evaporator mixer

The setpoint temperature of the heater is calculated through the software *FLUIDAT® on the Net* which is implemented by the producer Bronkhorst®.
It needs as inputs variables the liquid and gas flow rates, giving as a result the temperature needed to evaporate the liquid and to prevent vapor condensation at the outlet of the heater. The software interface is depicted in the following image:

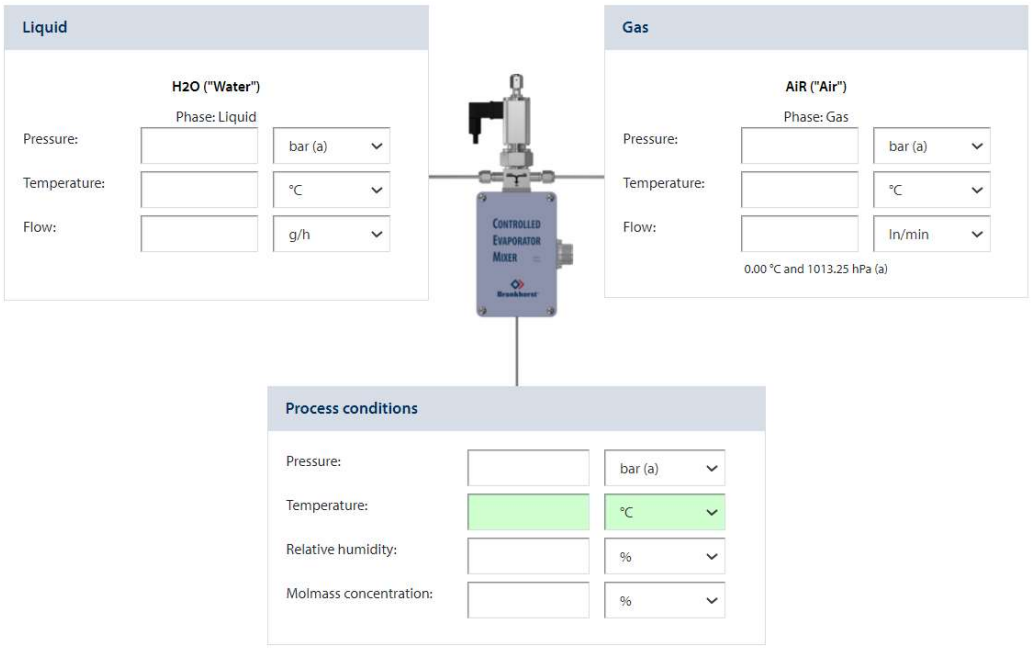

Figure 28 – Layout of FLUIDAT®

4.1.4 Oven

The oven hosts the cell, enabling and maintaining the desired temperature.

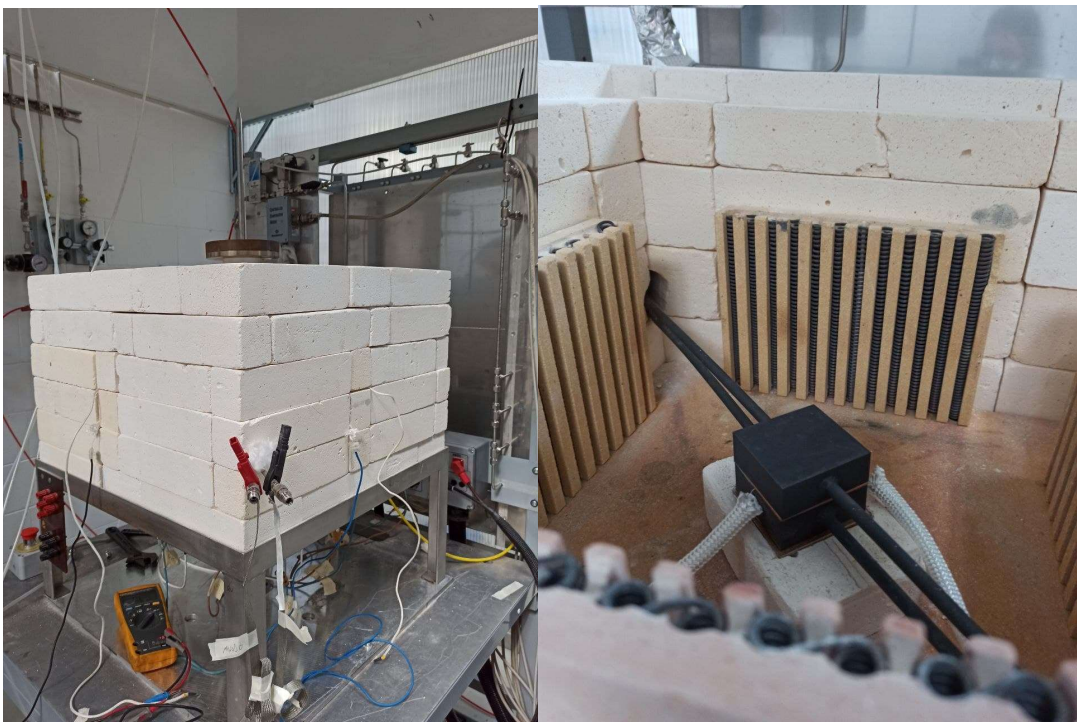

Figure 29 – Oven: external view (left), internal view (right)

In the oven, temperature is maintained at a fixed set-point during the whole experiment, by compensating for heat losses towards the external environment. The external structure of the oven is made up of movable refractory bricks and by four electrical resistors, placed at the four sides of the oven. The heating elements are fed by a dedicated power-supply, connected to a PID system that allows the control of the temperature of the oven using as process variable the temperature measured by a thermocouple inside one of the heating elements. The PID is integrated in the test-bench control system. Inside each resistor there is a thermocouple which is installed to keep track of the temperature during experiments with ceramic coating. Indeed, inside the oven, temperature is not uniform and so the temperature gradient must be taken into account. Temperature detected by the thermocouples placed inside the resistances is higher than the central one. The bricks of the oven have proper holes to allow the crossing of thermocouples and electrical connections.

4.1.5 Electronic auxiliaries for the oven and for the cell

The test bench under analysis is provided with two electronic auxiliaries: one for the oven resistances and one for the cell itself. In particular:

- The power supply dedicated to the oven sends a DC current to the electric resistances inside it. These components are connected in parallel with respect to the power supply;
- The electronic load for the cell is coupled with a compensation power supply, which amplifies the signal of the voltage cell, as it is very low. [45]

4.1.6 Data acquisition and control system

The test bench can be almost completely operated in remote. Through the Teachy software, in fact, tests and characterizations of the fuel cell can be performed. The devices just explained

can be operated and controlled through the software. Clearly, this is made possible by a proper data acquisition and control system.
Naturally, a local control is possible too, thanks to manually controlled terminals. The cabinet for the readout and for the control is depicted in the following image:

Figure 30 – Local control cabinet

The Eurotherm unit allows to manually impose set point temperature and ramp; the section dedicated to the MFCs allows the control and the readout of them; also the electronic auxiliaries can be locally controlled.
Furthermore, a manual switch allows to change from SOFC to SOEC operation mode, which is not possible through remote operation. It is also possible to put the test bench in emergency mode, switch it off or reset it.

4.2 Experimental setup

In this section, the procedure that has to be followed for the preparation of the test bench is explained.

4.2.1 Cell loading

The cell loading is obtained through the following steps:

1. The anode manifold is placed inside the furnace. A gasket is placed on the collector covering its perimeter;

2. A nickel grid is placed over the remaining area of the collector, sized such that it doesn't obstruct the gas flow ports;

3. A thin,platinum wire long enough to extend from the inside of the furnace to the outside is placed over the grid to allow for voltage monitoring. The portions of the wire not in contact with the cell are covered with insulation;

4. The cell is laid on the grid with the anode side facing down in contact with the platinum wire;

5. A second platinum wire is laid on the cathode side and pulled out of the furnace;

Figure 31 – Cell assembly

6. A silver grid is then placed on the cathode side of the cell and a new gasket is placed, making sure the two do not overlap;

7. The collector for the cathode is placed taking care that the anode and cathode tubes do not come in contact. Where necessary, insulation is placed between the two tubes;

8. The furnace is built covering all the cell structure and the four resistors on the four sides through the refractory bricks.

Figure 32 – Final setup

4.2.2 Cell conditioning

The furnace is programmed to heat up to 850°C. From room temperature to 300°C, with a temperature ramp of about 1°C/min and from 300°C to 850°C with a temperature ramp of about 0.5°C/min. The anode and cathode flows are increased to the desired flow rates for heating:

o Cathode: air @ 150 ml/min

o Anode: dry N2 @ 150 ml/min

4.2.3 Cell reduction

For reduction, the following steps are taken:

1. While maintaining 150 ml/min of N_2 on the anode, H_2 flow is increased to 50 ml/min.

2. The cathode air flow is increased to 250 ml/min.

3. The system is allowed to stand for 20-30 minutes or until the OCV begins to stabilize, whichever is longer.

4. Hydrogen is increased to 75 ml/min, after which the system is allowed to sit for another 10 minutes.

5. Transition the anode feed stream to 225 ml/min H_2 and 0 ml/min N_2 in 50 mil/min increments allowing the cell to sit at each condition for 5-10 minutes (or until the OCV begins to stabilize, whichever is longer).

6.Simultaneously, a flow of air up to 750 ml/min was sent in increments of equal duration to the previous ones.

7. Once the desired gas fluxes of 225 ml/min H_2 and 0 ml/min N_2 on the anode and 750 ml/min air on the cathode are achieved, the system is left at rest for 15 to 30 minutes to ensure steady state.

4.3 SOFC operation mode: setup and tests

In the following section, results from the experiments with the cell operating in SOFC are reported. The cell under analysis is an electrolyte-supported solid oxide planar cell produced by Nexceris with a size of 5 cm x 5 cm. The cell is made of a 150-micron thick Hionic™ scandium stabilized zirconia electrolyte support and state-of-the-art anode and cathode materials, the *NextCell* offers high performance over the temperature range of 750 to 850°C.

The complete Fuel Cell has the following specifications:

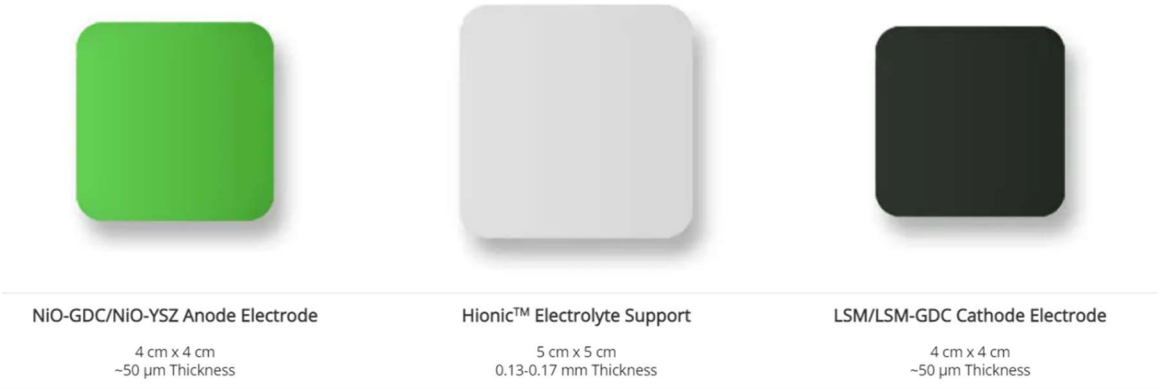

Figure 33 – Cell specifications [46]

Tests at two different temperatures are carried out: one at 800°C and one at 850 °C. For each temperature, different feed compositions are sent, and the polarization curves are reported. In the following table, all the compositions are depicted:

T, °C	Air, ml/min	N_2, ml/min	H_2 ml/min	H_2O ml/min
800	750	0	225	0
800	750	45	180	0
800	750	112,5	112,5	0
850	750	0	225	0
850	750	45	180	0
850	750	112,5	112,5	0
850	750	0	180	45
850	750	0	112,5	112,5

Table 4 – Feed compositions:SOFC

4.3.1 TEST 1: 800 °C

Once the set point temperature is reached, three different feed compositions are analyzed:

1. Air (MFC5) 750 ml/min, N_2 (MFC7) 0 ml/min (0%), H_2 (MFC1) 225 ml/min (100%):

I, A	V thin wires, V
0,0	1,086
0,2	0,998
0,4	0,907
0,6	0,822
0,8	0,733
1,0	0,65
1,2	0,572
1,4	0,494
1,6	0,418
1,8	0,344
2,0	0,272

Table 5 – Collection of data, feed composition 1

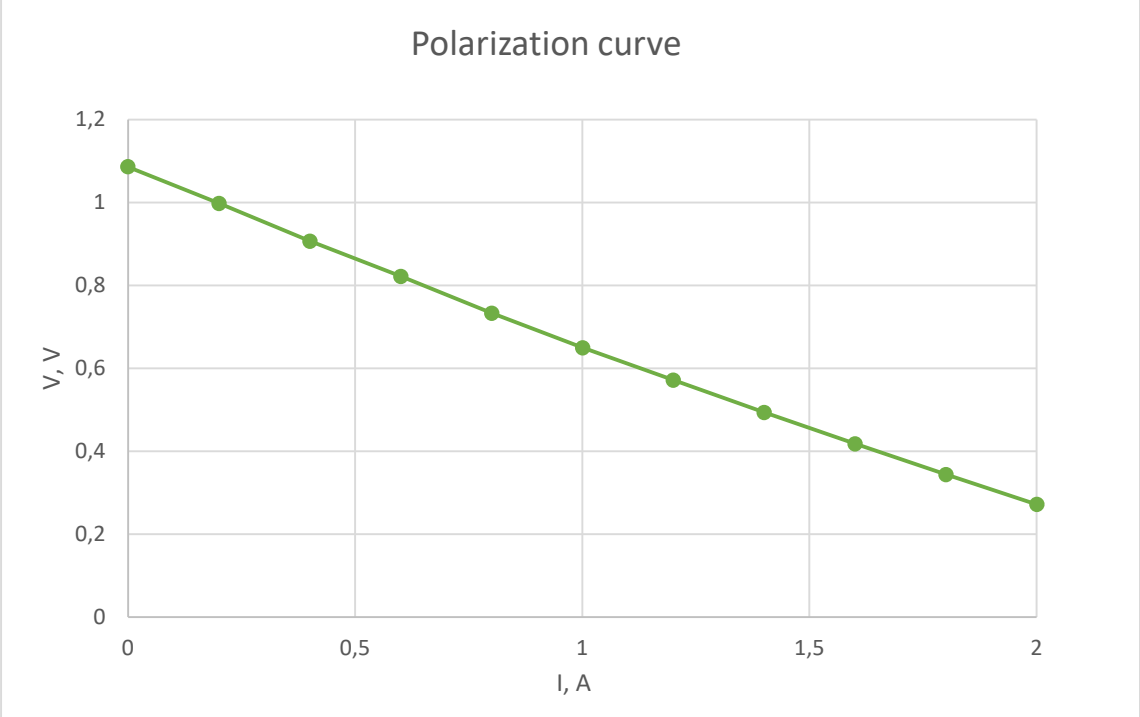

Figure 34 – Polarization curve, feed composition 1

2. Air (MFC5) 750 ml/min, N_2 (MFC7) 45 ml/min (20%), H_2 (MFC1) 180 ml/min (80%):

I, A	V thin wires, V
0,0	1,097
0,2	0,997
0,4	0,91
0,6	0,825
0,8	0,743
1,0	0,667
1,2	0,588
1,4	0,517
1,6	0,447
1,8	0,371
2,0	0,303

Table 6 – Collection of data, feed composition 2

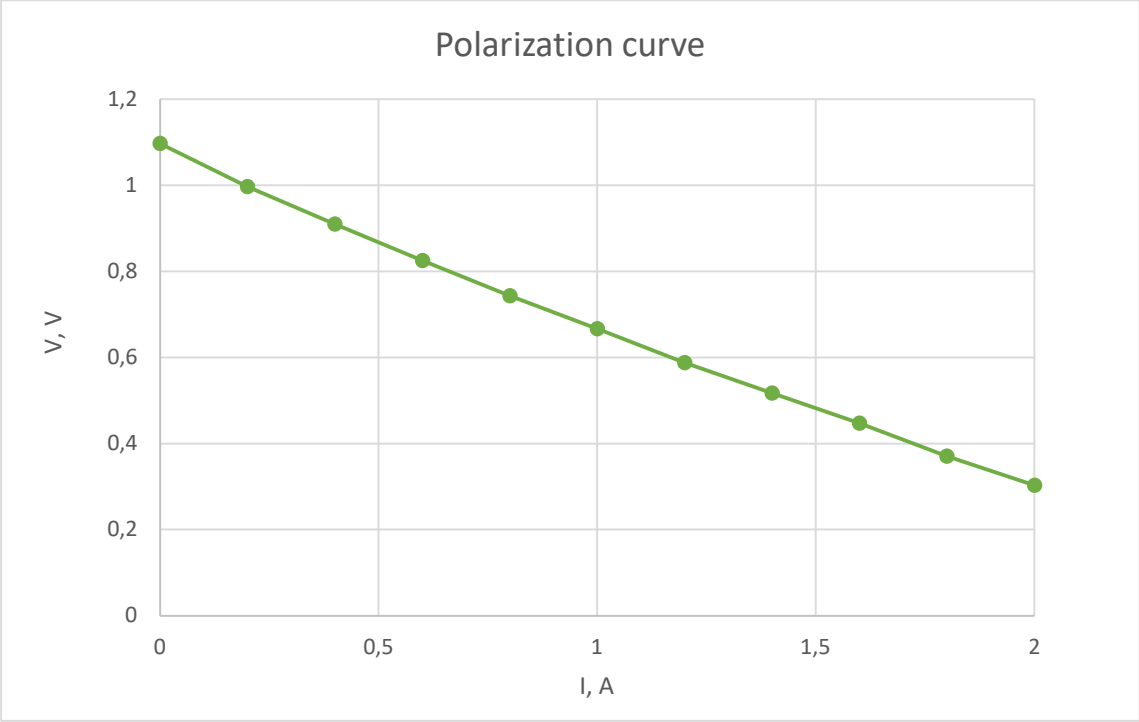

Figure 35 – Polarization curve, feed composition 2

3. Air (MFC5) 750ml/min, N_2 (MFC7) 112,5ml/min (50%), H_2 (MFC1) 112,5 ml/min(50%):

I, A	V thin wires, V
0,0	1,086
0,2	0,998
0,4	0,907
0,6	0,822
0,8	0,733
1,0	0,65
1,2	0,572
1,4	0,494
1,6	0,418
1,8	0,344
2,0	0,272

Table 7 – Collection of data, feed composition 3

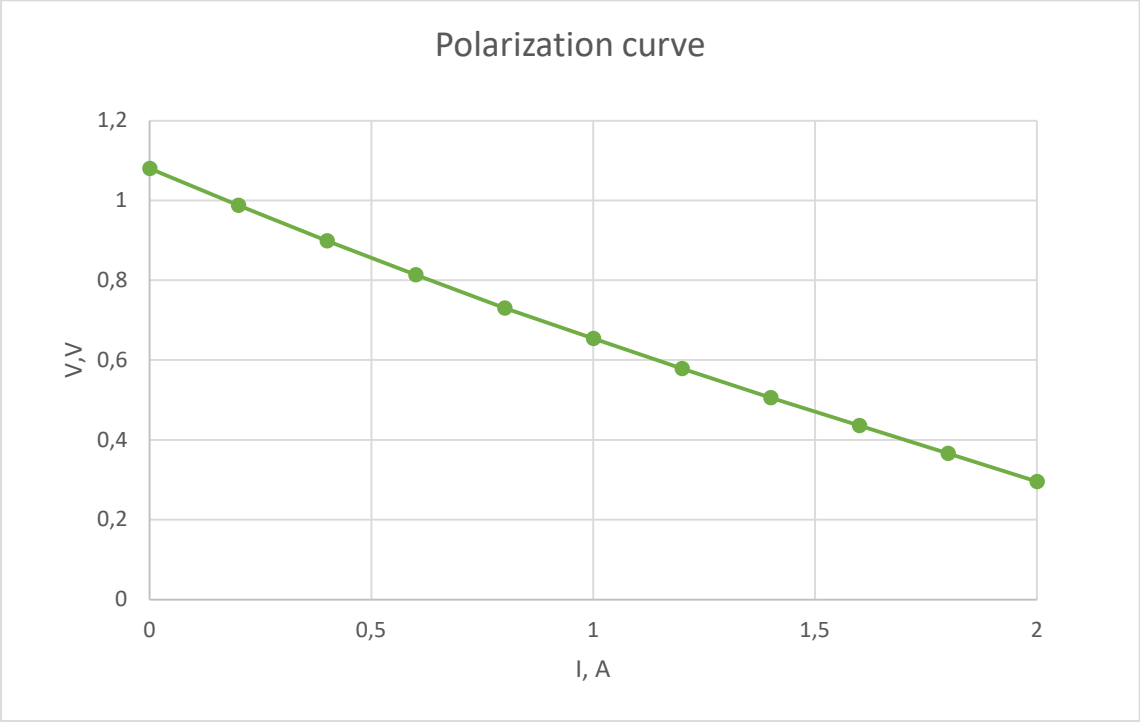

Figure 36 – Polarization curve, feed composition 3

From the graphs, it is remarkable the ohmic behavior of the cell as the polarization curve appears to be linear.

4.3.2 TEST 2: 850 °C

To have a countercheck for the measured voltage, in addition to the platinum cables required by regulations as explained in 4.2.1, a second couple of platinum wires are installed. These wires are ticker with respect to the formers and they cross the entire area of the cell, in both anode and cathode sides. The voltage from this last couple of wires was measured by an external voltmeter and its value are reported together with the voltage values of the thinner cables, which instead are read directly from the Teachy software or the local control cabinet.

To reach the desired temperature of 850 °C, the oven temperature is increased from 800°C with steps of 10 °C. Once the set point temperature is reached, tests with the same feed of the previous test are carried out. In addition, two tests with water in the feed are carried out.

1. Air (MFC5) 750 ml/min, N_2 (MFC7) 0 ml/min (0%), H_2 (MFC1) 225 ml/min (100%):

I, ampere	V thin wires, volt	V thick wires, V
0,0	1,073	1,074
0,2	1,008	1,026
0,4	0,945	0,981
0,6	0,883	0,937
0,8	0,823	0,894
1,0	0,764	0,852
1,2	0,706	0,811
1,4	0,648	0,77
1,6	0,593	0,728
1,8	0,538	0,688
2,0	0,485	0,649

Table 8 – Collection of data, feed composition 1

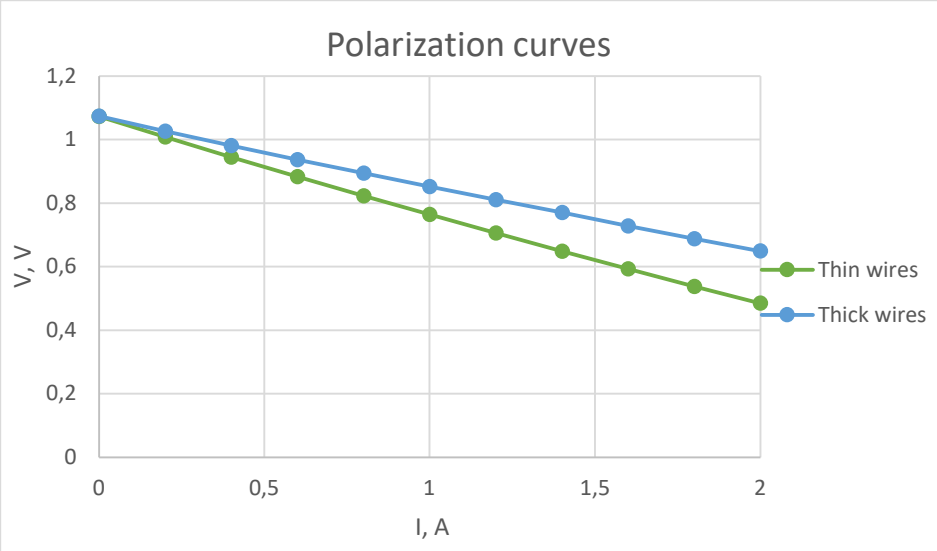

Figure 37 – Polarization curve, feed composition 1

2. Air (MFC5) 750 ml/min, N_2 (MFC7) 45 ml/min (20%), H_2 (MFC1) 180 ml/min (80%):

I, ampere	V thin wires, volt	V thick wires, V
0,0	1,074	1,075
0,2	1,006	1,027
0,4	0,939	0,975
0,6	0,875	0,929
0,8	0,811	0,884
1,0	0,753	0,843
1,2	0,692	0,802
1,4	0,638	0,759
1,6	0,576	0,715
1,8	0,522	0,672
2,0	0,468	0,631

Table 9 – Collection of data, feed composition 2

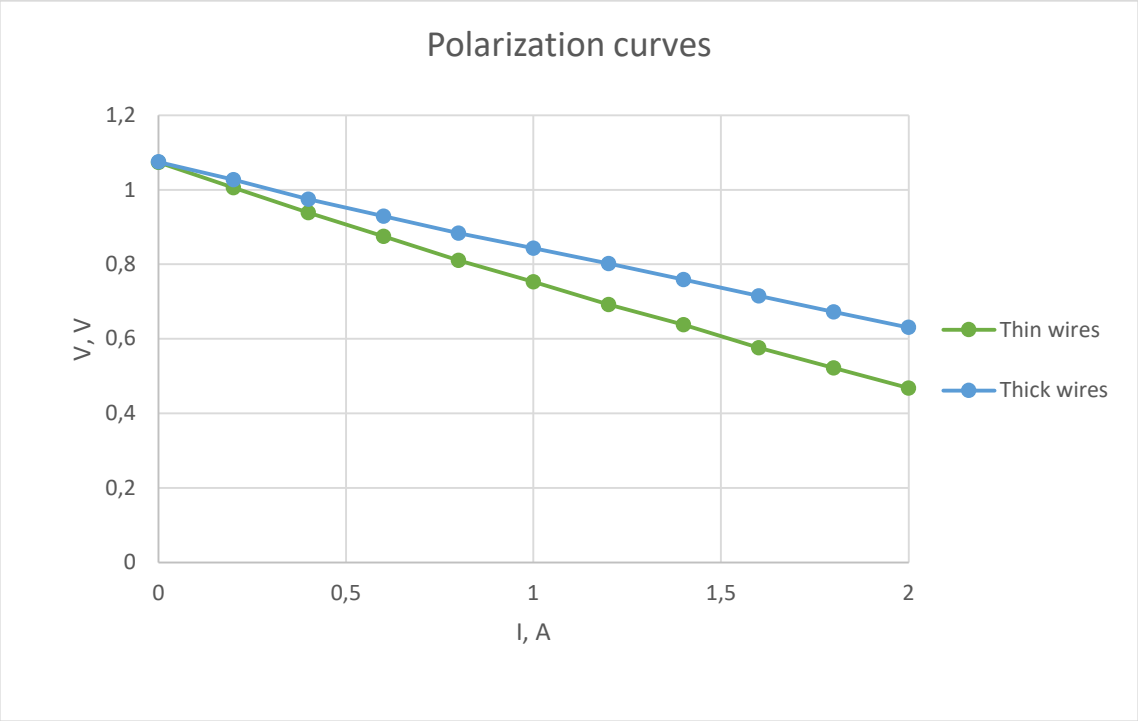

Figure 38 – Polarization curves, feed composition 2

3. Air (MFC5) 750 ml/min, N_2 (MFC7) 112,5 ml/min (50%), H_2 (MFC1) 112,5 ml/min (50%):

I, ampere	V thin wires, volt	V thick wires, V
0,0	1,06	1,061
0,2	0,989	1,008
0,4	0,918	0,956
0,6	0,85	0,907
0,8	0,786	0,86
1,0	0,717	0,814
1,2	0,655	0,77
1,4	0,595	0,727
1,6	0,539	0,684
1,8	0,489	0,644
2,0	0,438	0,603

Table 10 – Collection of data, feed composition 3

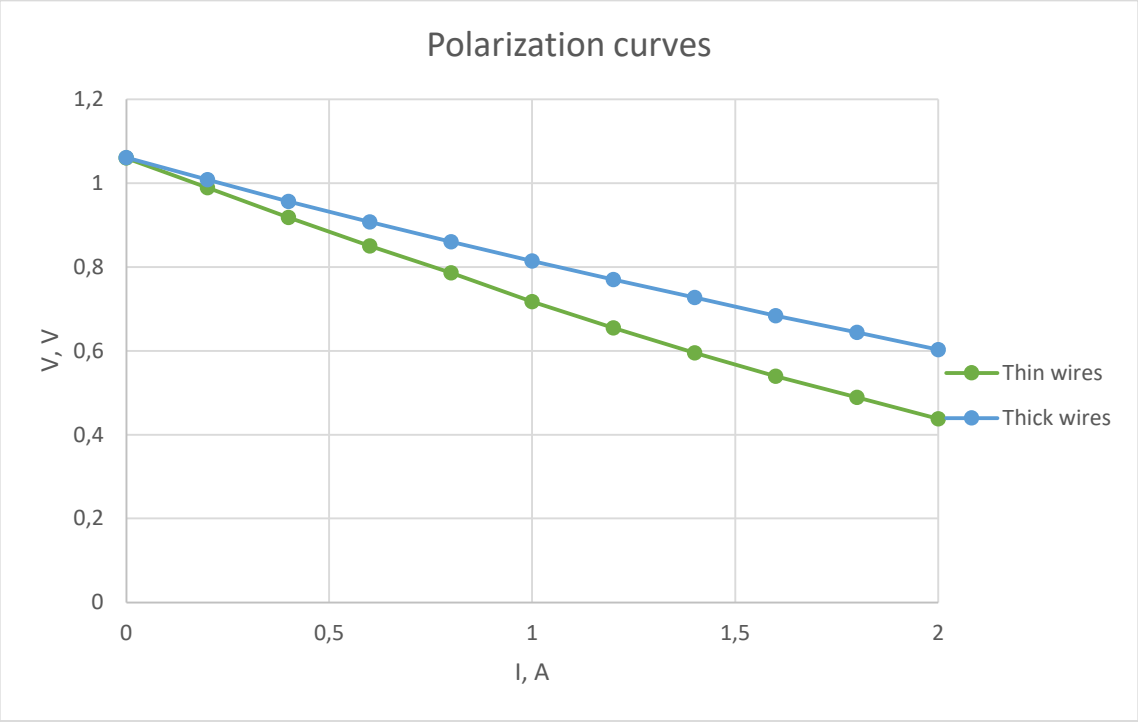

Figure 39 – Polarization curves, feed composition 3

Also for 850 °C it is possible to see the different values of voltage measured by the different couples of wires as well the general ohmic behavior of the cell.

4. Air (MFC5) 750 ml/min, H_2 (MFC1) 180 ml/min (80%), H_2O 45 ml/min (20%), T_{CEM}=61 °C:

I, A	V thick wires, V
0,0	0,936
0,2	0,882
0,4	0,827
0,6	0,77
0,8	0,706
1,0	0,644
1,2	0,581
1,4	0,526
1,6	0,464
1,8	0,412
2,0	0,352

Table 11 – Collection of data, feed composition 4

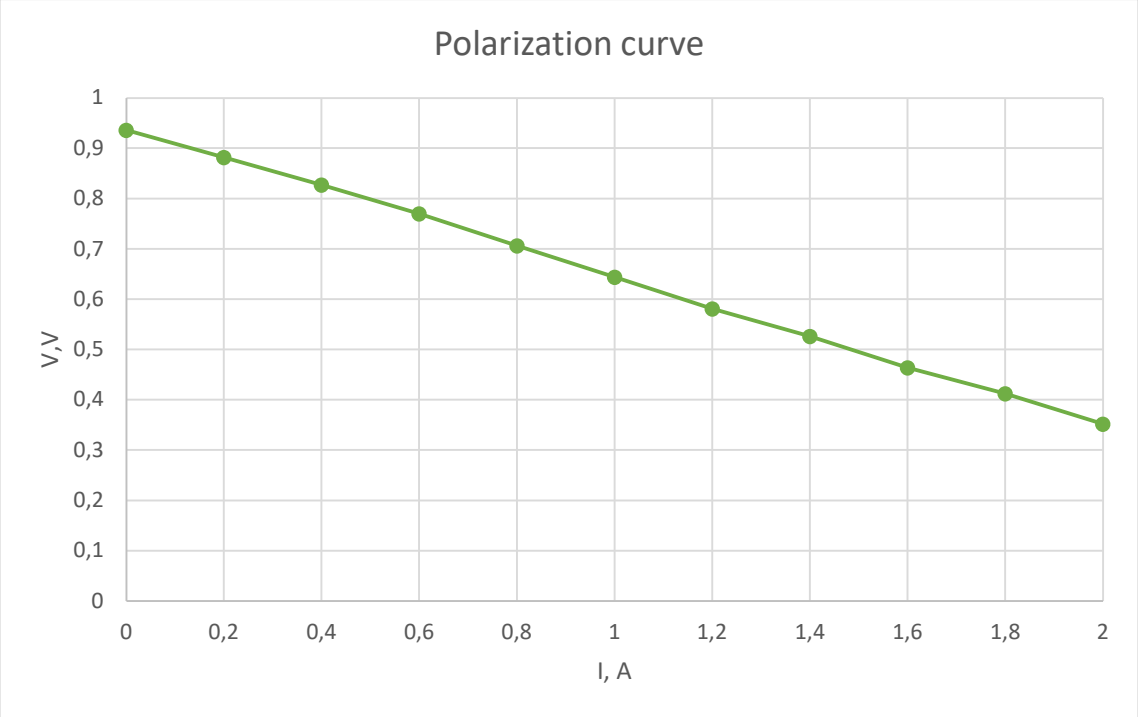

Figure 40 – Polarization curve, feed composition 4

5. Air (MFC5) 750 ml/min, H_2 (MFC1) 112,5 ml/min (50 %), H_2O 112,5 ml/min (50%) T_{CEM}=82 °C:

I, A	V thick wires, V
0,0	0,852
0,2	0,791
0,4	0,731
0,6	0,669
0,8	0,611
1,0	0,551
1,2	0,493
1,4	0,433
1,6	0,381
1,8	0,321
2,0	0,262

Table 12 – Collection of data, feed composition 5

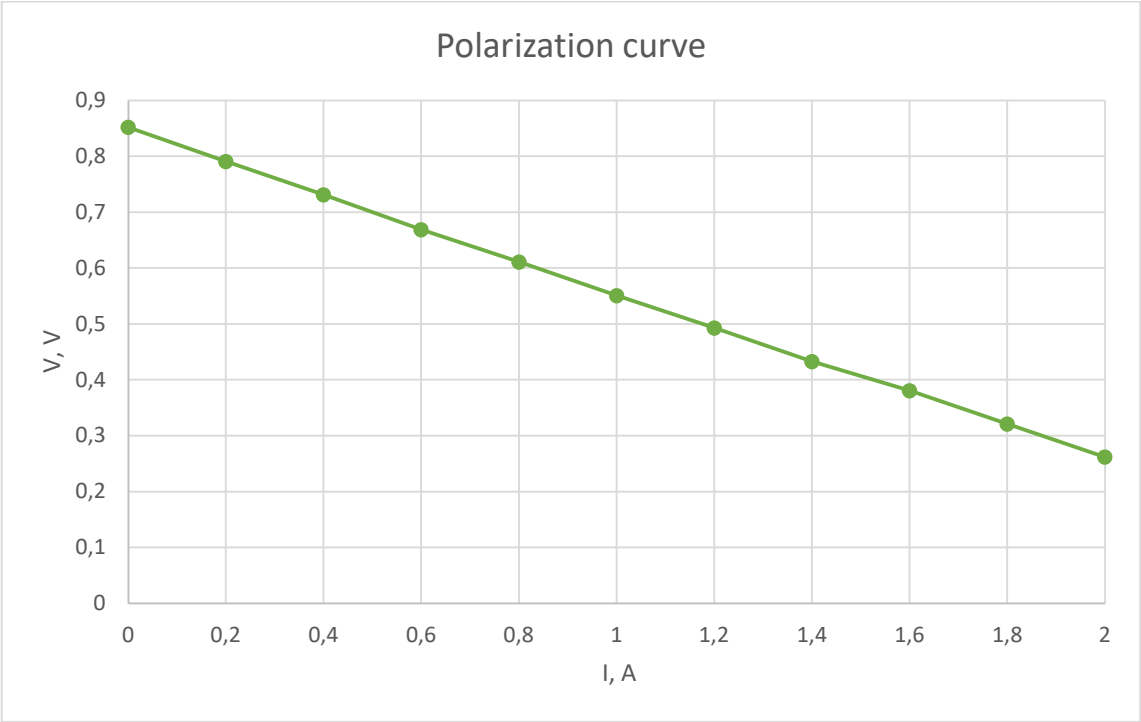

Figure 41 – Polarization curve, feed composition 5

4.4 SOEC operation mode: setup and tests

Before starting the SOEC experiment, the recommended feed composition sent to the cell is 50% N_2- 50% H_2 @ OCV.

Once the OCV is stable, it is possible to start the switching operation from SOFC mode to SOEC one. The procedure consists of the following steps:

1. Switching the three-way valve in the CEM unite in order to make possible the passage of the humified gases, and wait until the OCV stabilizes to a fixed value;
2. Verify that the resistance that heats up the line between the CEM and the inlet of the cells works properly;
3. Fix the feed composition of the dry gas – thus removing the N_2 and increasing the H_2 concentration;
4. Start sending the required water calculated through the *FLUIDAT® on the Net* software as mentioned in 4.1.3. It is recommended to reach the desired water flow rate through intermediate steps of 2 g/h, before each increment wait until both tension and flowrate stabilize;

Now it is possible to switch into the SOEC mode and start the polarization.

In the SOEC mode, both electrolysis and co-electrolysis are analyzed. Furthermore, a study on the outlet gases composition is carried on. In the following table, all the compositions are reported:

T, °C	Air, ml/min	CO_2, ml/min	H_2 ml/min	H_2O ml/min
850	750	0	112,5	112,5
850	750	0	45	180
850	750	101,25	22,5	101,25
850	750	33,75	22,5	168,75
850	750	168,75	22,5	33,75

Table 13 – Feed compositions:SOEC

4.4.1 TEST 1: electrolysis at 850 °C

For the electrolysis, the temperature of 850 °C is chosen. Two tests are carried out and their results are summarized. Even for electrolysis, the same two couples of wires are used ad the setup of the cell is not changed but it is just switched the cabinet into the SOEC mode.

Two feed composition are analyzed and for each of them, a different temperature of the CEM is required.

1. Air (MFC5) 750 ml/min, H_2O 112,5 ml/min (50%), H_2 (MFC1) 112,5 ml/min (50%), T_{CEM}=83 °C:

I, A	V thin wires, V	V thick wires,V
0,0	0,905	0,907
0,2	0,967	0,943
0,4	1,028	0,979
0,6	1,088	1,016
0,8	1,148	1,06
1,0	1,216	1,095
1,2	1,288	1,141
1,4	1,347	1,178
1,6	1,412	1,218
1,8	1,49	1,264
2,0	1,598	1,345

Table 14 – Collection of data, feed composition 1

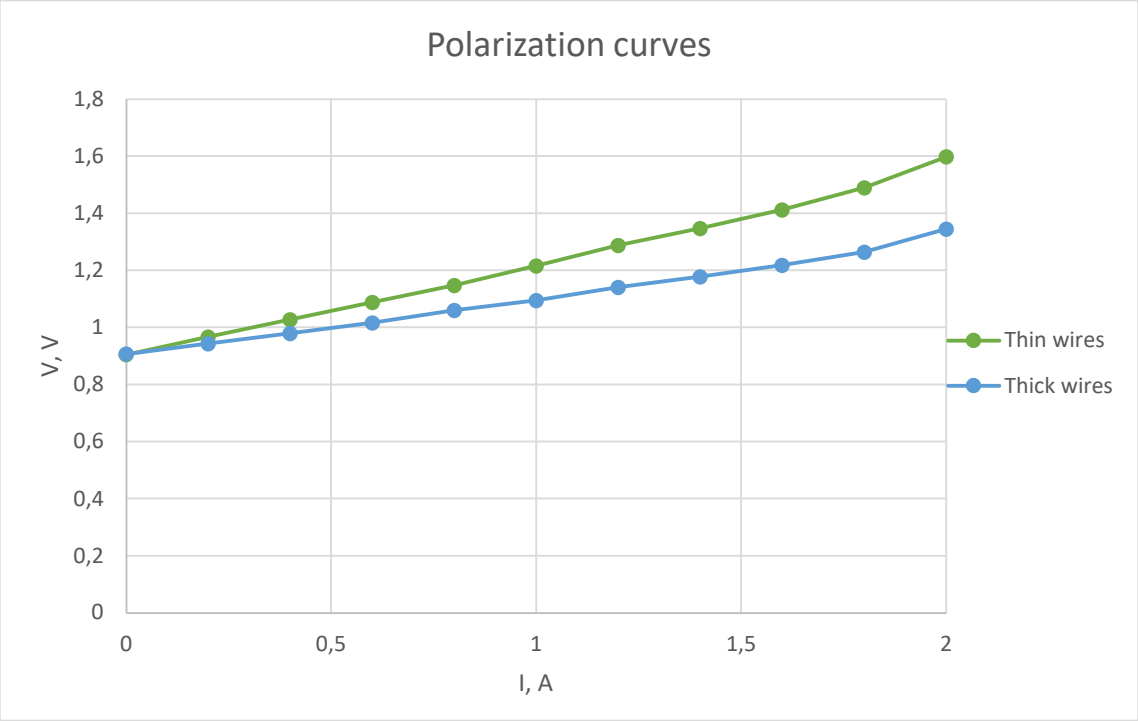

Figure 42 – Polarization curves, feed composition 1

2. Air (MFC5) 750 ml/min, H_2O 180 ml/min (80 %), H_2 (MFC1) 45 ml/min (20%), T_{CEM}=95 °C:

I, A	V thin wires, V	V thick wires, V
0,0	0,848	0,847
0,2	0,92	0,889
0,4	0,99	0,934
0,6	1,072	0,98
0,8	1,148	1,025
1,0	1,226	1,078
1,2	1,302	1,131
1,4	1,395	1,191
1,6	1,469	1,245
1,8	1,551	1,296
2,0	1,643	1,368

Table 15 – Collection of data, feed composition 2

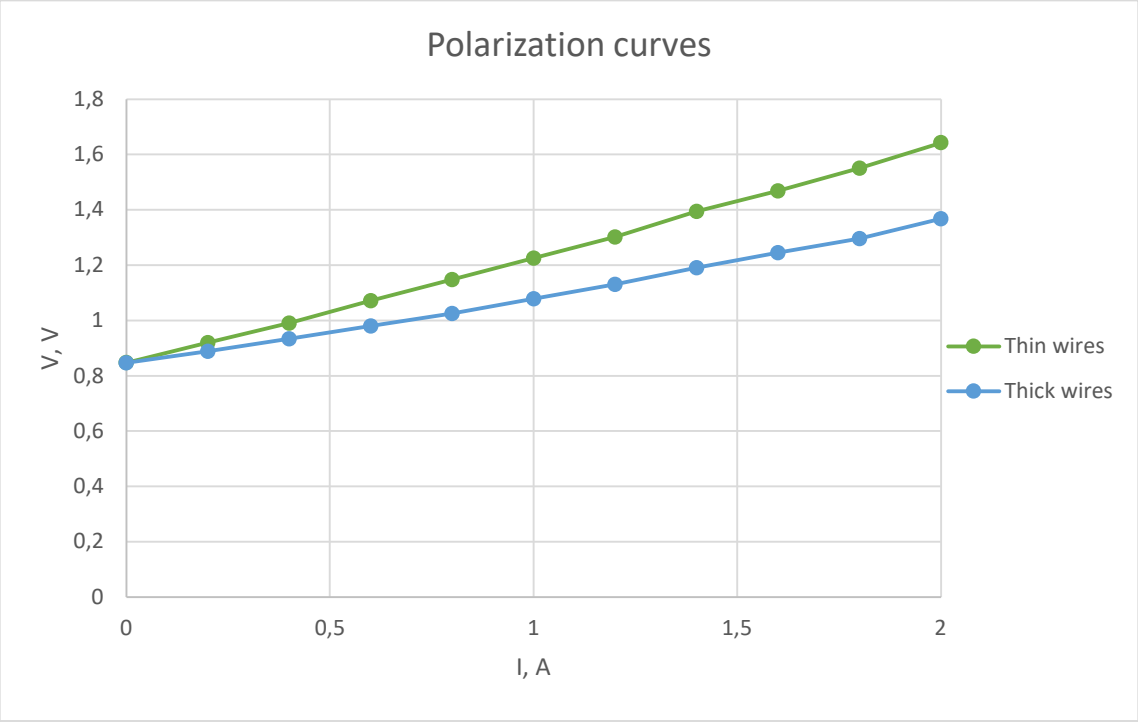

Figure 43 – Polarization curves, feed composition 2

4.4.2 TEST 2:co-electrolysis at 850 °C

Also for co-electrolysis the test is carried out at 850 °C. Three feed composition are analyzed:

1. Air (MFC5) 750 ml/min, H_2O 101,25 ml/min (45%), CO_2 101,25 ml/min (45 %), H_2 22,5 ml/min (10%), T_{CEM}=81 °C:

I, A	V thin wires, V	V thick wires, V
0,0	0,801	0,8
0,2	0,902	0,868
0,4	1,004	0,934
0,6	1,103	0,996
0,8	1,197	1,056
1,0	1,3	1,122
1,2	1,399	1,206
1,4	1,528	1,284
1,6	1,644	1,362
1,8	1,707	1,434
2,0	1,807	1,474

Table 16 – Collection of data, feed composition 1

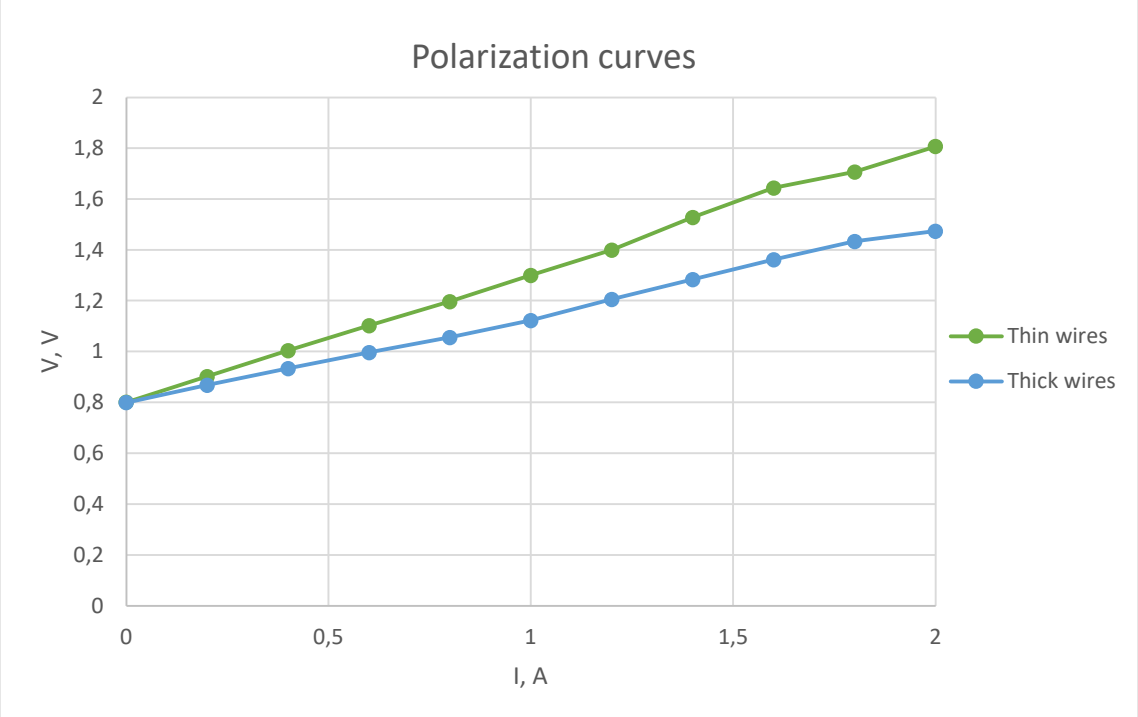

Figure 44 – Polarization curves, feed composition 1

2. Air (MFC5) 750 ml/min, H_2O 168,75 ml/min (75 %), CO_2 33,75 ml/min (15 %), H_2 22,5 ml/min (10%), T_{CEM}=93 °C:

I, A	V thin wires, volt	V thick wires, V
0,0	0,784	0,785
0,2	0,898	0,861
0,4	1,005	0,925
0,6	1,099	0,989
0,8	1,21	1,097
1,0	1,32	1,138
1,2	1,453	1,231
1,4	1,52	1,278
1,6	1,635	1,354
1,8	1,72	1,422
2,0	1,819	1,516

Table 17 –Collection of data, feed composition 2

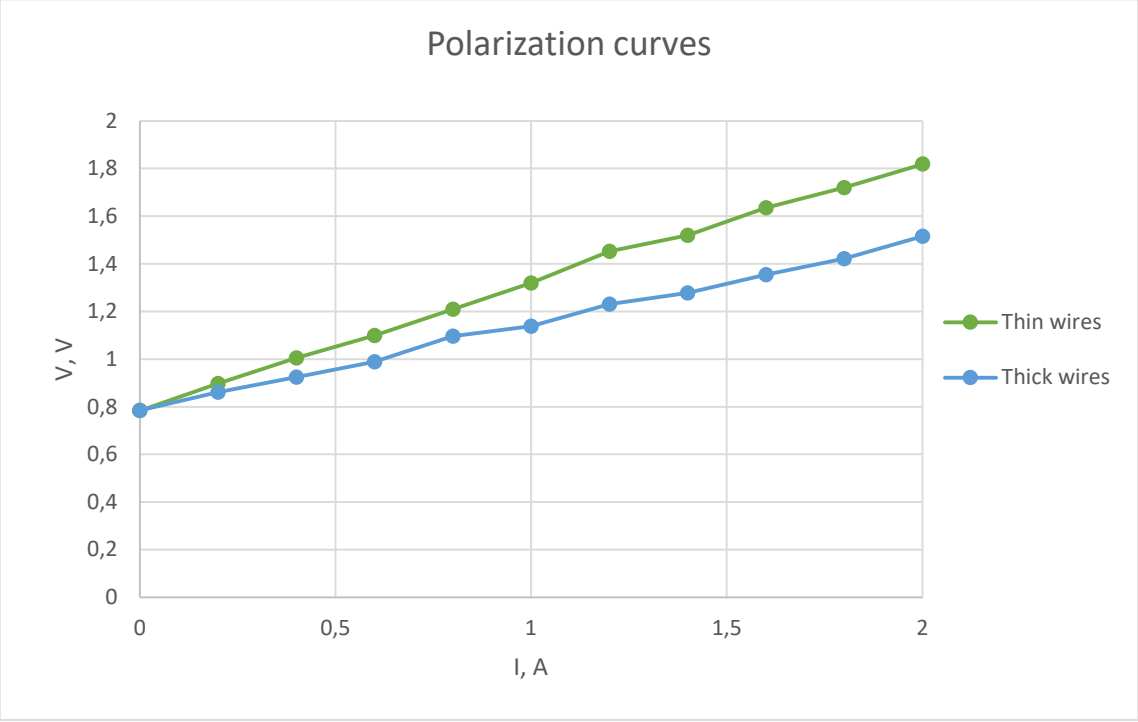

Figure 45 – Polarization curves, feed composition 2

3. Air (MFC5) 750 ml/min, H_2O 33,75 ml/min (15 %), CO_2 168,75 ml/min (75 %), H_2 22,5 ml/min (10%), T_{CEM}=55 °C:

I, A	V thin wires, volt	V thick wires, V
0,0	0,809	0,809
0,2	0,924	0,891
0,4	1,032	0,962
0,6	1,134	1,031
0,8	1,229	1,098
1,0	1,327	1,164
1,2	1,431	1,228
1,4	1,545	1,327
1,6	1,658	1,391
1,8	1,765	1,475
2,0	1,841	1,522

Table 18 – Data collection, feed composition 3

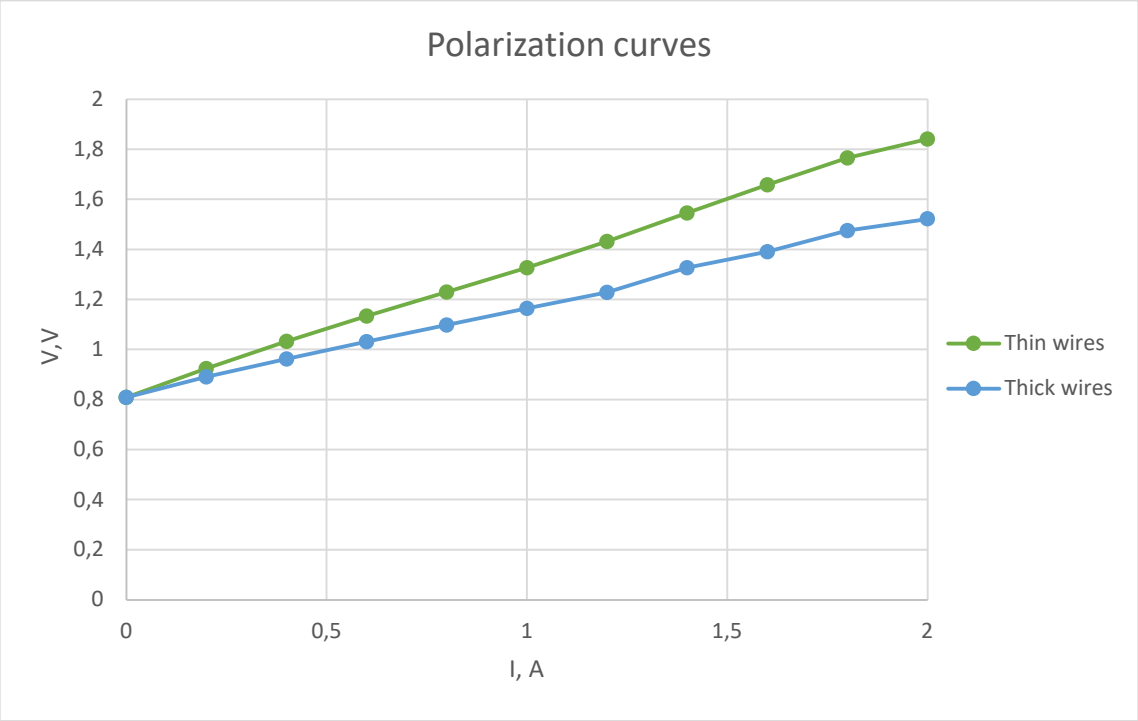

Figure 46 – Polarization curves, feed composition 3

4.4.3 Gas measurement

Continuing with the feed composition 3, the concentrations of the different molecules in the gas exiting the system are recorded.

It is used a gas analyzer, a device which continuously measure the volumetric concentrations of the stream under analysis.

The values for the methane are not reported as there are a hundred times lower than the other reported on the graph.

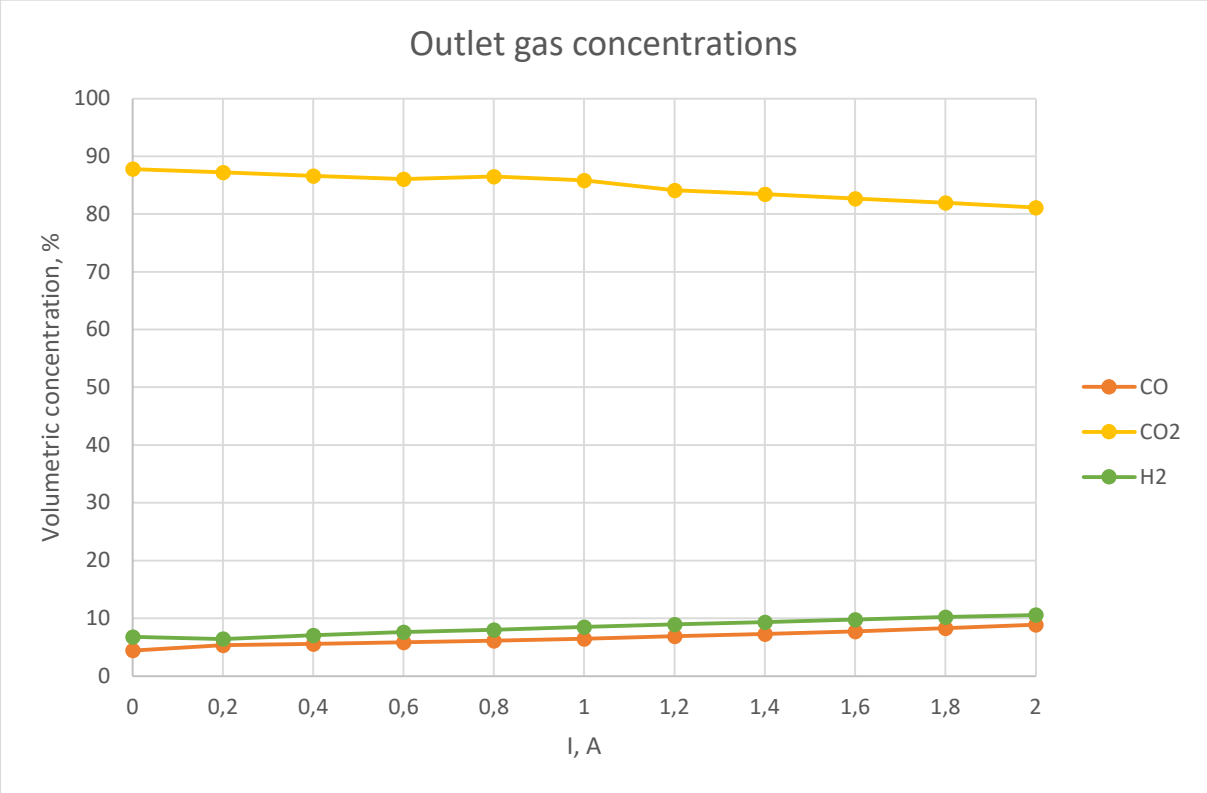

Figure 47 – Outlet gas concentrations

It can be seen that for low values of current (from 0 to 0,2 A), the concentration of hydrogen is subjected to a small decrease, this means that RWGS reaction takes place. However, as the current increases, hydrogen concentration increases too, as a proof of the electrolysis reaction occurred. Moreover, from 0 to 0,2 A, the measured CO increases, while CO_2 decreases: this is a sign that electrolysis of CO_2 is also occurring.

Otherwise, if CO was produced by RWGS the hydrogen would be consumed in the RWGS reaction and its concentration would not increase, (or it would increase slower than CO, while here they go up with the same rate: the curves of CO and H_2, in fact, in the graph are parallel above 0.2 A).

5.Plant modelling

After the theoretical study carried out in chapter 3 where SOEC and methanation were studied from the thermodynamic and chemical point of view, in this chapter it is discuss in detail their modeling on software. The model is built using the software Aspen Plus™.

The integration of high-temperature co-electrolysis with subsequent syngas methanation to produce SNG is investigated. The syngas produced in the SOEC plant undergoes a methanation process to obtain a stream of almost pure methane that is suitable (in term of density and heating value) to be injected in the NG grid.

It is important to notice that placing an electrolyzer upstream of the methanation simplifies the plant configuration: other sections, like gasification, air separation, sour shift and AGR are not required because, assuming to work with demineralized water and almost pure carbon dioxide, cleaning and correction issues are not present.
Having coal (or biomass) variable compositions, acid gas removal plays a "regulation" role to ensure FEED=3. In case of SOEC+methanation, by just fixing electrolysis operation conditions is possible to guarantee this target.

The plant starts from water and carbon dioxide to produce Synthetic Natural gas by high temperature co-electrolysis and methanation.
For all simulations the "Peng-Robinson Model" thermodynamic model is used, because using Ideal gas model could lead to considerable errors related to high pressures involved.

The simulation of the plant is of primary importance to investigate the benefits that can be drawn from this system, but above all, it allows to take note of the negative aspects that will have to be improved and studied in greater detail to further promote the technologies and make them competitive in their sectoral market.

The plant is modelled under the following hypothesis:

1. All the processes are assumed to be stationary. This means that the dynamic effects such as reaching the temperatures of the streams inside the components, the chemical, physical reactions and the electrical phenomena involved are neglected are not considered. This first hypothesis helps simplifying the treatment of the problem, adopting simpler models, characterized by a lower number of iterations to achieve the desired final result;

2. All the components are assumed to be adiabatic: the devices used are perfectly isolated from the external environment. This means that all the thermal losses that would actually occur are neglected.
3. No pressure drops are considered among components: the circulation does not cause any pressure loss, and that the presence of devices such as pumps and compressors have the sole function of increasing the pressures to the operating values of the subsequent components, without the need to consider no compensation for pressure drops.

The main features of the plant are:

- Stack pressure: 33,1 bar
- Stack temperature: 850 °C
- [H_2] at the cathode inlet: 10 %
- Reactant utilization: 80 %
- Methanators inlet temperature: 220 °C

5.1 Co-electrolysis in SOEC

5.1.1 Description of the system

The first block under analysis is the SOEC. The input streams are H2O-1 and CO2-1. It is assumed that this stream comes from flue gases of a cement plant, and its molar composition is: 98,4% CO_2, 1% N_2, 0,4% O_2, 0,2 % Ar [47] .

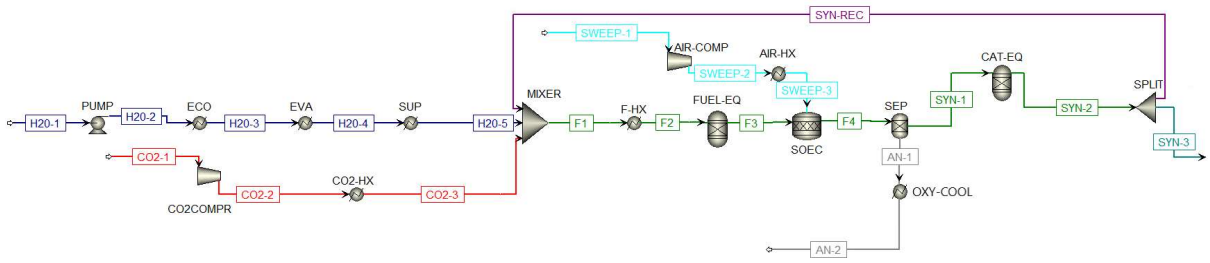

Figure 48 – SOEC on AspenPlus

The main blocks that make up the plant are:

PUMP which increases the pressure of water entering the system from 1 bar up to 33,1 bar, as the SOEC works in pressure.

ECONOMIZER, EVAPORATOR and SUPERHEATER perform namely the pre-heating, the evaporation and the superheating of the water. The economizer has the purpose of increasing the liquid water temperature, making it almost reach the change condition phase; in the evaporator occurs the transition of state from liquid water to steam, and finally the superheater allows the reaching of the required 850 °C temperature. Employing these three components in the water supply side is perfectly in line with the standard layout of energy generation systems in which water at high temperatures is involved, such as Rankine plants.

MIXER combines the H_2O flow and the CO_2 - which is heated up to 850 °C through the heat exchanger- with the recirculation of the cathode outlet.

After the mixer, a heat exchanger is used as the recirculation may decrease the temperature of the feed gas.

FUEL-EQ, SOEC, SEPARATOR and CAT-EQ simulate the SOEC.
Equilibrium modeling in Aspen Plus is performed using the RGibbs block which is based on the minimization of the Gibbs free energy of the system in terms of the mole numbers of the species present in all phases [48]: FUEL-EQ and CAT-EQ are two RGibbs blocks. SOEC is a stoichiometric reactor, used to simulate steam reduction. In addition to temperature and pressure, this block requires as input also reactants and products. The reactions put in the model are:

$$H_2O \rightarrow H_2 + \frac{1}{2}O_2$$

$$CO_2 \rightarrow CO + \frac{1}{2}O_2$$

Stoichiometric reactor also requires the specification of fractional conversion of the reactants. This value coincides with the Reactant Utilization (RU), and it is fixed do 80% for both the reactions.
This type of reactions does not simulate what actually happens, but being not possible to simulate an electrochemical device on Aspen Plus this version is the most reliable.

SEP is a separator which realizes the physical separation between anode and cathode side. Oxygen is mechanically separated from other substances, to simulate the fact that at anode side only oxygen production takes place.

SPLIT is a splitter block that performs the recirculation of a part of the cathode outlet stream. The quantity recirculated is fixed in order to obtain a fuel stream entering the SOEC with 10% molar concentration of H_2. This percentage avoids a too-oxidant atmosphere at the cathode side, in this way Ni oxidation does not occur.

A stream of air enters the STOICH block, simulating the air used to sweep.

5.1.2 DS e CB

Once the blocks are set and connected each other through material streams, it is necessary to set some targets to run the simulation.
This can be done through two specific tools: design specification (DS) and calculation block (CB).

The design specifications (DS), allow to set a specific value of a variable to be reached in the system simulation by varying one or more other variables, which can be, for example, a temperature value, the quantity of flow rate in a certain component and so on. Furthermore, equations can be set with the use of a section with Fortran language. Aspen obtains the results with various degrees of accuracy based on the tolerance value set.

A calculator block (CB) is a section of the Aspen program that allows to perform a specific calculation, choosing the input variables and obtaining export variables that are overwritten to the generic values previously set.

With the use of these two tools, Aspen simulates the process by performing a series of iterations, to reach convergence dictated by compliance with all the specifications set.

For the co-electrolysis part, two DS and one CB are used.

1° DS

The first design specification allows to obtain a fuel stream entering the SOEC with 10% molar concentration of H_2. This is done by varying the split fraction of the block SPLIT. In addition, the variation in flow rate also optimizes the flow rates at the cathode and anode inlet.

2°DS

With the second DS the FEED ratio introduced in chapter 3 is fixed to 3. This is done by modifying the mole flow of H_2O entering the system.

1° CB

At this point, it is necessary to calculate the electric power consumed by the process of co-electrolysis: this is done though the calculator block and then its Fortran section for the coding. Fixing an inlet mole flow of CO_2, the second DS calculates the requested input stream of H_2O. Considering the mole flows of H_2 and CO produced in the stoichiometric reactor, through the Faraday Law (1) it is possible to calculate the total current. Starting from the hypothesis of fixed ASR, V_{gibbs}, V_{TN} and the area of a single cell, is possible to calculate the current density trough eq.27 and so the single cell current as: $I_{cell} = j \cdot A_{cell}$.
With this value the total number of the cells needed to operate at the total current is calculated. Finally, the power is obtained.

5.2 Methanation and cleaning section

When a large amount of methane is synthesized in a reactor via the highly exothermic methanation reaction, the reactor temperature will dramatically increase. To avoid an high reactor temperature which can cause catalyst deactivation, as explained in chapter 3, inlet gas temperature of each reactor is adjusted to 220 °C.

The methanation section process starts with the injection of the syngas (TOMETH-1), at the initial conditions of 220 °C and 33,1 bar.

5.2.1 Description of the system

For the methanation section, two different setups are implemented. The first, CASE A, employs four methanators, as the majority of the existing plants do. The second, CASE B, is made up of three methanators. As the SOEC works in pressure, and so methane is present already at the cathode outlet, the aim of the analysis of the latter configuration is to verify if the final composition still has grid qualities even if the fuel undergoes to only three methanation steps.

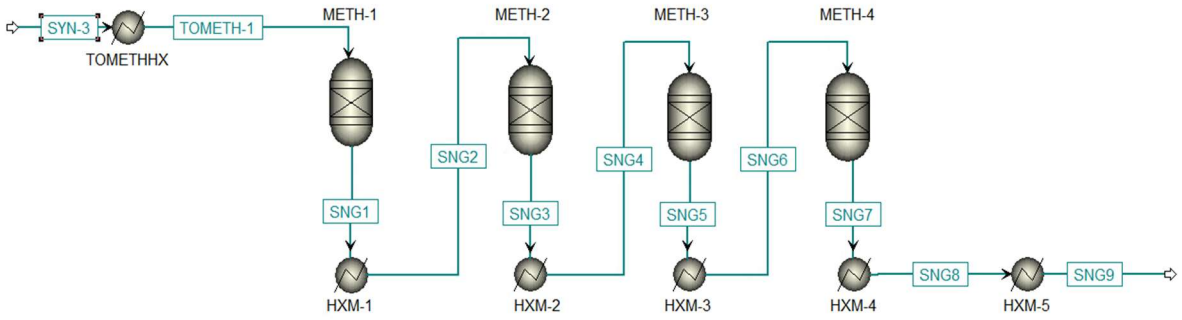

Figure 49 – Methanation on AspenPlus: CASE A

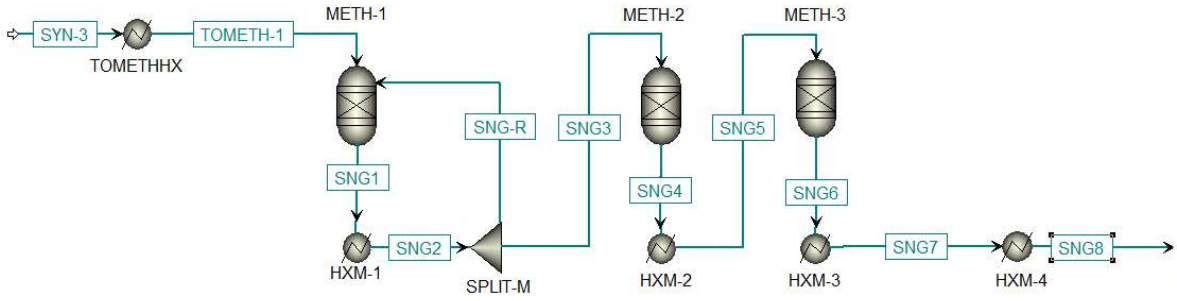

Figure 50 – Methanation section on AspenPlus: CASE B

Referring to fig.49:

METH-1, METH-2, METH-3 and METH-4 are the four methanation reactors, they are simulated with a Gibbs Reactor and considered to be adiabatic.

HXM-1, HXM-2, HXM-3, HXM-4 and HXM-5 are intermediate coolers which cool down the mixture from the previous methanation, in order to allow a subsequent equilibrium which will increase the fraction of methane in the mixture. Their outlet temperature is set to 220°C except for HXM-5 which cools the mixture down to 35°C.

Also for CASE B (fig.50), methanators are considered adiabatic and the inlet temperature is kept at 220 °C by the intercoolers. In order to have a final stream with higher content of methane, a recirculation after the first reactor is implemented.

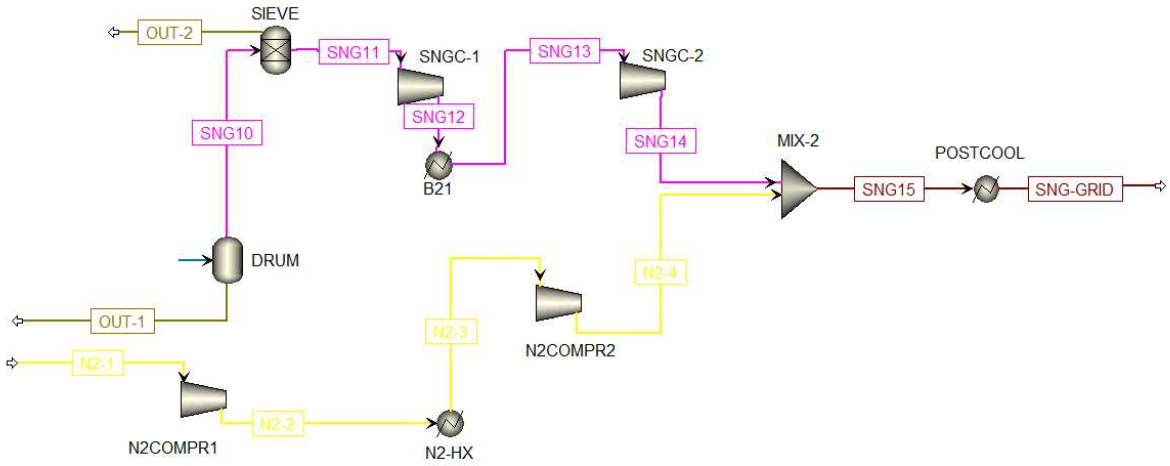

Figure 51 – Cleaning section on AspenPlus

With reference to fig.51, the main blocks of the cleaning section are:

DRUM which is a Flash separator and performs the thermodynamic equilibrium between liquid and gaseous phase. It allows the separation from the syngas of a huge fraction of water (OUT-1). This water can be recirculated before pumping, at the beginning of the plant, in order to minimize the consumption of demineralized water.

SIEVE which simulates a molecular sieve which retains substances as water and carbon dioxide (OUT-2). According to [49], it is hypothesized that sieve retains almost all the water and 98.5% of carbon dioxide.

SNGC-1, SNGC-2 are compressors that bring gas pressure to a value of 60 bar, which is a typical value of natural gas pipelines pressure.

Natural Gas Correction

In order for the gas to be introduced into the national network, it must respect certain parameters. For this thesis work, prescriptions established by Snam for pumping natural gas into pipelines are used [50].

The main constraints regard three parameters:

- Gas Gravity;
- Wobbe Index;
- Higher Heating Value of produced SNG.

Gas Gravity is the ratio between densities of produced SNG and air, both calculated at "Standard conditions", i.e. 101.325 Pa and 288,15 K (according to [50] and ISO 13443).

$$GG = \frac{\rho_{SNG}}{\rho_{air}}$$

Where ρ_{air} is set to 1,22 kg/Sm^3 assuming a mole mass of 28,84 kg/kmol.

Wobbe Index is expressed by the following equation:

$$WI = \frac{HHV}{\sqrt{GG}}$$

HHV is the Higher Heating Value of SNG.

Note that, during evaluation of HHV related to pipeline prescriptions, only methane (and not hydrogen) contribution was prudently considered, despite also hydrogen is a fuel.

Acceptability boundaries for these parameters are summarized in following table:

HHV, MJ/Sm^3	34,95-45,28
WI, MJ/Sm^3	47,31-52,33
GG	0,5548- 0,8

Table 19 – Acceptable boundaries by SNAM

The produced SNG has too low density, and consequently too low Gas Gravity. Being the SNG mostly composed by light molecules such as hydrogen and methane, it is too light.
So, it is necessary to "correct" SNG with a diluent. Nitrogen is chosen, and the target value of GG is set to 0,555.

6. Analysis of the performance

In this chapter all the results of the model are presented. Efficiencies of the plants are calculated considering the results obtained in the thermal integration section.

6.1 Simulation results

Results of the electrochemical section are obtained starting from the following hypothesis data.

SOEC features:

- OCV= 1,031 V
- ASR= 0,262 $\Omega \cdot cm^2$
- A_{CELL}= 300 cm^2
- V_{TN}= 1,029 V

The input stream of CO_2 is set to 12 mol/s which correspond to around 2 t/h. As already stated, the corresponding input stream of water is calculated through the second DS, and the fraction of syngas recirculated is calculated through the second DS, obtaining:

	CASE A	CASE B
Input water, mol/s	44,33	44,89
Recirculated fraction of syngas, %	22	23

Table 20 – Results of DSs

Through the CB, the following operating data are obtained:

	CASE A	CASE B
I_{TOT}, A	$9{,}13 \cdot 10^6$	$9{,}23 \cdot 10^6$
I_{CELL}, A	198	198
j_{tn}, A/cm2	0,66	0,66
n_{CELL}	46077	46600
W_{el}, MW	10,99	11,11

Table 21 – Results from CB

The molar compositions at the cathode outlet differ slightly from each other due to the small difference in water input:

Component	CASE A	CASE B
H_2, %	49,40	49,7
H_2O, %	25,2	25,2
CH_4, %	10,4	10,4
CO, %	10,2	10,0
CO_2, %	4,8	4,7

Table 22 – Cathode outlet gas compositions

Considering cathode outlet composition it can be seen that mole fractions for hydrogen and steam are respectively higher than that of carbon monoxide and dioxide, highlighting a larger quantity of water involved respect to carbon dioxide: this is just due to the "Feed Constraint": $FEED = \frac{[H_2]-[CO_2]}{[CO]+[CO_2]}$.

The presence of methane confirms the methanation already in the cathode. The simultaneous presence of H_2 & CO_2 and H_2 & CO in the same environment, under the operating conditions of the SOEC, cause the methanation reactions [8]. The concentration of methane in the outlet gas is directly proportional to the operating pressure, reaching approximately 10% at 33,1 bar. Fig.51 shows the molar concentrations of the cathode flow during co-electrolysis. The trend is almost constant for all components except for hydrogen and methane: the decrease in the molar percentage of hydrogen is due to the methanation reactions, favored by increasing pressure.

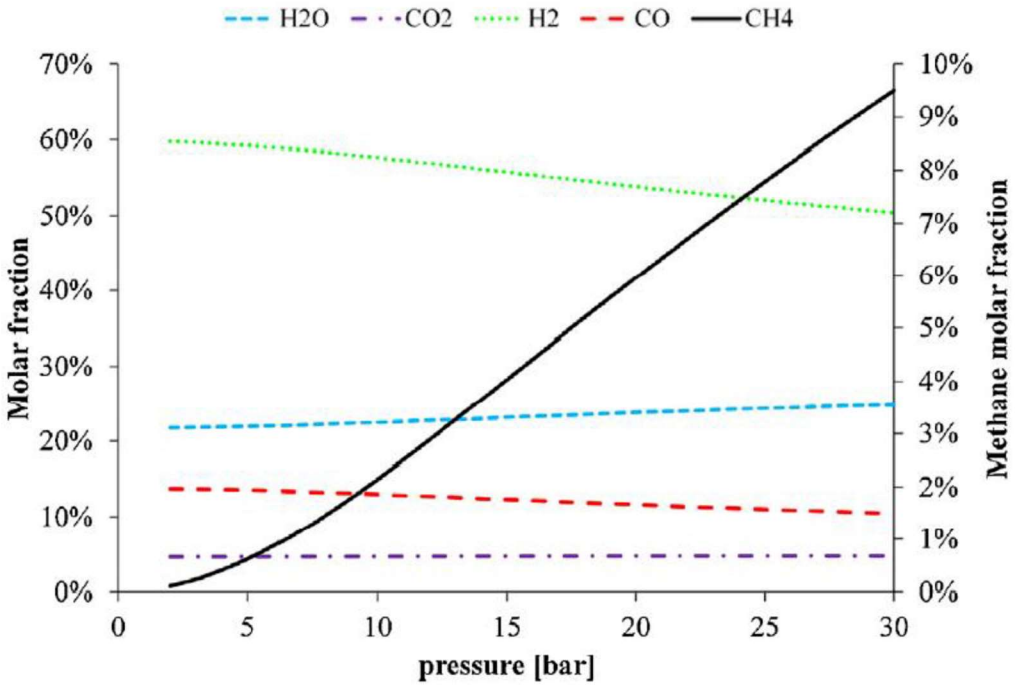

Figure 52 – Molar concentration of components during co-electrolysis [34]

As already stated, the methanation reactions are exothermic, and so they produce heat and increase the cathode temperature of the SOEC, leading two very important effects:

1. From a thermodynamic point of view, an increase in temperature brings to a decrease in the enthalpy of the reactions involved. Indeed, the high temperature is generated by the heat of the reactions, meaning a lower internal energy content. This lower energy content leads to a lower thermoneutral current, decreasing the productivity of the device [8]:

$$V_{cell} = V_{TN} \rightarrow \frac{\Delta h}{Z \cdot F} = \frac{\Delta g}{Z \cdot F} + ASR \cdot i_{TN} \rightarrow i_{TN} = \frac{\Delta h - \Delta g}{ASR \cdot Z \cdot F} \quad (53)$$

2. An increase in temperature favors the kinetics of reactions and it also improves the diffusivity of the reactant streams in the electrodes, up to the activation point of the reaction (TPB), allowing overall to obtain a greater number of electrochemical reactions. Moreover, higher temperatures can bring advantages in terms of resistivity, in fact the electrolyte lowers its capacity to oppose the passage of ions, allowing the passage of more electrical charges in the connected external circuit. Overall, this results in better productivity.

The two effects are conflicting, but considering the contemporaneity of them, the first prevails over the second, marking a net decrease in performance. Consequently, cathode heating must be avoided by exporting a greater amount of heat to maintain the temperature at operating conditions [8].

After the methanation and the cleaning section, a SNG with the following composition is obtained:

Component	CASE A	CASE B
CH_4, %	96,8	92,5
H_2, %	1,6	3,6
N_2, %	1,6	3,9

Table 23 – SNG final composition

For both the plants, a blending of nitrogen is necessary to obtain an acceptable value of GG:

	CASE A	CASE B
N_2-blending, mol/s	0,2	0,5
GG	0,555	0,555

Table 24 – Final value of GG after N_2 blending

6.1.1 Results analysis

The technical specification UNI/TS 11537:2019 ("Introduction of biomethane into natural gas transport and distribution networks" – "Immissione di biometano nelle reti di trasporto e di distribuzione del gas naturale") sets a technical acceptability limit of 1% of hydrogen volume in biomethane that can be injected into the grid.
According to this limit, the SNG produced do not respect the actual technical limits.

However, in November 2020, the MISE published the first "Guidelines for the National Hydrogen Strategy" ("Linee Guida per la Strategia nazionale sull'idrogeno) in which the future increment of green hydrogen is underlined, identifying the sectors in which it will become competitive in the short term.

In this document, the Italian Government focuses on the role that hydrogen can play in the national decarbonization pathway, in accordance with the Integrated National Energy and Climate Plan, and the EU Hydrogen Strategy, within the framework of the Long-Term Strategy for full decarbonization in 2050.

From the document, it is possible to read that: "For the next decade, the Government envisages the application of hydrogen in the transport sector, particularly heavy duty (e.g. long-haul trucks), in railways and in industry, with specific reference to those segments where hydrogen is already used as a raw material, for example in the chemical sector and in oil refining. In addition to this, hydrogen blending in the gas grid can be used to anticipate and stimulate the growth of the hydrogen market.
Blending low-carbon hydrogen into the grid can be an effective way to contribute to decarbonization goals and stimulate the hydrogen market while investing in the development of the production and distribution chain. In the case of green hydrogen, overgeneration from renewable sources can be leveraged to produce the hydrogen for blending at a lower cost. (…) Although in Italy an official technical limit is still to be defined, it is plausible to think that by 2030 an average of up to 2% of natural gas distributed can be replaced with hydrogen." [51]

Considering the results obtained in the simulations, certainly, the SNG produced in CASE A will be injectable in the next future.

6.2 Thermal Integration

6.2.1 Pinch Analysis theory

Pinch Analysis is an extension of the second principle of Thermodynamics to the energy management of a whole plant. Its aim is to optimize the heat exchange between the process streams, as well as the use of utilities [52]. Pinch Analysis is used to model energy systems characterized by a heat exchangers network.

The process data is represented as a set of energy streams, as a function of heat load (product of specific heat and mass flow rate) against temperature. These data are combined for all the streams in the plant to give composite curves, one for all hot streams (those which must be cooled down) and one for all cold streams (those which must be heated up) [53].

Pinch point represents the point in which there is the minimum temperature difference between a hot and a cold fluid in the entire system.
Pinch point allows representing the system as separated in two parts:

- Above pinch point: system requires a heat input and is therefore a net heat sink
- Below pinch point: system rejects heat and so is a net heat source

The energy targets can be achieved using heat exchangers to recover heat between hot and cold streams in two separate systems, one for temperatures above pinch temperatures and one for temperatures below pinch temperatures.

The energy targets can be, for example, minimum of external heat requirement or minimum of heat exchange area. In this work the target will be the minimization of heat requirement.
In addition to fluids temperatures, another constraint is the minimum temperature difference (ΔT_{min}) between hot and cold fluids which has to be maintained in each heat exchanger: in this work it has been chosen ΔT_{min}=20°C.
For the analyzed systems it has been supposed that for external heating an electrical source will be used, whereas for external cooling water at 15°C will be involved [16].

As shown in following figure, for both the two parts thermal balance is obtained without heat exchange through the pinch point.

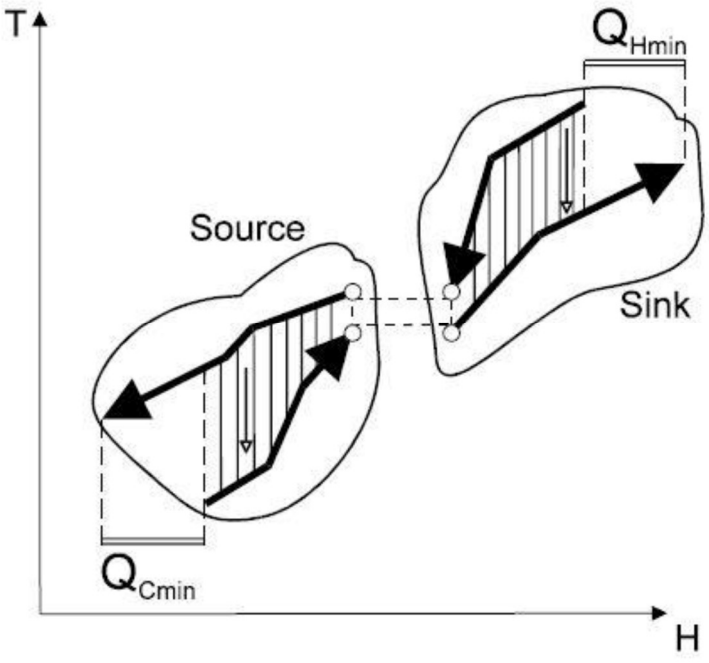

Figure 53 – Schematic of the system [16]

To summarize, there are three rules that must be observed to achieve the minimum energy targets for a process:

- Heat must not be transferred across the pinch;
- There must be no external cooling above the pinch;
- There must be no external heating below the pinch.

Minimize energy requirements

The procedure starts with definition of temperature intervals trough the "fictitious temperatures" (T*) defined as follows:

- Inlet and outlet temperature of each cold fluid are increased of $\frac{1}{2}\Delta T_{min}$;
- Inlet and outlet temperature of each hot fluid are decreased of $\frac{1}{2}\Delta T_{min}$.

All T* are overlapped and sorted from largest to smallest, defining several temperature intervals.

For each interval so defined, the global heat flux required is calculated as follows:

$$\phi_i = (T_i^* - T_{i+1}^*) \cdot \left(\sum Gc_h - \sum Gc_c\right)$$

Where:

- G is mass flow in kg/s;
- c is specific heat in kJ/kgK.

A positive value of ϕ_i means a deficit of thermal flux in the corresponding interval, otherwise it stands for a surplus.

Then is possible to define a cumulate of ϕ_i which is the sum, for a generic interval, between cumulate at interval *i-1* and ϕ_i, starting from the assumption that external heat input at first interval is 0.

Negative values of the cumulate are not acceptable, then the external heat is increased until each value of the cumulate will be ≥ 0, so the lowest value of the cumulative heat is found, and its absolute value is added to each cumulative heat previously calculated. The lower bound of T* of the interval with cumulate equal to 0 is the pinch point (T_{PP}^*).

This means that pinch point temperature for hot fluids is $T_{PP,h} = T_{PP}^* + \frac{1}{2}\Delta T_{min}$ and pinch point temperature for hot fluids is $T_{PP,h} = T_{PP}^* - \frac{1}{2}\Delta T_{min}$

6.2.2 Results: CASE A

In following table fluids involved in analysis and key variables are presented:

N°	Process	Fluid Type	G·c, kW/K	T_{in}, °C	T_{out}, °C	Φ, kW
1	Water Heating	COLD	3,35	20,2	239,1	733,0523
2	Evaporation	COLD	1338,90	239,1	240,1	1338,9
3	Steam superheating	COLD	1,60	239,1	850	977,44
4	CO2 heating	COLD	0,66	395,7	850	300,1906
5	Fuel heating	COLD	2,57	849,1	850	2,315249
6	Air heating	COLD	2,10	538,3	850	654,7103
7	O2 cooling	HOT	0,70	850	35	-570,5
8	SNG cooling	HOT	1,75	850	220	-1099,94
9	M1 cooling	HOT	1,27	698,3	220	-605,256
10	M2 cooling	HOT	1,13	517,7	220	-337,07
11	M3 cooling	HOT	1,08	334,3	220	-123,606
12	M4 cooling	HOT	1,06	238,9	202	-39,179
13	M5 cooling	HOT	6,00	202	35	-1002
14	SNG intercooling	HOT	0,43	68,6	35	-14,5226
15	N2 cooling	HOT	0,01	647,8	35	-6,38538
16	SNG post-cooling	HOT	0,42	60,6	35	-10,8638

Table 25 – Streams scheme: CASE A

The evaporation outlet temperature has been increased fictitiously of 1°C.

Remembering that ΔT_{min}=20°C, the following results are obtained:

N°	Process	T_{in}, °C	T_{out}, °C	T^*_{in}, °C	T^*_{out}, °C
1	Water Heating	20,2	239,1	30,2	249,1
2	Evaporation	239,1	240,1	249,1	250,1
3	Steam superheating	239,1	850	249,1	860
4	CO2 heating	395,7	850	405,7	860
5	Fuel heating	849,1	850	859,1	860
6	Air heating	538,3	850	548,3	860
7	O2 cooling	850	35	840	25
8	SNG cooling	850	220	840	210
9	M1 cooling	698,3	220	688,3	210
10	M2 cooling	517,7	220	507,7	210
11	M3 cooling	334,3	220	324,3	210
12	M4 cooling	238,9	202	228,9	192
13	M5 cooling	202	35	192	25
14	SNG intercooling	68,6	35	58,6	25
15	N2 cooling	647,8	35	637,8	25
16	SNG post-cooling	60,6	35	50,6	25

Table 26 – Fictitious temperatures: CASE A

Cumulative heats have the following values:

T* intervals	$\Sigma G \cdot c_{HOT} - \Sigma G \cdot c_{COLD}$	Φ, kW	Cum 1	Cum2
-	-	-	0	177,5
860-859,1	-6,93	-6,24035	-6,24035	171,3
859,1-840	-0,16	-3,06223	-9,30258	168,2
840-688,3	2,29	346,7261	337,4235	514,9
688,3-637,8	-0,65	-32,8182	304,6053	482,1
637,8-548,3	-0,64	-56,9106	247,6947	425,2
548,3-507,7	1,46	59,31682	307,0116	484,5
507,7-405,7	2,59	263,4745	570,4861	748,0
405,7-324,3	3,25	264,878	835,364	1012,9
324,3-250,1	4,34	321,6903	1157,054	1334,6
250,1-249,1	-1334,56	-1334,56	-177,51	0,0
249,1-228,9	2,59	52,25029	-125,26	52,3
228,9-210	2,95	55,72495	-69,535	108,0
210-192	-1,58	-28,3791	-97,9142	79,6
192-58,6	3,36	448,4401	350,5259	528,0
58,6-50,6	3,79	30,35071	380,8767	558,4
50,6-30,2	4,22	86,05141	466,9281	644,4
30,2-25	7,57	39,34843	506,2765	683,8

Table 27 – Results: CASE A

As said before, negative values for cumulates are unacceptable. So, in this plant an external energy input is necessary.

T^*_{pp} is 249,1 °C so it's possible to calculate pinch point temperatures for hot and cold fluids, which are reported in following table:

$T_{PP,hot}$, °C	259,1
$T_{PP,cold}$, °C	239,1

Table 28 – Pinch point temperatures: CASE A

Pinch point coincides with water inlet into the evaporator, and the external heat that must be provided to the system has a value of around 177,5 kW.

6.2.3 Results: CASE B

N°	Process	Fluid Type	Gc, kW/K	Tin	Tout	Fi, kW
1	Water Heating	COLD	3,39066	20,2	239,1	742,2155
2	Evaporation	COLD	1338,9	239,1	240,1	1338,9
3	Steam superheating	COLD	1,62	239,1	850	989,658
4	CO2 heating	COLD	0,6607761	395,7	850	300,1906
5	Fuel heating	COLD	1,7230342	849,1	850	1,550731
6	Air heating	COLD	2,06025	538,3	850	642,1799
7	O2 cooling	HOT	0,7	850	35	-570,5
8	SNG cooling	HOT	1,7381516	850	220	-1095,04
9	M1 cooling	HOT	1,1002202	476,91	220	-282,658
10	M2 cooling	HOT	1,0531572	304	220	-88,4652
11	M3 cooling	HOT	1,0531572	227,3	202	-26,6449
12	M4 cooling	HOT	1,0531572	202	35	-175,877
13	SNG intercooling	HOT	1,6850208	68,7	35	-56,7852
14	N2 cooling	HOT	0,01042	647,8	35	-6,38538
15	SNG post-cooling	HOT	0,4426159	61,7	35	-11,8178

Table 29 – Streams scheme: CASE B

As before, evaporation outlet temperature has been increased fictitiously of 1°C.

It is obtained:

N°	Process	T_{in}, °C	T_{out}, °C	T^*_{in}, °C	T^*_{out}, °C
1	Water Heating	20,2	239,1	30,2	249,1
2	Evaporation	239,1	240,1	249,1	250,1
3	Steam superheating	239,1	850	249,1	860
4	CO2 heating	395,7	850	405,7	860
5	Fuel heating	849,1	850	859,1	860
6	Air heating	538,3	850	548,3	860
7	O2 cooling	850	35	840	25
8	SNG cooling	850	220	840	210
9	M1 cooling	476,91	220	466,91	210
10	M2 cooling	304	220	294	210
11	M3 cooling	227,3	202	217,3	192
12	M4 cooling	202	35	192	25
13	SNG intercooling	68,7	35	58,7	25
14	N2 cooling	647,8	35	637,8	25
15	SNG post-cooling	61,7	35	51,7	25

Table 30 – Fictitious temperatures: CASE B

Cumulative heats have the following values:

T* intervals	$\Sigma G \cdot c_{HOT} - \Sigma G \cdot c_{COLD}$	Φ, kW	Cum 1	Cum2
-	-	-	0	628,0861
860-859,1	-6,911026065	-6,21992	-6,21992	621,8662
859,1-840	-0,220526065	-4,21205	-10,432	617,6541
840-637,8	2,217625519	448,4039	437,9719	1066,058
637,8-548,3	-1,892454481	-169,375	268,5972	896,6833
548,3-466,9	0,167795519	13,65856	282,2558	910,3419
466,9-405,7	1,268015696	77,60256	359,8583	987,9445
405,7-294	1,928791761	215,446	575,3044	1203,39
294-250,1	2,981948939	130,9076	706,2119	1334,298
250,1-249,1	-1334,298051	-1334,3	-628,086	0
249,1-217,3	1,211288939	38,51899	-589,567	38,51899
217,3-210	2,264446117	16,53046	-573,037	55,04944
210-192	-1,627082822	-29,2875	-602,324	25,76195
192-58,7	3,31976	442,524	-159,8	468,286
58,1-51,7	3,881433587	24,84117	-134,959	493,1271
51,7-30,2	4,324049442	92,96706	-41,9919	586,0942
30,2-25	7,714709442	40,11649	-1,87542	626,2107

Table 31 – Results: CASE B

Again, T^*_{pp} is 249,1 °C, obtaining:

$T_{PP,hot}$, °C	259,1
$T_{PP,cold}$, °C	239,1

Table 32 – Pinch point temperatures: CASE B

Pinch point coincides with water inlet into the evaporator, and the external heat which must be provided to the system has a value of around 628 kW. The higher value of external heat required in CASE B is mostly due to the fact that while the heat requirement in SOEC are almost equal for both plants, the cooling demand is lower in CASE B due to the lower temperatures reached at the outlet of each methanator.

6.3 Plant efficiency

From aspen, it is possible to read the power requested from SOEC (in DC):

	CASE A	CASE B
$W_{IN\text{-}SOEC}$, MW	10,99	11,11

Table 33 – SOEC DC requirement

Efficiency of the plant is calculated as the ratio between Chemical Power associated to SNG and the total electric power in input (A.C.).

Total electrical input is made up of several contributions:

- electrical input in AC into the stacks (electrolysis cells operate in DC);
- electricity to drive pump and compressors;
- electricity for external heat requirements.

So, efficiency can be calculated as follows:

$$\eta = \frac{POWER_{SNG}}{W_{el}} = \frac{LHV_{SNG} m_{SNG}}{W_{el}}$$

LHV is calculated considering the final molar composition of SNG, after the correction section (both methane and hydrogen are considered as fuels).
For the electricity to drive pumps and compressors both isentropic and electric efficiency are considered, their values are:

LHV methane, MJ/kg	50
LHV hydrogen, MJ/kg	120
$\eta_{is,COMPR}$	0,75
$\eta_{is,PUMP}$	0,8
$\eta_{INVERTER}$	0,96

Table 34 – Hypothesis

Bringing to the following results:

	CASE A	CASE B
$W_{IN\text{-}SOEC\ AC}$, kW	114478	11573
$W_{IN\text{-}COMPR\text{-}CO2}$, kW	245	245
$W_{IN\text{-}COMPR\text{-}SNG}$, kW	29	30,3
$W_{IN\text{-}COMPR\text{-}N2}$, kW	4,7	13,5
$W_{IN\text{-}PUMP}$, kW	3,2	3,2
$W_{EXT\text{-}COOLING}$	177,5	628,1
$W_{EL\text{-}TOT}$, MW	11907,4	12493,1
LHV_{SNG}, MJ/kg	48,7	46,8
m_{SNG}, kg/s	0,19	0,20
CHEMICAL POWER, kW	9253	9834,3
η	0,78	0,79

Table 35 – Plant results

6.3 Overall efficiency

In this section the overall efficiency is calculated considering the technology used to produce the electric power needed as input in the plant. Two technologies are taken into account: photovoltaic (PV) and wind power.

Considering conversion efficiency of these two technologies, is possible to evaluate an overall efficiency from renewable sources to Synthetic Natural Gas, coupling electricity production from RES with Power-to-Gas technologies.

For photovoltaic, a value of 18% is considered according to literature, while for wind power, a value of 46% is set [16].
Overall efficiencies are obtained multiplying efficiency of Power-To-Gas (P2G) plant by chosen RES efficiency:

Efficiencies	CASE A	CASE B
η_{SNG}	0,777	0,787
η_{PV}	0,18	0,18
η_{PV+P2G}	0,139	0,142
η_{WIND}	0,46	0,46
$\eta_{WIND+P2G}$	0,357	0,362

Table 36 – Overall efficiencies

7. Economic analysis

The economic analysis is a very useful tool to compare different configurations of the methanation plant coupled with the same SOEC, because the price of the product clearly explains the economic competitiveness of the process.
Both the capital and the operating costs of the P2G plant are estimated, the information necessary for the quantification of costs are mainly obtained from the literature. Considering capital and annual costs allows to build a detailed cash flow analysis.
In this work plant capital and annual costs have been considered in order to build a detailed cash flow analysis. Annual costs account for operating and maintenance items, energy input as well as material streams input cost. In the following section, each item will be analyzed.

The analysis is carried for both CASE A and CASE B. Even if for current gas parameters, the plant B cannot produce grid quality SNG, it is still interesting to see the possible economic benefits of this plant in a future perspective of increased N_2 blending.

7.1 Methodology

The economic evaluation pursued in this work is based on the concept of Net Present Cost (NPC), i.e. the determination of the total expenses attributable to a plant during the entire duration of its life referring to the present [8]. This data is the very useful for the comparison between different plants and technologies.

$$NPC = CAPEX_0 + \sum_{j=1}^{N} \left[\frac{OPEX_j}{(1+d)^j} + \frac{CAPEX_j}{(1+d)^j} \right] \tag{54}$$

Where:

- $CAPEX_0$ represents the capital expenditures due to the investments done at the beginning of the analysis period;
- $OPEX_j$ represents the cost of the operational phase in the j-th year. It accounts for the maintenance of the plant as well as all the expenditures necessary during the year.
- $REPL_j$ accounts for the replacement cost as periodically it is necessary a periodic substitution of components to maintain reliable the operation of the system.

- d is the corrected discount rate, considering an expected inflation rate. It represents the economic interest to which a certain component is subject in a year different from the reference year (today), bringing a future value back to the present value, hence by calculating its real cost [8];
- N represents the plant lifetime.

The discount rate variable, d, extends the economic analysis to the entire life of the plant and it can be calculated through an economic formulation used in reference [54]. In this way it is possible to determine any future cost at the present value:

$$d = \frac{d^I - i}{1 + i} \tag{55}$$

Where:

- d^I is the nominal discount rate, fixed at 7%;
- i is the inflation rate fixed at 2% [54].

The discount rate carriable has so a value of 4.9%.

Another hypothesis that has to be fixed is the capacity factor of the plant, defined as the ratio between the operating hours of the system and the total yearly hours:

$$CF = \frac{working\ hours}{8760}$$

For the analysis, a CF equal to 90% is fixed, so the total working hours of the plant are 7884. This ratio is important for assessing the total production of SNG as well as the consumption of fuels and the frequency of substitutions.

7.2 CAPEX

The capital expenditures are composed by the investment costs for the electrolysis part and for the methanation part.

For SOEC plants, according to [55], the capex is so composed:

	CASE A	CASE B
SOEC stack, M€	3,14	3,17
Auxiliaries, M€	3,14	3,17
Installation, M€	0,79	0,79
TOTAL COST, M€	7,07	7,13

Table 37 – SOEC CAPEX breakdown

These values depend on the size of the SOEC, which are calculated in the calculator block in the electrolysis section on Aspen.

The CAPEX of the methanation section depends on the power of the SNG obtained at the end of the process, with the reference to its HHV [56].

The obtained values are:

	CASE A	CASE B
SNG POWER (HHV basis), MW	10,27	10,40
TOTAL COST, M€	5,84	5,88

Table 38 – Methanation CAPEX

These value include:

- Equipment;
- Installation and buildings;
- Instrumentation and piping;
- Engineering costs.

The total capital expenditure are:

	CASE A	CASE B
TOTAL CAPEX, M€	12,90	13,03

Table 39 – Total CAPEX

7.3 OPEX

In the Operating Expenditure are included all the cost for activities that occur once the system starts to operate.

In particular, the following expenditures are considered:

- Operation and maintenance costs:
  The general maintenance cost is fixed at 3% [56] of the total CAPEX per year, reaching a value of around 0,45 M€ for CASE A and 0,46 M€ for CASE B.

- Personnel costs:
  Costs related to staff salaries amount to 135208 €/year for CASE A and 136934 €/year for CASE B, as it is according to [56], a function of the HHV of the SNG produced.

- Catalyst substitution costs:
  It is supposed to employ a catalyst with a lifetime of 24000 hours and a substitution cost of 570588 € for CASE A and 577874 € for CASE B, even in this case, the cost is a function of the HHV of the SNG [56]. According to the capacity factor of the plant, the substitution of the catalyst is required every three years.

- SOEC stack substitution costs:
  The stack substitution cost is fixed to the 30% of the total SOEC investment cost and the substitution is performed every 5 years. This cost is of around 2,12 M€ for CASE A and 2,14 M€ for CASE B.

- Electricity costs:
  As the substitutions costs, the expenditure relating to electricity depend on plant utilization. Electricity is used to run both SOEC and methanation sections, and its cost is fixed to 50 €/MWh.
  The following table summarizes the obtained values:

		CASE A	CASE B
SOEC section	$W_{el\text{-}AC}$, MW	11,45	11,57
	Electricity cost, M€	4,5	4,6
METHANATION section	SNG POWER (LHV basis), MW	10,27	10,40
	Electricity demand, kW/MW	25	25
	Demand, kW	257	260
	Electricity cost, M€	0,10	0,11

Table 40 – Electricity costs

- Fuel costs:
  For the CO2, the case in which only transportation cost through a pipeline is considered is chosen. In this work, carbon dioxide transportation cost has been set equal to 4 $/t. This is an acceptable value for transportation cost through a 200 km-length pipeline [57].
  Demineralized water is assumed to cost 1$/t [57].

		CASE A	CASE B
Water	Specific cost, €/t	0,90	0,90
	Mass flowrate, kg/s	0,80	0,81
	Mass flowrate, t/h	2,88	2,92
	Water costs, €	20435	20719
CO_2	Specific cost, €/t	3,6	3,6
	Mass flowrate, kg/s	0,528	0,528
	Mass flowrate, t/h	1,9	1,9
	CO_2 costs, €	53927	53927

Table 41 – Fuels costs

7.4 Results

The aim of this section is to consider and quantify in economic terms the fruits of the sizing and operations carried out by the P2G plant.

According to (54):

	CASE A	CASE B
TOTAL NPC, M€	85,34	85,13

Table 42 – NPC values

Starting from NPC, it is possible to calculate other variables to provide even more accurate indications from the point of view of convenience of the plant.

To quantify the SNG produced in monetary terms, another cost value can be considered as a function of the intrinsic thermal energy contained, to be able to compare it with the other variables. The following equation therefore allows to estimate the cost at which 1 kWh produced by the SNG should be sold [8]:

$$LCOE_{SNG} = \frac{NPC}{\sum_{i=1}^{N} E_{SNG}} \tag{56}$$

To estimate the LCOE costs, the following data are used:

	CASE A	CASE B
SNG flowrate, kg/s	0,19	0,2
SNG LHW, MJ/kg	48,7	46,83
Chemical power, kW	9253	9366
Yearly kWh (LHV basis), kWh	72950652	73841544

Table 43 – Values for LCOE calculation

The results are:

	CASE A	CASE B
LCOE, €/MWh	58,5	57,6

Table 44 – LCOE values

For an electricity cost of 50 €/MWh, the obtained values of the LCOE of the SNG are almost two times the 2019 prices of industrial fossil natural gas (29,30 €/MWh, LHV basis), while are lower than the 2019 prices of household fossil natural gas (95,10 €/MWh, LHV basis). [58]
The process analyzed in this thesis work could be economically competitive if the SOEC technology is improved. Electrolytic section costs, in fact, account for most of the CAPEX and OPEX.
Even if nowadays SOEC technology represents the best available path for power-to-H_2 process due to its high efficiency at the thermoneutral point, it is still a small-scale technology, its cost is still very high for plant with sizes of around 10MW.

7.5 Sensitivity analysis

With the base case price of electricity, it is possible to notice how it influences on the total cost of the plant. Costs related to electricity accounts for around 22% in both the scenarios studied.

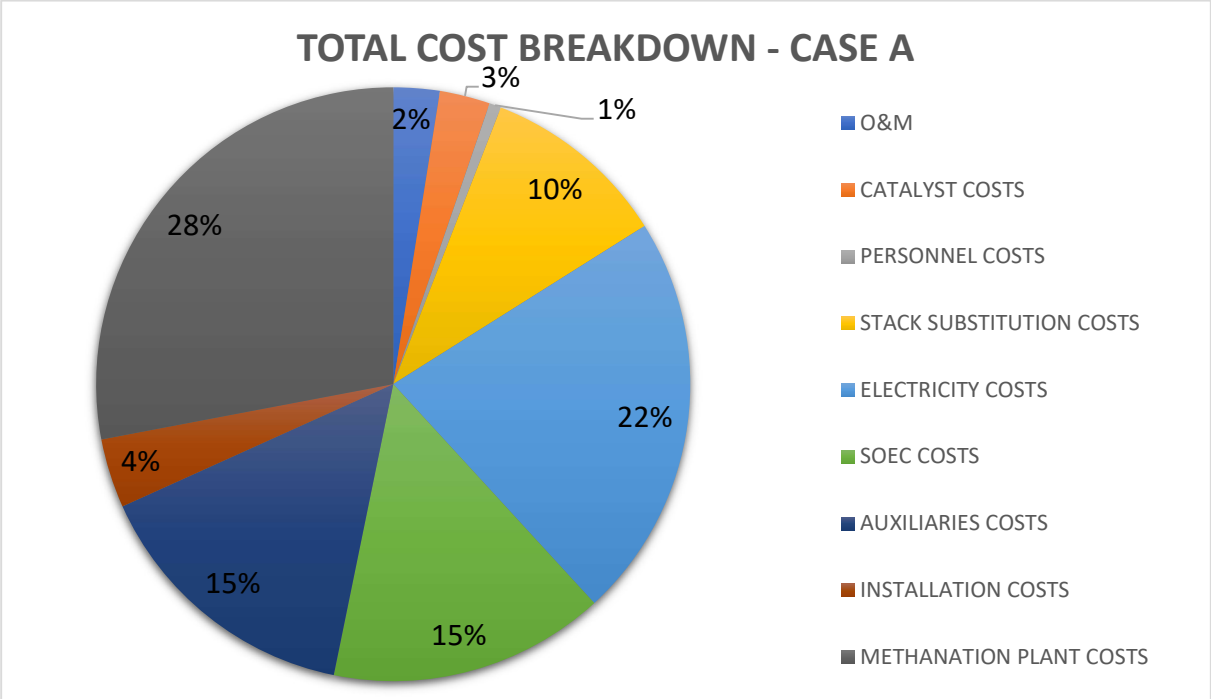

Figure 54 – Cost breakdown: CASE A

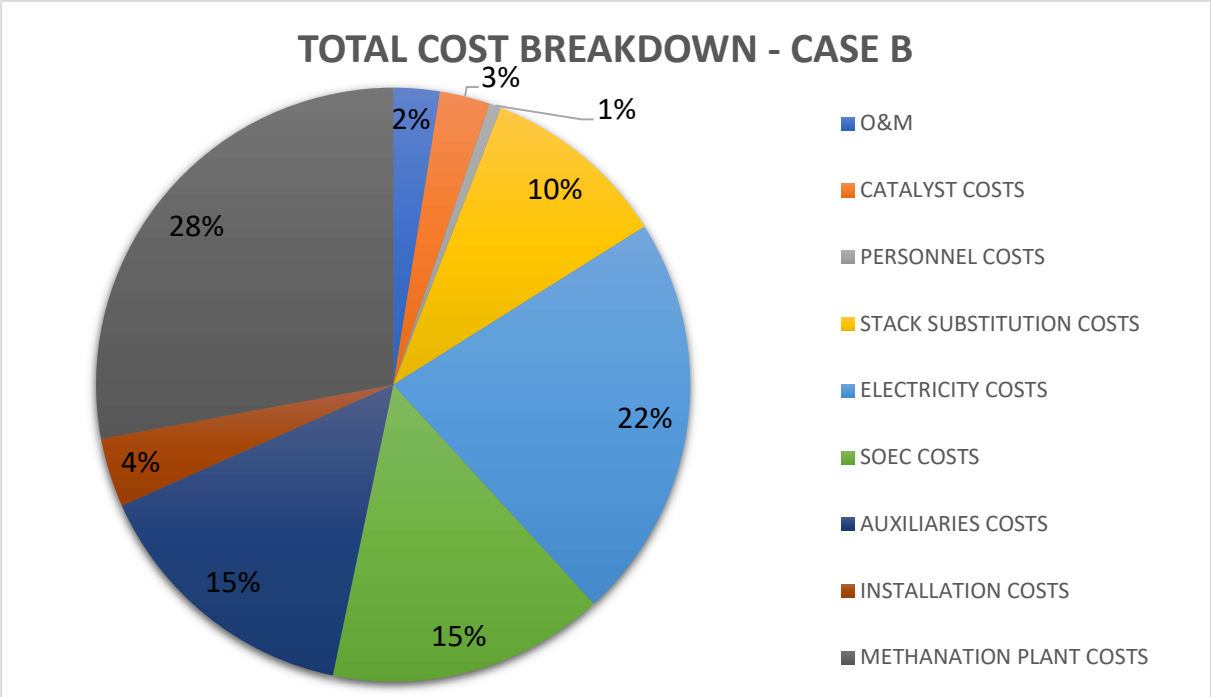

Figure 55 – Cost breakdown: CASE B

It is useful to perform a sensitivity analysis varying the cost of electricity to see how the NPC of the plant vary as well as the final LCOE. Electricity cost is supposed to be variable in a range between 0 and 80 €/MWh. Even if the lowest values are not comparable with the actual market price, their choice is justifiable starting from the consideration that Power to Gas could have a development only in a "low electricity price" scenario.

Starting from these hypotheses, the obtained results of the sensitivity analysis are reported in the following sections.

7.5.1 Case A

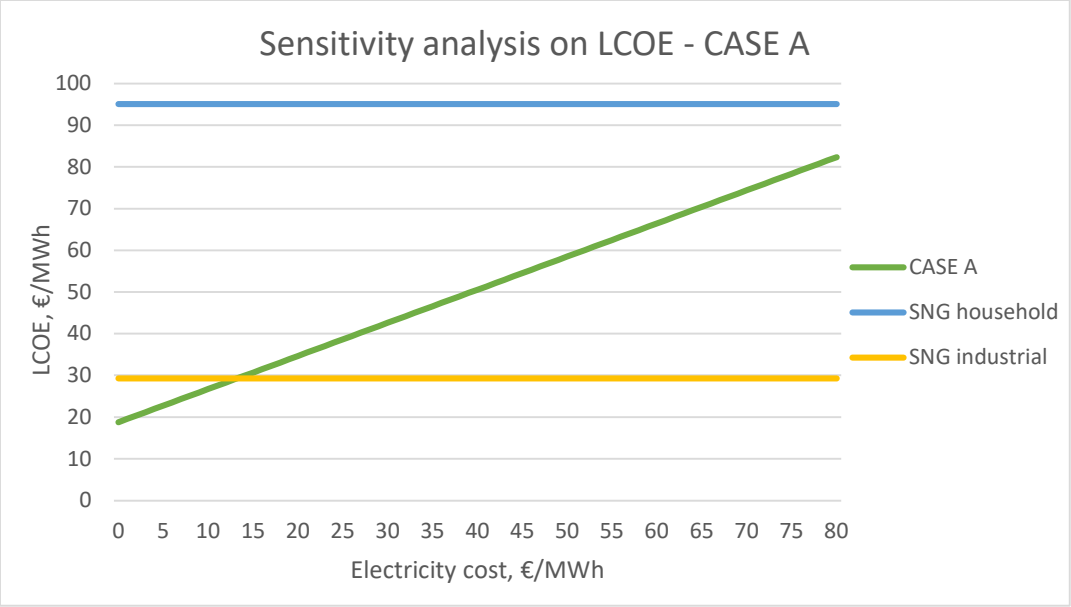

Figure 56 – Electricity cost vs LCOE

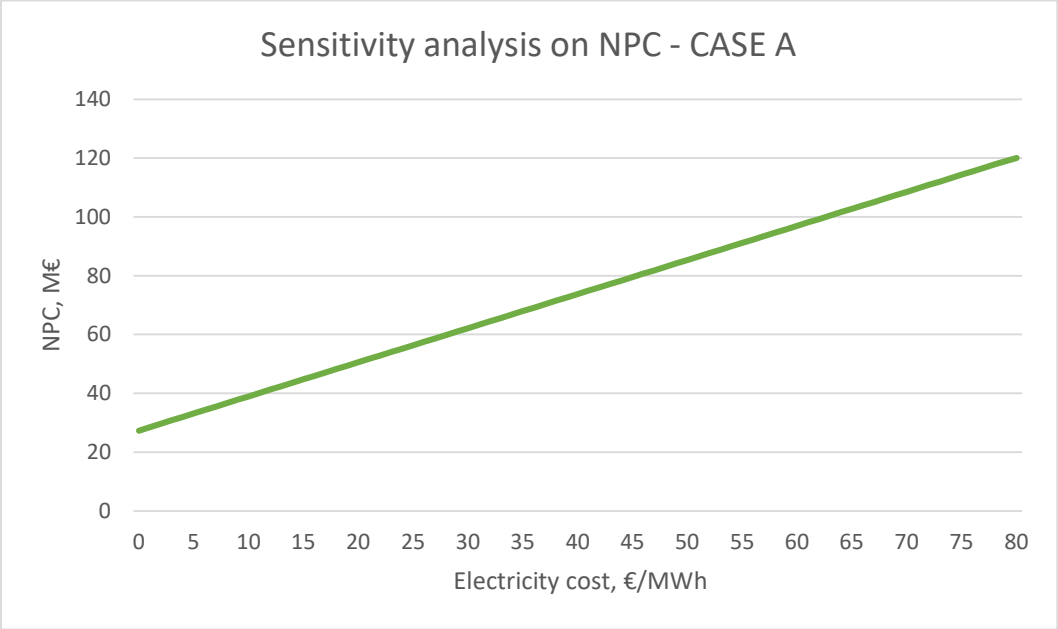

Figure 57 – Electricity cost vs NPC

7.5.2 Case B

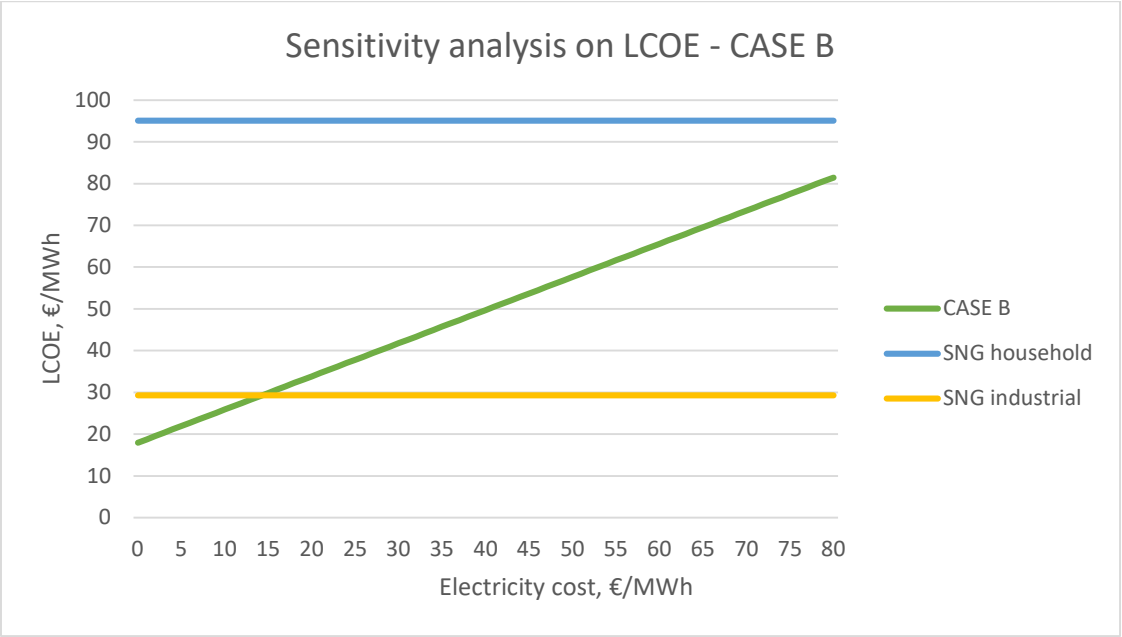

Figure 58 – Electricity cost vs LCOE

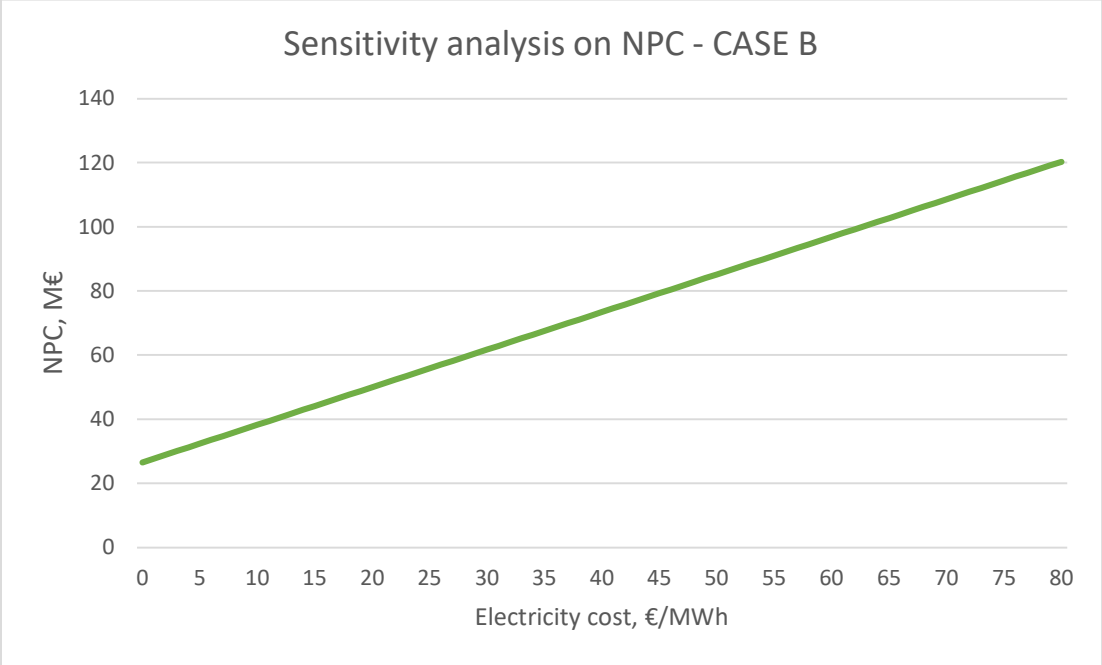

Figure 59 – Electricity cost vs NPC

In the scenario of a P2G plant operated with a low-priced surplus of electricity, the convenience of the plant is significant because the LCOE of the SNG would be lower than both the industrial and domestic SNG sold.

These results confirm the high potentiality of this process.

Conclusions

The growth of renewable energy sources as an alternative to fossil fuels represent a valid alternative to disjoin the society from carbon sources.
The strong dependence of RES from atmospheric conditions underlines the needing of an efficient way to store electric excess of production. The most promising technologies to achieve this purpose, seems to be the Power-to-gas.

This work of thesis aims to assess both qualitatively and quantitatively the technical and economic aspects of the coupling between a P2G plant and a SOEC.

Since the surplus cannot be fed into the grid so as not to cause stability issues, the electricity can be stored in chemical fuels that can be converted back into electricity when needed or directly used as SNGs.

In this paper, a new approach of converting renewable electricity into methane via syngas methanation is presented. Electricity from RES is used to electrolyze H_2O and CO_2 to H_2 and CO by using a SOEC (Solid Oxide Electrolysis Cell). Syngas produced is then converted into methane via TREMP™ methanation process.

For this thesis work, solid oxide electrolyzers are used. Co-electrolysis can be run by demineralized water coming from a Wastewater Treatment plant and CO_2 coming from flue gasses of an oxycombustion process, reducing the emission of this gas dangerous for global warming. Moreover, working in pressure brings methanation to occur yet at the cathode.

Pressurized working condition results to be advantageous as the exothermic methanation lowers energy requirements (good from a thermodynamic point of view). However, this leads to a reduction of current density at thermoneutral conditions and so to an increase of active area, resulting a disadvantage in economic analysis.

Coupled with the SOEC working at 850 °C and 33,1 bar, two different layouts of methanation are implemented and studied: CASE A has the traditional layout with four adiabatic TREMP reactors while CASE B has only three reactors and a recirculation after the first methanation step. Between the reactors, intercoolers are employed to lower the inlet temperature of the gas feed of the successive reactor.

Even if a partly methanation occurs already in the SOEC, this is not sufficient to have a SNG with grid quality with the layout of CASE B. However, this configuration can result to be interesting in the next future when higher values of hydrogen blending in SNG will be accepted.

Pinch analysis results a fundamental tool to maximize the exploitation of excess heat all over the plant and so, to maximize the efficiency of the system which results to be 78% for CASE A and 79% for CASE B.

The economic feasibility of SNG production via high temperature co-electrolysis is eventually assessed.

From the cash flow analysis, the LCOE of the SNG produced is lower than the NG sold to households (2019) but higher than the one sold to industries (2019). The main expenditures are related to the SOEC, since it is still a new technology and the use in large scale results to be still too much expensive.

In conclusion, the potentiality of P2G technology is confirmed, a foretaste of its increasing implementation resulting from the interesting economic results obtained. Taking into account the methodology of NPC used, in the economic analysis were not considered any kind revenue and especially no incentives, which would be an enormous source of income and would make this technology competitive.

References

[1] O. Edenhofer, R. Pichs-Madruga, Y. Sokona, K. Seyboth, S. Kadner, T. Zwickel, P. Eickemeier, G. Hansen, S. Schlömer, C. von Stechow and e. al, "RenewableEnergy sources and climate change mitigation: special report of the Intergovernmental Panel on Climate Change," Cambridge University, 2011.

[2] *https://news.climate.columbia.edu/2021/02/25/carbon-dioxide-cause-global-warming/.*

[3] D. Archer, "Atmospheric lifetime of fossil fuel carbon dioxide," *Annual Review of Earth and Planetary Science,* 2009.

[4] *https://www.iea.org/data-and-statistics.*

[5] A. Eitan, " “Promoting Renewable Energy to Cope with Climate Change”," *Sustainability 2021,* 2021.

[6] D. Grosso, *Uso Ottimale e sicurezza degli impianti energetici, notes of lectures,* Torino, 2019.

[7] *https://unfccc.int/process/bodies/supreme-bodies/conference-of-the-parties-cop.*

[8] V. Cascio, "Modelling and analysis of CO2 reuse in a PtX system based on reversible Solid Oxide Cell," Politecnico di Torino, Master Thesis.

[9] *https://www.rte.ie/news/world/2021/1109/1258831-climate-action-tracker/.*

[10] *https://www.isprambiente.gov.it/it/archivio/notizie-e-novita-normative/notizie-ispra/2021/11/26a-conferenza-delle-parti-sul-cambiamento-climatico.*

[11] https://ourworldindata.org/energy-mix.

[12] https://ourworldindata.org/electricity-mix.

[13] C. H. Arredondo, G. Aguilar-Lira, I. Perez-Silva, J. A. Rodriguez, G. Islas and P. Hernandez, "Characterization and Application of Agave salmiana Cuticle as Bio-membrane in Low-temperature Electrolyzer and Fuel Cells," *Applied sciences,* 2019.

[14] W. Wang, X. Wei, D. Choi, X. Lu, G. Yang and C. Sun, Electrochemical cells for medium- and large-scale energy storage: fundamentals, Pacific Northwest National Laboratory, Richland, WA, USA; 2UniEnergy Technologies, LLC,Mukilteo, WA, USA.

[15] L. Peng and Z. Wei, Catalyst Engineering for Electrochemical Energy Conversion from Water to Water: Water Electrolysis and the Hydrogen Fuel Cell.

[16] E. Giglio, "Modeling of High Temperature Electrolysis and Methanation processes for Synthetic Natural Gas Production," Politecnico di Torino, Master Thesis.

[17] S. Ebbesen, "Durable SOC stacks for production of hydrogen and synthesis gas by high temperature electrolysis," *Hydrogen Energy,* 2011.

[18] M. Mogensen, "Production of synthetic fuels by Co-Electrolysis of Steam and Carbon Dioxide," *International Journal of Green Energy,* 2009.

[19] S. Jensen, "Hydrogen and synthetic fuel production using pressurized solid oxide electrolysis cells," *Hydrogen Energy,* 2010.

[20] E.-J. Liu, Y.-H. Hung and C.-W. Hong, "Improved Metaheuristic Optimization Algorithm Applied to Hydrogen Fuel Cell and Photovoltaic Cell Parameter Extraction," 2021.

[21] P. D. Giorgio and U. Desideri, "Potential of Reversible Solid Oxide Cells as Electricity Storage System," *Energies,* 2016.

[22] L. Barelli, G. Bidini and G. Cinti, "Airflow Management in Solid Oxide Electrolyzer (SOE) Operation: Performance Analysis," *Chemengineering,* 2017.

[23] M. Carmo, D. L. Fritz, J. Mergel and D. Stolten, "A comprehensive review on PEM water electrolysis," *International Journal of Hydrogen Energy,* vol. 38, no. 12, pp. 4901-4934, 2013.

[24] S. Slade, S. A. Campbell, T. Ralph and F. Walsh, "Ionic Conductivity of an Extruded Nafion 1100 EW Series of Membranes," *Journal of The Electrochemical Society,* 2022.

[25] J. Russell, N. LJ and F. AP, "Hydrogen generation by solid polymer electrolyte water electrolysis," 1973.

[26] *https://blog.csiro.au/green-blue-brown-hydrogen-explained/.*

[27] *https://en.wikipedia.org/wiki/Coal_gasification#Process.*

[28] *https://www.turbomachinerymag.com/view/what-is-power-to-x.*

[29] *https://www.prosperoevents.com/power-to-x-energy-of-the-future/.*

[30] P. Deiana, C. Bassano and P. Gislon, "Tecnologie e prospettive del Power To Gas," 2020.

[31] E. Giglio, A. Lanzini, M. Santarelli and P. Leone, "Synthetic natural gas via integrated high-temperature electrolysis and methanation: Part I—Energy performance," *Lournal of energy storage,* 2015.

[32] P. Schmidt, W. Weindorf, A. Roth, V. Batteiger and F. Riegel, "Power-to-Liquids: potenstial and perspectives for the future supply of renewable aviation fuel," German Environment Agency, 2016.

[33] *https://www.ise.fraunhofer.de/en/business-areas/hydrogen-technologies-and-electrical-energy-storage/thermochemical-processes/power-to-liquids.html.*

[34] M. Santarelli, *Notes from "Polygeneration and advanced energy systems" course,* 2020.

[35] C. Graves, S. Ebbesen and M. Mogensen, "Co-electrolysis of CO2 and H2O in solid oxide cells: Performance and durability," *Solid State Ionics,* pp. 398-403, 2011.

[36] C. Wendel, P. Kazempoor and R. Braun, "Novel electrical energy storage system based on reversible solid oxide cells: System design and operating conditions," *Journal of Power Sources,* pp. 133-144, 2015.

[37] D. M. Bierschenk, J. R. Wilsona and S. A. Barnett, "High efficiency electrical energy storage using a methane–oxygen solid oxide cell," *Energy & Environmental Science,* 2011.

[38] X. Zhang, S. Chan, G. Li, H. Ho, J. Li and Z. Feng, "A review of integration strategies for solid oxide fuel cells," *Journal of Power Sources,* pp. 685-702, 2010.

[39] W. L. Becker, R. J. Braun, M. Penev and M. Melaina, "Production of Fischer–Tropsch liquid fuels from high temperature solid oxide co-electrolysis units," pp. 99-115, 2012.

[40] M. H. Bocanegra-Bernal and S. D. D. l. Torre., "Phase transitions in zirconium dioxide and related materials for high performance engineering ceramics," *Journal of Materials Science,* 2002.

[41] C. Graves, S. D. Ebbesen, S. H. Jensen, S. B. Simonsen and M. B. Mogensen, "Eliminating degradation in solid oxide electrochemical cells by reversible operation.," 2014.

[42] X. Zhang, J. E. O. Brien, R. C. O. Brien, J. J. Hartvigsen, G. Tao and G. K. Housley, "Improved durability of SOEC stacks for high temperature electrolysis," *International Journal of Hydrogen Energy,* pp. 20-28, 2013.

[43] H. Topsoe, "From solid fuels to substitute natural gas (SNG) using TREMP".

[44] J. H. Jensen, J. M. Poulsen and N. U. Andersen, "From coal to green energy," 2011.

[45] G. Bazzara, *Setup of an experimental test-bench for remote testing of solid oxide cells.Test-bench commissioning and test-protocols definition for the characterization of single cells for fuel cells applications,* Politecnico di Torino, Master Thesis, 2021.

[46] https://fuelcellmaterials.com/products/cells/electrolyte-supported-cells/nextcell-electrolyte-supported-planar-cell/.

[47] N. Meunier, S. Laribi, L. Dubois, D. Thomas and G. D. Weireld, "CO2 capture in cement production and re-use: first step for the optimization of the overall process," 2014.

[48] *https://onlinelibrary.wiley.com/doi/10.1002/ceat.202000068.*

[49] DOE/NETL, *Cost and performance baseline for fossil energy plants volume 2: coal to synthetic natural gas and ammonia,* 2011.

[50] *SNAM Rete Gas. Codice di rete - Allegato 11/A..*

[51] MISE, *Linee guida per la Strategia Nazionale sull'idrogeno,* 2020.

[52] A. C. Dimian, C. S. Bildea and A. A. Kiss, "Integrated design and simulation of chemical processes," *Computer Aided Chemical Engineering,* 2003.

[53] https://en.wikipedia.org/wiki/Pinch_analysis.

[54] A. Calvo, A. Lanzini, M. Santarelli and P. Marocco, "Modeling of stand-alone H2-based energy storage systems for electricity production and H2 mobility".

[55] H. Ammermann, P. Hoff, M. Atanasiu, J. Aylor, M. Kaufmann and O. Tisler, "Advancing Europe's energy systems: Stationary fuel cells in distributed generation".

[56] F. Mörs, S. Ruth, J. Gorre and R. Leonhard, "Innovative large-scale energy storage technologies and power-to-ga concept after optimization," 2020.

[57] E. Giglio, A. Lanzini and P. Leone, "Synthetic natural gas via integrated high-temperature electrolysis and methanation: part II-Economic analysis," *The journal of energy storage,* 2015.

[58] *https://www.sipotra.it/wp-content/uploads/2019/05/Natural-gas-price-statistics.pdf.*